AD-A147 799 APPLICATION OF ELECTROCHEMICAL ENGINEERING METHODS AND THEORY TO SOLVING..(U) ELECTROCHEMICAL TECHNOLOGY CORP SEATTLE WA R T RUGGERI ET AL. APR 84 NADC-84107-60 1/2

UNCLASSIFIED N62269 82 C-0261 F/G 11/6 NL

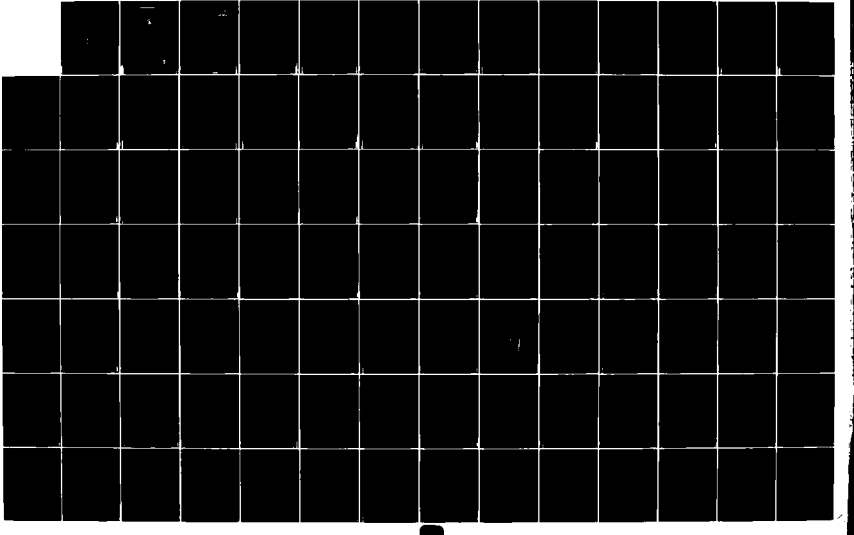

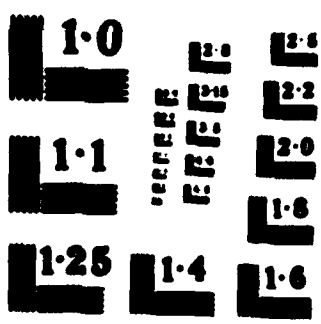
1.0
1.1
1.25
1.4
1.6
1.8
2.0
2.2

REPORT NO. NADC-84167-60

APPLICATION OF ELECTROCHEMICAL ENGINEERING METHODS AND THEORY TO SOLVING CORROSION AND ADHESION PROBLEMS WITH ORGANIC COATINGS

ELECTROCHEMICAL TECHNOLOGY CORP
Seattle, Washington 98107

APRIL 1984

INTERIM SUMMARY REPORT
For Period April 24, 1982 through April 30, 1984
Contract No. N62269-82-C-0281

APPROVED FOR PUBLIC RELEASE. DISTRIBUTION UNLIMITED

Prepared for
NAVAL AIR DEVELOPMENT CENTER
Department of the Navy
Warminster, Pennsylvania 18974

AD-A147 799

UNCLASSIFIED

SECURITY CLASSIFICATION OF THIS PAGE (When Data Entered)

REPORT DOCUMENTATION PAGE	READ INSTRUCTIONS BEFORE COMPLETING FORM
1. REPORT NUMBER: NADC-84107-60	2. GOVT ACCESSION NO.
3. RECIPIENT'S CATALOG NUMBER	
4. TITLE (and Subtitle): Application of Electrochemical Engineering Methods and Theory to Solving Corrosion and Adhesion Problems with Organic Coatings	5. TYPE OF REPORT & PERIOD COVERED: Interim Summary 24 April 1982 - 30 April 1984
6. PERFORMING ORG. REPORT NUMBER	
7. AUTHOR(s): Robert T. Ruggeri; Theodore R. Beck (Principal Investigator)	8. CONTRACT OR GRANT NUMBER(s): N62269-82-C-0261
9. PERFORMING ORGANIZATION NAME AND ADDRESS: Electrochemical Technology Corp. 3935 Leary Way N.W. Seattle, WA 98107	10. PROGRAM ELEMENT, PROJECT, TASK AREA & WORK UNIT NUMBERS
11. CONTROLLING OFFICE NAME AND ADDRESS: Naval Air Development Center Aero Materials Division Warminster, PA 18974	12. REPORT DATE: April 1984
	13. NUMBER OF PAGES: 109
14. MONITORING AGENCY NAME & ADDRESS (if different from Controlling Office)	15. SECURITY CLASS. (of this report): UNCLASSIFIED
	15a. DECLASSIFICATION/DOWNGRADING SCHEDULE

16. DISTRIBUTION STATEMENT (of this Report)

Approved for Public Release; Distribution Unlimited.

17. DISTRIBUTION STATEMENT (of the abstract entered in Block 20, if different from Report)

18. SUPPLEMENTARY NOTES

None.

19. KEY WORDS (Continue on reverse side if necessary and identify by block number)

Paint, Permeability, Solubility, Diffusion, Transference number, Mathematical model, Corrosion

20. ABSTRACT (Continue on reverse side if necessary and identify by block number)

The general objective of this work is to develop quantitative models for correlation and prediction of corrosion of aluminum under paint films. Transport properties for water and sodium and chloride ions were determined for five paints used on Navy aircraft as a basis for the models. Generic models for typical corrosion situations under paint films were developed.

DD FORM 1 JAN 73 1473 EDITION OF 1 NOV 65 IS OBSOLETE S/N 0102-LF-014-6601

UNCLASSIFIED

TABLE OF CONTENTS

	Page
INTRODUCTION	4
SUMMARY	4
EXPERIMENTAL RESULTS AND DISCUSSION	6
Hittorf Experiments	6
$SrCrO_4$ Leaching from YP-Epoxy	15
Humidity Chamber Experiments	17
Water solubility	17
Water Diffusivity	20
Solubility of Sodium and Chloride in Paints	26
Density of Paint Films	31
Average Water Permeability in Thick Paint Films	31
Adhesion Experiments	33
MATHEMATICAL MODELS	35
Introduction	35
Models	37
The Role of Inhibitors	39
Anodic Reaction	39
Cathodic Reaction	43
Mass Transport	45
Boundary Conditions	46
Simplifications	47
Corrosion-Geometry Models	47
Flat Surface	47
Paint Edge	48
Crack	48
Wedge	48
Blister	49
Examples	49
Inhibitor Depletion Through the Topcoat	49
Permeation of NaCl to the Metal Surface	50

Page

Depletion of Inhibitor Near a Crack 51
Reduction of the Effective Cathode Area by Paints . . .53
Discussion 55

APPENDIX A (Hittorf Experiments). 60
Apparatus 60
Procedure 64

APPENDIX B (Humidity Chamber Experiments) 73
Crystal Oscillator Theory 73
Diffusion Theory 76
Apparatus 78
Procedure 80
Experimental Results 84
Water Solubility 84
Water Diffusivity 103

INTRODUCTION

The basic objective of this work is to help solve corrosion problems on aircraft with the application of electrochemical techniques. Specific objectives include the determination of the mass transport properties, mechanism of corrosion initiation, and inhibitor leaching rate of various Navy paints. The paints received from NADC for this study are identified in Table 1.

The program has been divided into three phases or tasks. In the first phase the physical and transport properties of the paints listed in Table 1 were to be determined. The transport properties include water permeability and solubility, ionic diffusivities and transference numbers, and other mass transport parameters required by the mathematical models. The first phase proceeded as originally conceived and is substantially complete. The second phase of work has also begun. In the second phase, an attempt is being made to quantitatively understand mass transport in paints through the use of mathematical models. Several mathematical models have been developed and tested. It is apparent from this analysis that a wide range of mass transport behavior is exhibited by paints of interest to the Navy and that the transport property exhibiting the greatest influence on corrosion is a function of a number of physical parameters, geometry, and time. The third phase is correlation of the model results with field performance of paint systems. It is contingent upon the successful completion of phase two.

SUMMARY

Phase one is now substantially complete; the mass transport properties have been determined. Adhesion tests were unsuccessful and have been discontinued. Phase two is currently in progress. A detailed mathematical model of the transport mechanism in paints was developed and tested. The results showed even more complex transport behavior than was originally envisaged.

TABLE 1

Paints with Physical Properties
Given in this Report

Mil Spec.	Binder	Color	ETC Designation Code
I. Paints delivered by NADC			
MIL-C-83286 B	polyurethane	gray, flat	FP-PUR
MIL-C-83286	polyurethane	white, glossy	GP-PUR
MIL-P-23377 D	epoxy polyamid	yellow	YP-Epoxy
MIL-C-85054	silicone alkyd	clear	WD 2
MIL-P-85658	silicone alkyd (a)	white	WDPT
II. Reference paints from prior contract work (b)			
MIL-C-83286	polyurethane (c)	clear	O-PUR
MIL-C-81773 B A/S	polyurethane (d)	clear	N-PUR

(a) Same binder as WD 2 but with added pigment.

(b) See Ref. 4.

(c) Desoto, Inc., Chemical Coatings Div., Berkeley, CA (Meets Boeing Materials Specification BMS-10-60D-TYII).

(d) Formulated at ETC (Ref. 4).

A second mathematical model has been developed based on the original model and experimental results. Certain aspects of the complex mass transport behavior of paints have been simplified in this model. The effects of the aluminum oxide on the aluminum substrate have been included in the expressions for the electrochemical reaction kinetics. The kinetic expressions are also simplified models of real behavior. Although this model incorporates many simplifications, it is anticipated that the essential characteristics of the corrosion mechanism have been retained. If the model can be confirmed by correlation with corrosion tests it can be used to prescribe the characteristics of the coating system which determine its corrosion performance. It is anticipated that the relative importance of various transport properties will depend on the geometry and other physical properties of the corrosion cell. Once the physical properties have been specified and the relative importance of the transport properties assessed, the relative merits of various coating systems will be evaluated.

The development of the mathematical model partially completes task two of the work statement. The transport of mobile species in the paint has been modeled and a computer program is available; however, it has been determined that the model must include surface reaction kinetics as well in order to accurately describe the corrosion process. Experiments have not been conducted to determine the kinetic parameters. The mathematical model has not yet been correlated with corrosion experiments; this work constitutes task three of the work statement.

EXPERIMENTAL RESULTS AND DISCUSSION

Hittorf Experiments

Hittorf experiments were performed to determine the transport properties of ions and water in paint films. The films were prepared by spray painting sheets of decal paper. When the paint had dried, the paint films could easily be removed from the decal paper by soaking in water. Detached paint films prepared in this manner have been termed "free films."

Hittorf experiments were conducted in sodium chloride solution to determine permeability coefficients and transference numbers of sodium and chloride ions and water through free films of paint. Radiotracers (^{22}Na or

^{36}Cl) were used to determine the flux of the appropriate ion across paint membranes. Tritium (^{3}H) was used to trace the water flux. The basic Hittorf experiment consists of measuring the fluxes of the mobil species which pass through the paint film from one aqueous solution to another. The two aqueous solutions were identical except that one contained radiotracers. Figures 1 and 2 show how the radiotracer activity in the solution originally devoid of tracers (top solution) changed with time. In this experiment two different applied voltages were tested. Figure 3 shows a linear relationship between the sodium and the total charge passed through the membrane, despite the fact that the current density varied more than a factor of two over the course of the experiment.

Hittorf experiments were conducted with all paints listed in Table 1. Attempts were made to complete experiments with WD-2 in 1.0 N NaCl solution, but these attempts repeatedly failed because of the physical properties of this coating. All Hittorf results are presented in Appendix A and a summary is presented in Table 2. (Corrections were made to some of the data previously given in quarterly reports.)

The Hittorf results show considerable variability in many of the transport properties. The conductivity and ionic permeability coefficients show order of magnitude variations between specimens as well as large changes with time. The source of these variations has not been determined, but if the classic theory is adopted they must represent changes in either the ion solubility or diffusion coefficient. The relationship between permeability coefficient, diffusion coefficient, and dimensionless solubility is

$$P = DS \qquad (1)$$

The data obtained here were insufficient to determine if the changes in permeability resulted primarily from variations in either the diffusion coefficient or the solubility.

Table 2 shows the arithmatic average transference numbers and the geometric average conductivities obtained in Hittorf experiments. One interesting result illustrated in Table 2 is that the transference numbers of sodium and chloride ions do not sum to unity. It is generally assumed that coatings immersed in aqueous sodium chloride solution will transfer charge by ionic migration of sodium and chloride ions. Clearly this assumption is not accurate for many paints. The standard deviation of transference

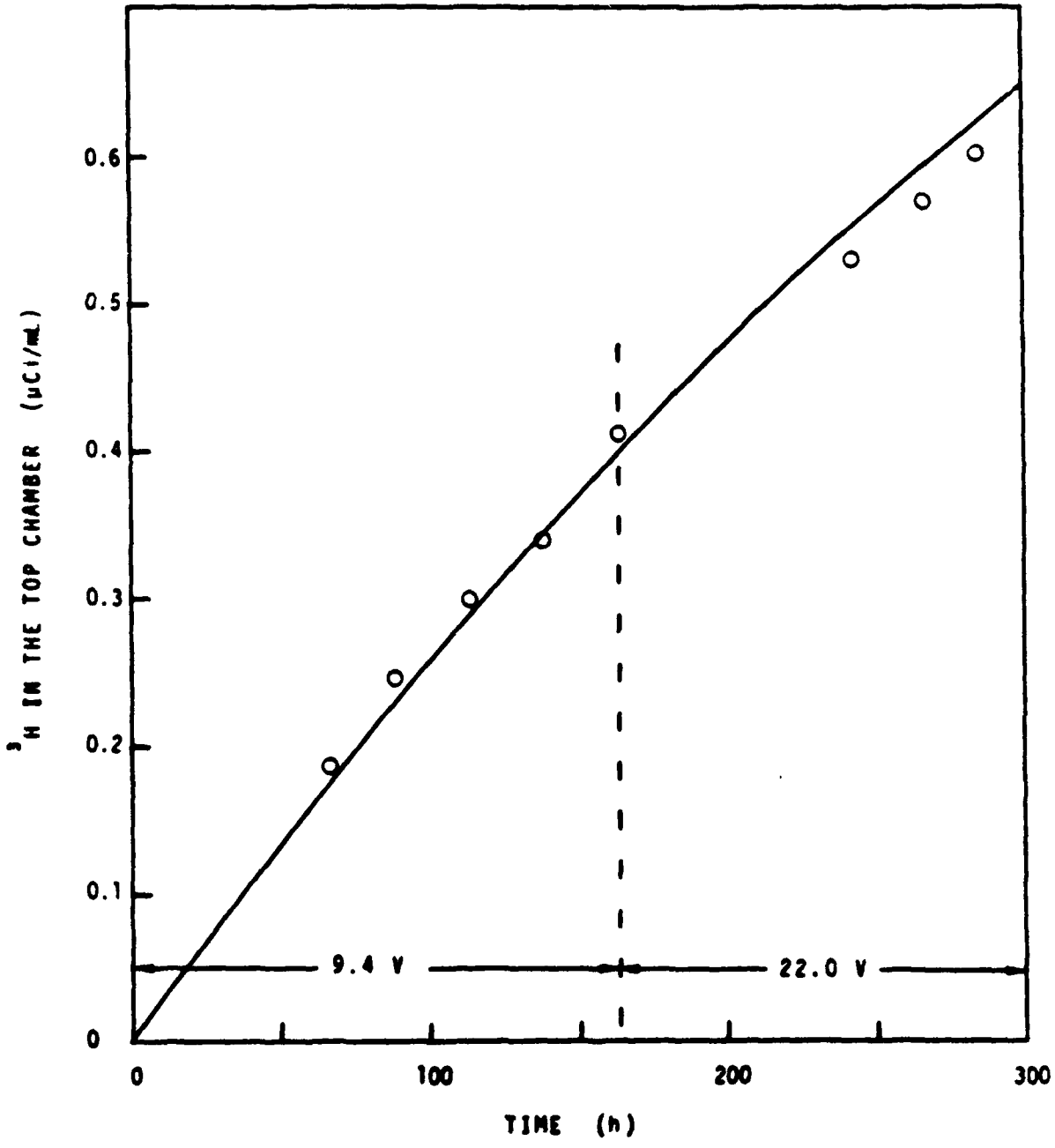

Fig. 1. Tritium activity in the top compartment of a Hittorf experiment conducted with GP-PUR. O = experimental points. —— = the theoretical $^3H_2$ activity for a constant permeability coefficient (P = 7.14 x 10^{-10} cm^2/s).

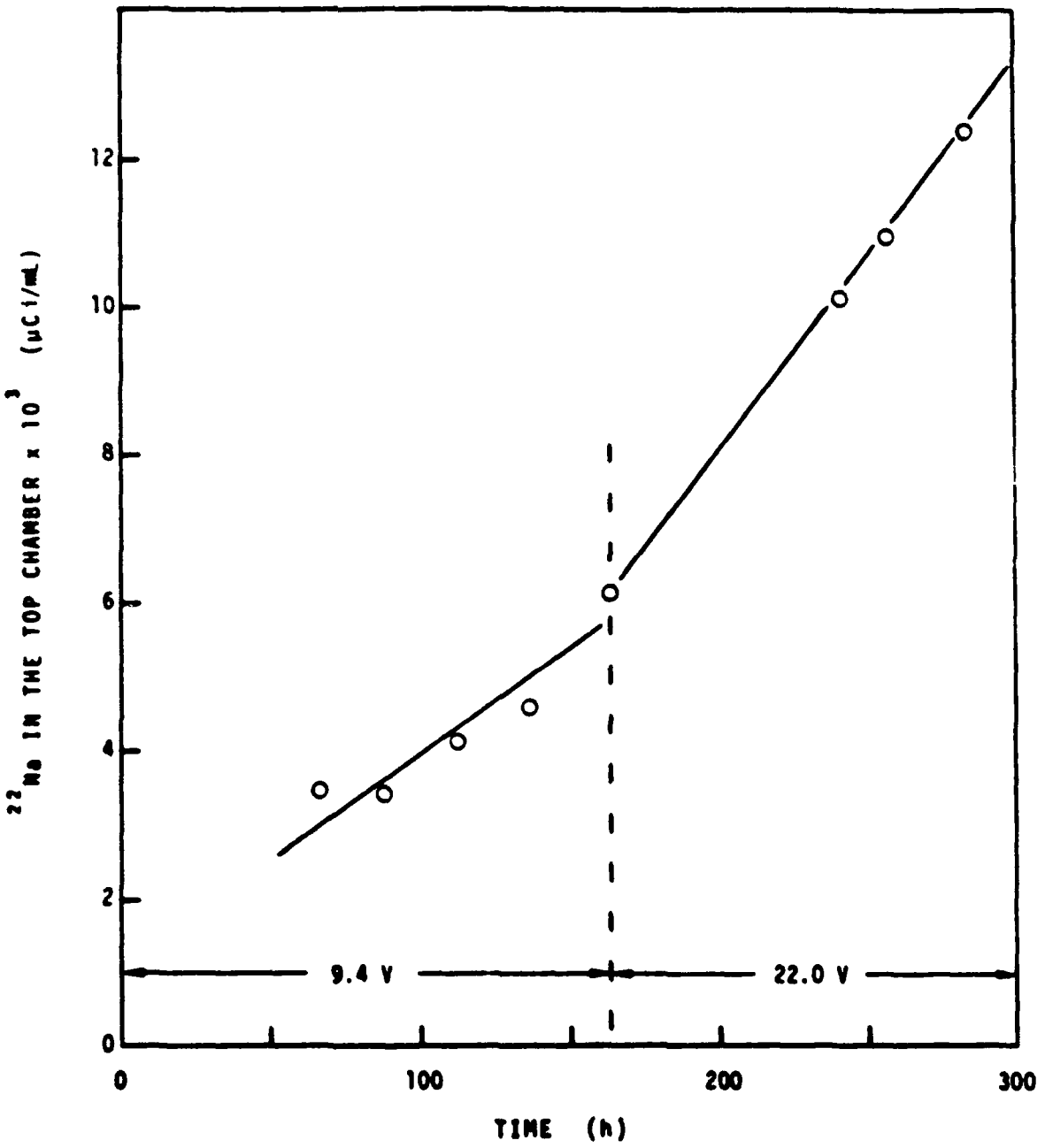

Fig. 2. Radioactive sodium-22 activity in the top compartment of a t experiment with GP-PUR. O = experimental points. The curve straight line segments through the data obtained at constant

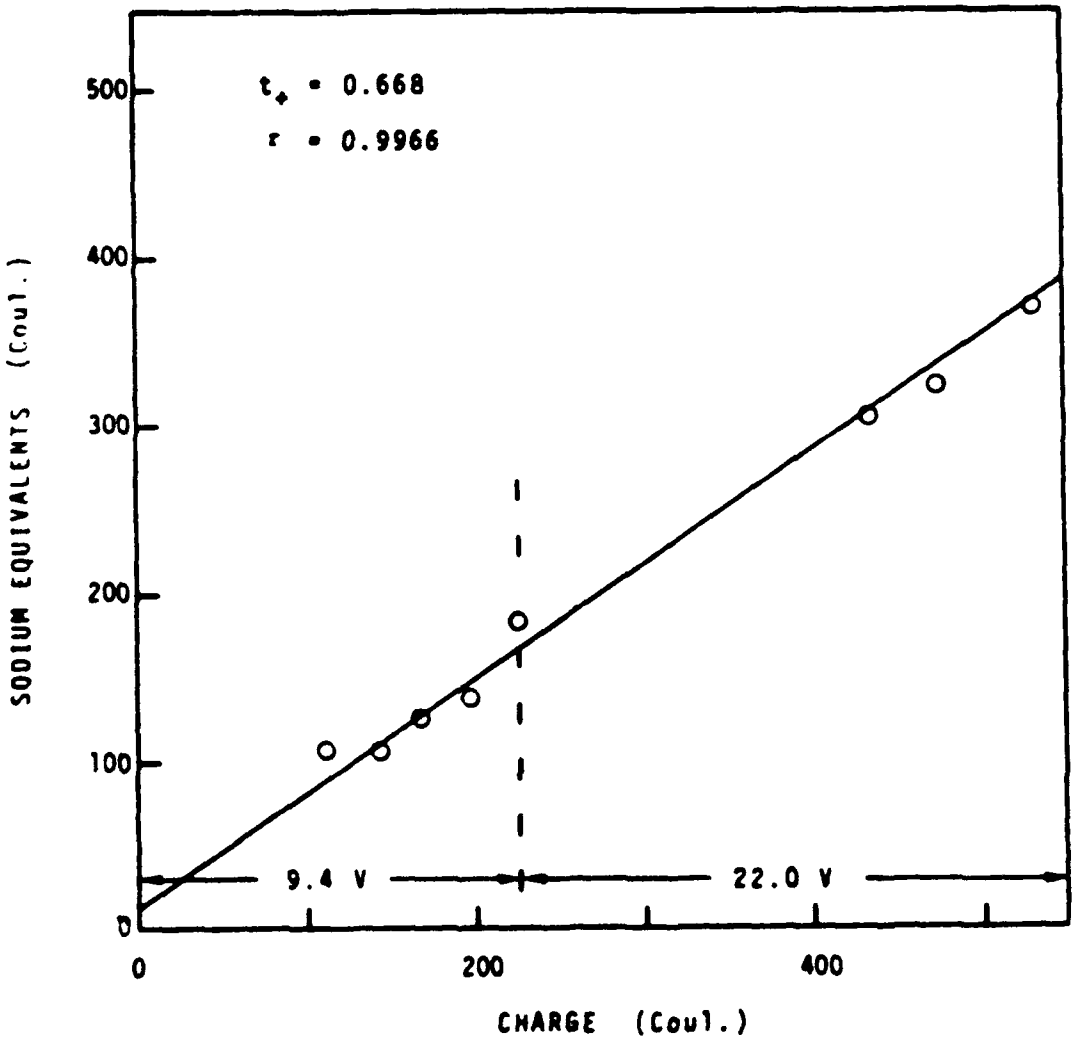

Figure 3. Equivalents of sodium passed through GP-PUR versus total charge. The slope of the best straight line through the data was taken as the transference number. Least squares slope (t_+) and correlation coefficient (r) are shown.

Table 2

Average Transference Numbers of Sodium and Chloride in Paints in Aqueous Solution at 25°C

Paint	NaCl Conc. (N)	Average Transference Number t_-	t_+	t_-+t_+	Average dc Conductivity (S/cm)
O-PUR	0.1	0.31	0.41	0.72	4.1×10^{-11}
N-PUR	0.1	0.20	0.42	0.62	4×10^{-10}
FP-PUR	0.1	0.12	0.48	0.60	1.9×10^{-9}
	1.0	0.20	0.29	0.49	1.2×10^{-8}
GP-PUR	0.1	0.13	0.54	0.67	$6. \times 10^{-12}$
YP-Epoxy	0.1	0.40	0.14	0.54	2.8×10^{-7}
	1.0	0.59	0.28	0.87	2.1×10^{-6}
WDPT	0.1	0.11	0.56	0.67	$1. \times 10^{-7}$
	1.0	0.38	0.44	0.82	3.0×10^{-8}
WD-2	0.1	0.63	0.33	0.99	$5. \times 10^{-8}$

numbers obtained in duplicate experiments is about 0.1 and it may be assumed that the error in the sum is about 0.2. Seven of ten entries in Table 2 therefore show that a significant portion of the current is not carried by sodium and chloride. In another study a larger number of experiments were performed with O-PUR. Statistical analysis of those data showed that the sum of the transference numbers for sodium and chloride is significantly less than unity. This finding was confirmed here for six of the seven paints tested in 0.1 N NaCl solution (Table 2), but for only one of three paints tested in 1.0 N NaCl solution.

The fact that sodium and chloride do not carry 100% of the current raises the question of which species carry the remainder. This question has been addressed in previous reports but has not yet been resolved. YP-Epoxy presents a special case. This primer contains a soluble inorganic inhibitor, $SrCrO_4$. Strontium chromate composes about 52% of the coating mass (1) and has a solubility in water of about 4×10^{-3} m. It is therefore expected that Sr^{+2} and $CrO_4^{=}$ ions carry some current, and that the fraction of current carried by these ions increases as the sodium chloride concentration decreases. This type of behavior is observed, as shown in Table 2. It is possible that pigments in other paints provide a source of ions, but more study will be required to clarify this point.

Another possible source of ions is the production of hydrogen and hydroxyl ions in the paints by water splitting. Such a process is known to occur in dilute boundary layers near membranes and electrodes (2). Since the solubility of sodium chloride in paints is low, paints immersed in aqueous electrolyte can be considered as dilute solutions in which water splitting takes place. Another possibility is simply that hydrogen or hydroxyl ions have a much higher solubility in paints than do sodium and chloride. The ion solubility experiments discussed later in this report tend to support this hypothesis.

If hydrogen and hydroxyl ions do carry part of the current then the pH of both solutions adjacent to the membrane should change in Hittorf experiments. Changes in pH have been observed, but no trends have been noted, as would be expected if water splitting occurred. Most of the Hittorf experiments require several weeks to complete, and the expected pH changes are small so that some

secondary process may be masking the effects of water splitting. It is therefore not yet possible to identify the ions other than sodium and chloride which carry current in these paints.

Table 3 presents a summary of the average transport properties of seven paints. The tabulated concentrations of chloride and sodium in the paints are the results of ion solubility experiments discussed in a later section. The permeability coefficients which are tabulated are the geometric means of normalized permeability coefficients. The normalization was performed to reduce time dependent scatter in the data. It was observed that the conductivity of paint membranes varied with time in the course of a single Hittorf experiment, and that the ionic permeability coefficients also changed in a corresponding manner. This type of behavior would be expected if the coating had been tested in several solutions with different sodium chloride concentrations, but it was not expected in individual Hittorf experiments. It was therefore decided to normalize the permeability coefficients obtained, not only in single experiments but also for different experiments. The normalization factor was based on coating conductivitiy according to the equation

$$P_n = \frac{P_e k_e}{k_{Ave}} \qquad (2)$$

P_n = the normalized permeability
P_e = the experimental permeability
k_e = the experimental conductivity
k_{Ave} = the geometric mean conductivity.

Each apparent diffusivity listed in Table 3 was calculated from the corresponding permeability coefficient and solubility according to Eq. 1.

The flux of a species through a membrane can be written as

$$F_i = -P_i \frac{\Delta C_i}{L} - P_i \bar{C}_i \frac{\Delta\psi}{L} \qquad (3)$$

$\Delta\psi$ = the change in dimensionless potential across the membrane = $\frac{z_i F}{RT} \Delta\phi$.

$$\bar{C}_i = (1/\Delta\psi) \int_0^L C_i \nabla\psi dx \qquad (4)$$

L = membrane thickness
C_i = concentration in the aqeuous electrolyte in equilibrium with the membrane.

Table 3

Average Transport Properties of Ions in Paints

Paint	NaCl Concentration in Solution (N)	Concentration in Paint (mol/ml.)		Average Permeability Coefficient (cm^2/s)		Apparent Diffusivity (cm^2/s)	
		Cl	Na	Cl	Na	Cl	Na
O-PUR	0.1	1.5×10^{-7}	3.0×10^{-8}	1×10^{-14}	1×10^{-14}	7×10^{-12}	3×10^{-11}
N-PUR	0.1	2.7×10^{-8}	1.7×10^{-8}	3×10^{-13}	7×10^{-13}	1×10^{-9}	4×10^{-9}
FP-PUR	0.1	4.6×10^{-6}	5.8×10^{-5}	7×10^{-13}	2×10^{-12}	2×10^{-11}	3×10^{-12}
	1.0	9.0×10^{-5}	3.3×10^{-5}	6×10^{-13}	8×10^{-13}	7×10^{-12}	2×10^{-11}
CP-PUR	0.1	1.4×10^{-6}	3.3×10^{-6}	3×10^{-15}	1×10^{-14}	2×10^{-13}	3×10^{-13}
YP-Epoxy	0.1	2.6×10^{-5}	3.4×10^{-5}	3×10^{-10}	1×10^{-10}	1×10^{-9}	3×10^{-10}
	1.0	1.3×10^{-4}	5.3×10^{-5}	4×10^{-10}	6×10^{-11}	3×10^{-9}	1×10^{-9}
MDPT	0.1	3.1×10^{-5}	1.1×10^{-4}	1×10^{-11}	1×10^{-10}	3×10^{-11}	9×10^{-11}
	1.0	1.0×10^{-4}	1.9×10^{-4}	3×10^{-12}	4×10^{-12}	3×10^{-11}	2×10^{-11}
MD2	0.1			7×10^{-11}	4×10^{-11}		

Equation 3 is based on two assumptions: the diffusivity is a constant, and the dimensionless concentration is a constant. It is clear from Eq. 3 that, for a given set of circumstances, the flux of the mobile species is proportional to its permeability coefficient.

The time required to reach a steady state condition depends on the diffusivity not the permeability. The time constant for diffusion is

$$t_i = \frac{L^2}{D_i} \tag{5}$$

In practical applications both the time constant and the steady-state flux are important. Table 4 shows how the six paints studied here rank with respect to both the permeability coefficient and diffusivity. The paints are ranked in order from 1 to 6 with 1 being the minimum value of permeability or diffusivity and 6 being the maximum value. According to these results GP-PUR should provide the best protection both in terms of time required for ions to penetrate through the coating to the metal surface and in terms of the maximum flux of ions which can flow. If the permeability and diffusivity are of equal importance in a given application then the paints can be scored by summing the four entries in Table 4. The results of this procedure are shown in Table 5. This procedure illustrates one way the experimental data can be used to rate coating performance, but to be of practical value an appropriate weighting factor must be applied to each parameter (diffusivity or permeability). The weighting factor will describe the relative importance of each parameter in the particular environment in which the paint will be used. For example, the diffusivity is of little importance if the paint was applied over a dirty surface contaminated with sodium chloride. Also the results in Table 5 apply to single-coat systems, and would therefore not apply to two-coat systems such as GP-PUR over YP-Epoxy. These results do however show the kind of ranking procedure which could be employed once the use and physical conditions the coating will be subjected to have been specified.

$SrCrO_4$ Leaching from YP-Epoxy

Leaching experiments were conducted with YP-Epoxy. A weighed specimen of paint was placed in 50 mL of well-stirred distilled water. Periodically

Table 4

Relative Ranking of Sodium Chloride Transport in Paints Exposed to 0.1 N NaCl Solution at 25°C

Rank	Permeability		Diffusivity	
	Cl	Na	Cl	Na
1	GP-PUR	GP-PUR	GP-PUR	GP-PUR
2	O-PUR	O-PUR	O-PUR	FP-PUR
3	N-PUR	N-PUR	FP-PUR	O-PUR
4	FP-PUR	FP-PUR	WDPT	WDPT
5	WDPT	WDPT	YP-Epoxy	YP-Epoxy
6	YP-Epoxy	YP-Epoxy	N-PUR	N-PUR

Table 5

Total Score of Paints Listed in Table 4

Rank	Paint	Total
1	GP-PUR	4
2	O-PUR	9
3	FP-PUR	13
4	N-PUR	18
5	WDPT	18
6	YP-Epoxy	22

300 µL of the solution were withdrawn and a 200 µL portion of this sample was added to 25 mL of distilled water. Then the electrical conductivity of the resulting mixture was determined. The conductivity obtained in this way was subtracted from the conductivity of the original 25 mL of distilled water which was determined immediately prior to the addition of the 200 µL sample. The time constant for diffusion of inhibitor out of YP-Epoxy was about 1000 m. Assuming the leaching rate is controlled by diffusion in the paint, a diffusivity can be calculated from the time constant and the paint thickness (about 150 µm). The diffusivity calculated in this manner is 9×10^{-10} cm^2/s). This compares with the diffusivity of NaCl: 7×10^{-10} cm^2/s. The diffusivity of NaCl was estimated from permeability coefficients obtained in Hittorf experiments and solubilities obtained by using radio-isotopes.

Humidity Chamber Experiments

Water Solubility

A crystal oscillator apparatus was used to determine the solubility of water in paints. A detailed description of apparatus and procedure are given in Appendix B. Typical results are shown in Fig. 4 as mass of water absorbed per kilo Pascal of water pressure versus the mass of paint applied to the quartz crystal. The slope of the curve represents the solubility of water in GP-PUR. The solubility of water in GP-PUR exposed to partial pressure of water of 3.52 kPa at 31.6°C was 0.028 g-H_2O/g-paint. The data in Fig. 4 have a significant negative intercept which may indicate some type of error or curvature in the oscillator's frequency response as mass is added. Another possibility is that the solubility of water is a function of coating thickness.

The solubility of water in the paints examined here is summarized in Table 6. These results are based on the slopes of the least-squares lines through data similar to that shown in Fig. 4. These results show that the solubility is relatively constant for all the paints tested. YP-Epoxy exhibits the lowest solubility partially because of the large volume fraction of dense solids and partially because epoxies sorb little water. GP-PUR exhibits the greatest water solubility. The solubility of water in GP-PUR, on a pigment-free basis, is about 2.4 times that of unpigmented M-PUR (3). Since the pigments are generally inorganic crystalline materials with

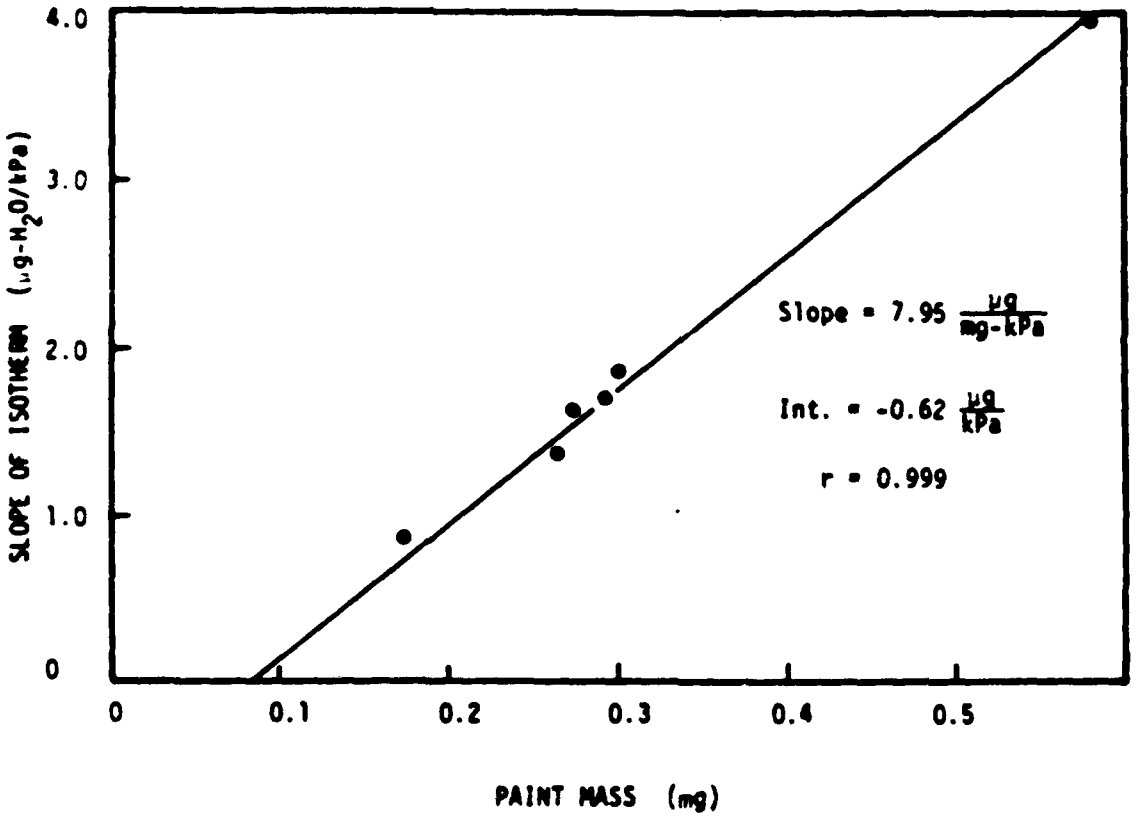

Fig. 4. Solubility of water in GP-PUR at 31.6°C.

Table 6

Average Transport Properties of Water
in Paints at 30°C

Paint	Solubility $\left(\frac{g\text{-}H_2O}{(g\text{-paint})(Pa)}\right)$	Permeability Coefficient x 10^{10} (cm^2/s)	Diffusivity x 10^9 (cm^2/s)
O-PUR	5.6	4.0	15.
N-PUR	6.7	3.6	11.
GP-PUR	7.9	5.6	11.
FP-PUR	8.0	10.9	21.
YP-Epoxy	3.7	2.0	7.1
WDPT	4.0	5.4	19.
WD2	5.8	1.0*	3.5**

* Data obtained with crystal oscillator apparatus

** Calculated from P = DS

low solubility in water it is unlikely that a significant volume of water is incorporated into the pigment particles themselves. These data therefore indicate that the pigment interacts with the binder in some way to enhance the solubility of water. Water has been shown to concentrate near some paint-metal interfaces (4-6). Perhaps a similar phenomenon occurs at the paint-pigment interface. In any case it is apparent that pigments have a great effect on the solubility and thermodynamics of water in paints.

Water Diffusivity

Analysis of the time transient data obtained with the crystal oscillator apparatus provides diffusivities of water in the paints. Average diffusivities of water in five different paints are shown in Table 7. More detailed results are presented in Appendix B. Diffusivities obtained with the crystal oscillator apparatus are also shown in Figs. 5-7. These results show that the diffusivity is in general a function of water concentration, or water activity in the paint. The diffusivity of water in the three paints illustrated here tends to decrease as the activity of water increases. This same trend was found previously for unpigmented polyurethane coatings, N-PUR and O-PUR, but the effect was more pronounced in the unpigmented materials (4). The effect of coating thickness was also greater with unpigmented paints. Both O-PUR and N-PUR show a significant increase in apparent diffusivity with increasing thickness when the coatings are thinner than about 10 μm. The diffusivities obtained with thick membranes in Hittorf experiments did not depend on thickness. The average diffusivity obtained from Hittorf experiments is also shown in Figs. 5-7. These values were obtained by dividing the permeability coefficients obtained in Hittorf experiments by the dimensionless solubility obtained with the crystal oscillator. The Hittorf diffusivities are generally greater than those obtained with the crystal oscillator. This result was assumed to be due to the fact that thicker membranes were used in Hittorf experiments, but it may also be related to differences in experimental conditions or membrane history.

The data obtained with the humidity-chamber apparatus suggest a number of generalizations. The absorption isotherms of individual paint specimens are adequately represented by Henry's law. Some curvature of the isotherms may be present, but the error introduced by the Henry's law approximation is

Table 7

Average Diffusivity of Water in Paints at 30°C
Exposed to a Partial Pressure of Water Equal to 3.5 kPa

Paint	$\bar{D}$ (cm^2/s)
FP-PUR	3×10^{-9}
GP-PUR	1×10^{-9}
YP-Epoxy	5×10^{-10}
O-PUR	1×10^{-9}*
N-PUR	8×10^{-10}**

* Sample thickness approx. 2 μm

** Sample thickness approx. 4 μm

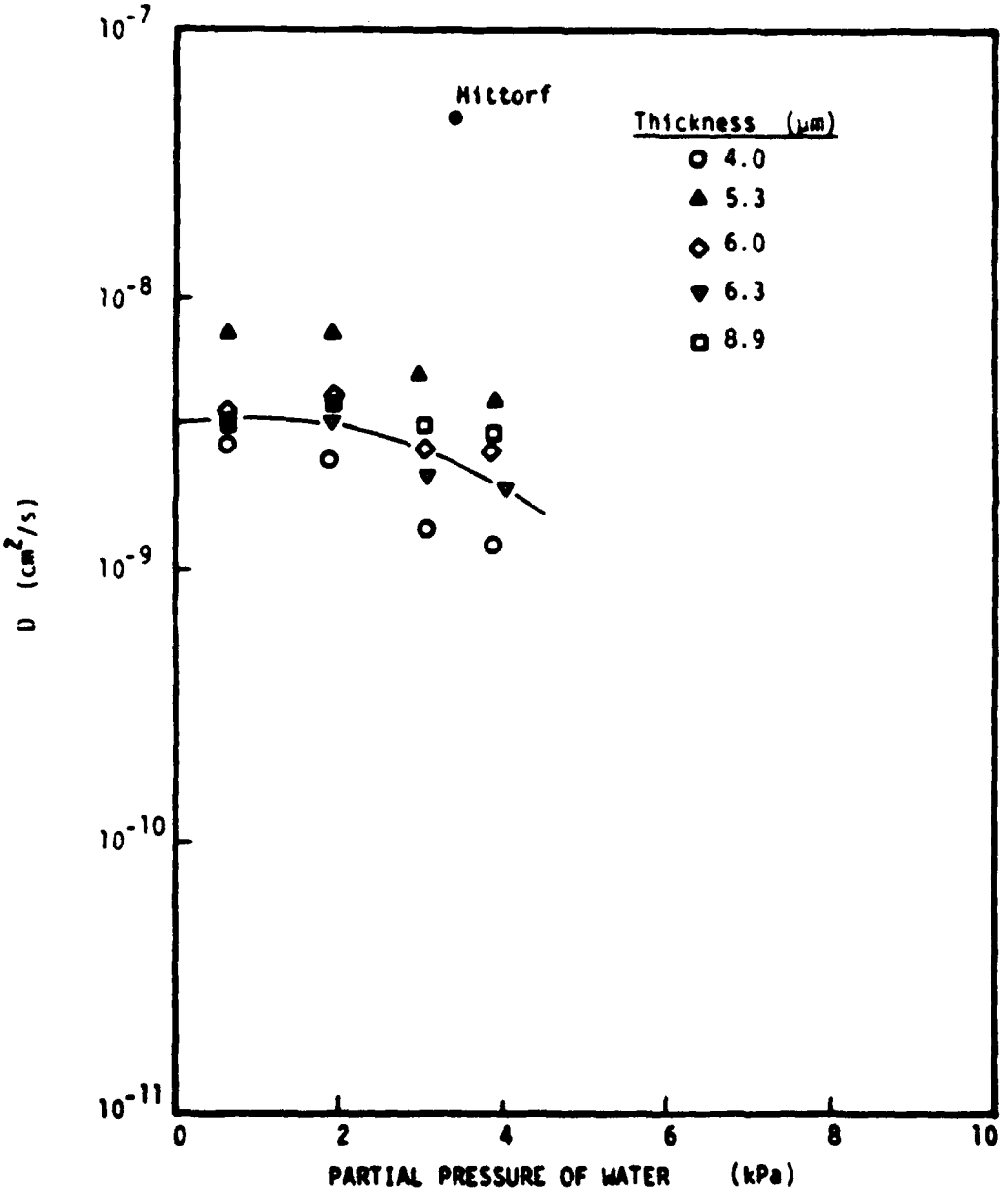

Fig. 5 Diffusivity of water in FP-PUR at 30°C.

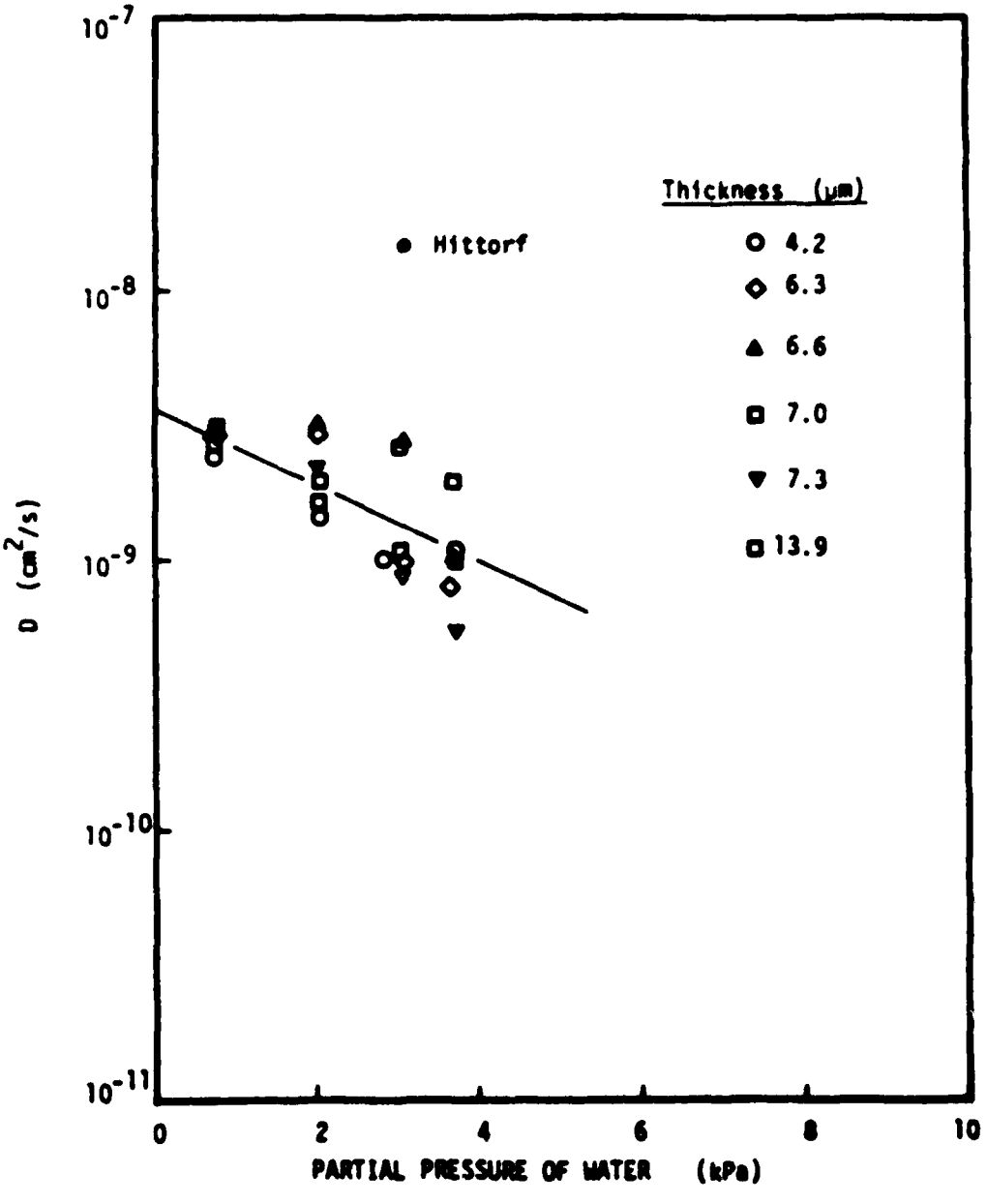

Fig. 6. Diffusivity of Water in GP-PUR at 30°C.

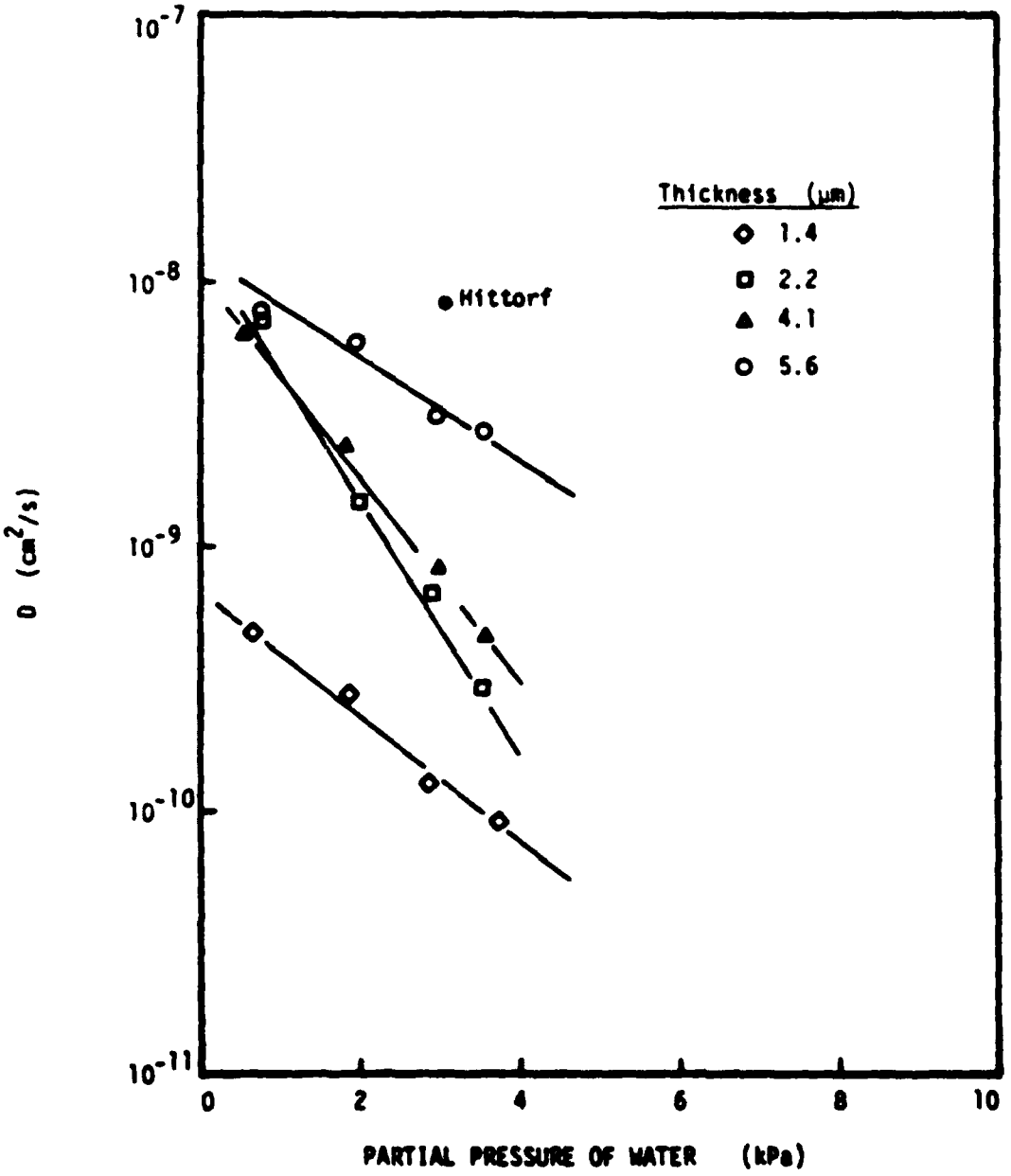

Fig. 7. Diffusivity of water in YP-Epoxy at 30°C.

smaller than other uncertainties inherent in these experiments. In general the solubility data are more reproducible than the diffusivity results. The average solubility depends on the coating thickness. This effect can be interpreted as either a variation in solubility with position in the coating, or as a result of two different phases absorbing different quantities of water (4). In addition to the effect of thickness, the solubility also depends on temperature. The diffusivity is a function of temperature, water concentration, and coating thickness.

These results explicitly show the complex nature of diffusion and sorption in paints. It is expected that other solutes will exhibit similar, equally complex behavior, but some simplification is possible if it can be assumed that the temperature and water concentration are constant. This is a reasonable assumption for isothermal exposure to an electrolyte of fixed concentration, as in a standard salt spray test. Table 6 shows typical values of the transport parameters for water in paints. It is interesting that the three different parameters each fall in relatively narrow bands. Presumably this result is a consequence of the function these paints have been formulated to perform.

The results shown in Table 6 are representative of what one might find in a salt spray test. Under these conditions water quickly penetrates the coating and is present at unit activity near the paint-metal interface in a few minutes. The time constants for diffusion of water cover the range, 20 m < L^2/D < 120 m, for a 50 μm thick coating. The maximum water flux for 50 μm thick coatings has also been calculated. The flux ranges between 1.1×10^{-9} mol/(cm^2·s) and 1.2×10^{-8} mol/(cm^2·s). Assuming two electrons per water molecule, the corresponding current densities are 2.2×10^{-4} A/cm^2 and 2.4×10^{-3} A/cm^2 respectively. The average corrosion current for aluminum in a solution with pH equal to three is about 1.5×10^{-6} A/cm^2 (7-9). Thus water diffusion is not generally a rate limiting step in the corrosion process, but it could become rate limiting in a corrosion cell where the local corrosion rate is orders of magnitude greater than the average.

Solubility of Sodium and Chloride in Paints

The solubility of chloride and sodium ions in paints was determined with radiotracers. First a known mass of paint was equilibrated with 2 mL of 0.1 N NaCl solution containing a known activity of either sodium-22 or chloride-36. The paint remained in this "hot" solution for approximately three weeks. The temperature was 25°C ± 3°C. Next the paint was removed from the "hot" solution and briefly rinsed in three separate 0.1 N NaCl solutions containing no radiotracers. The paint was then allowed to equilibrate with 2 mL of radiotracer-free 0.1 N NaCl solution. Periodically 10 µL samples were withdrawn from this solution and analyzed for radiotracer content. The solubility of the radiotracer species was calculated according to the formula

$$C_p = \frac{V_2 C_2}{M_p} \left[\frac{C_2^*}{C_1^* - C_2^*} \right] \qquad (6)$$

where C_p = concentration of radiotracer species (Na or Cl) in the paint, mol/g

V_2 = the volume of the leaching solution, cm^3

C_2 = the concentration of radiotracer species in the leach solution, mol/cm^3

M_p = mass of paint, g

C_1^* = equilibrium activity of radiotracer in the "hot" solution, $\mu Ci/cm^3$

C_2^* = equilibrium activity of radiotracer in the leach solution, $\mu Ci/cm^3$

The concentration of sodium and chloride in paints exposed to aqueous electrolytes is shown in Table 8. No data were obtained with WD2 because the free films made of this brittle material cracked and crumbled into many small pieces. Mayne and others have suggested that paints exhibit ion exchange properties (10-14). These properties result from a large excess of one type of bound charge. The ratio of the concentration of chloride to that of sodium is shown in Table 8. In no case is a large excess of one charge type found.

Table 8

Concentration of Sodium and Chloride in Paints
in Equilibrium with Aqueous Electrolytes at 25°C

Paint	Electrolyte	Concentration (N)	Chloride Concentration (mol/g-paint)	Sodium Concentration (mol/g-paint)	Na:Cl Ratio	Dimensionless Solubility Cl	Dimensionless Solubility Na
O-PUR	NaCl	0.1	1.31 E-7	2.61 E-8	5.0	1.5 E-3	3.0 E-4
H-PUR	NaCl	1.0	1.42 E-5 (± 8%)	8.10 E-6 (± 12%)	1.8	1.6 E-2	9.4 E-4
H-PUR	NaCl	0.1	2.33 E-8	1.48 E-8	1.6	2.7 E-4	1.7 E-4
H-PUR	HCl	0.01	6.87 E-7 (± 8%)			8.0 E-2	
H-PUR	NaOH	0.01		1.08 E-6 (± 20%)			1.2 E-1
FP-PUR	NaCl	1.0	5.83 E-5 (± 5%)	2.15 E-5 (± 16%)	2.7	9.0 E-2	3.3 E-2
FP-PUR	NaCl	0.1	2.96 E-6 (± 10%)	3.75 E-5 (± 6%)	0.1	4.6 E-2	5.9 E-1
FP-PUR	HCL	0.01	2.35 E-6 (± 7%)			3.6 E-1	
FP-PUR	NaOH	0.01		3.17 E-5 (± 30%)			4.9
CP-PUR	NaCl	1.0	7.10 E-5 (± 6%)	1.85 E-5 (± 10%)	3.8	1.1 E-1	2.9 E-2
CP-PUR	NaCl	0.1	9.12 E-7 (± 35%)	2.15 E-6 (± 15%)	0.4	1.4 E-2	3.3 E-2
CP-PUR	HCl	0.01	2.95 E-7 (± 6%)			4.6 E-2	
CP-PUR	NaOH	0.01		7.49 E-7 (± 25%)			1.2 E-1

Table 8 (Continued)

Concentration of Sodium and Chloride in Paints
in Equilibrium with Aqueous Electrolytes at 25°C

Paint	Electrolyte	Concentration (N)	Chloride Concentration (mol/g-paint)	Sodium Concentration (mol/g-paint)	Na:Cl Ratio	Dimensionless Solubility	
						Cl	Na
MDPT	NaCl	1.0	5.95 E-5 (± 7%)	1.10 E-4 (± 12%)	0.5	1.0 E-1	1.9 E-1
MDPT	NaCl	0.1	1.81 E-5 (± 10%)	6.13 E-5 (± 5%)	0.3	3.1 E-1	1.1
MDPT	HCl	0.01	6.58 E-6 (± 5%)			1.1	
MDPT	NaOH	0.01		2.30 E-5 (± 25%)			4.0
YP-Epoxy	NaCl	1.0	7.36 E-5 (± 7%)	2.92 E-2 (± 10%)	2.5	1.3 E-1	5.3 E-2
YP-Epoxy	NaCl	0.1	1.44 E-5 (± 5%)	1.89 E-5 (± 5%)	0.8	2.6 E-1	3.4 E-1

According to the theory of ion exchange membranes, sodium and chloride should be present inside the membrane as either coions or counterions. Donnan exclusion should govern the absorption of coions. Figure 8 shows the qualitative behavior of both types of ions in ion exchange materials The concentration inside the membrane is $\bar{C}$. The concentration in the external aqueous electrolyte is C_b, and C_m is the excess fixed charge which is bound to the membrane. Figure 8 shows that the dimensionless solubility ($\bar{C}_i/C_b$) of coions increases as the concentration of electrolyte in the aqueous solution increases. The dimensionless solubility of coions asymptotically approaches zero at low aqueous concentration and a higher value at high concentration. At any concentration (C_b) the value of the net fixed charge is equal to the difference between the counterion and coion concentrations.

The data illustrated in Table 8 do not conform to the Donnan-exclusion-ion-exchange-membrane theory. Sodium and chloride solubilities both increase with increasing NaCl concentration for N-PUR. An opposite trend is observed with YP-Epoxy and WDPT. With FP-PUR and GP-PUR in NaCl one of the solubilities increase and the other decreases, but the chloride to sodium ratio is both above and below one for both these polyurethanes. This behavior is prohibited by the Donnan theory of ion exchange membranes. We therefore conclude that none of the coatings tested behaves as a classic ion exchange membrane. Neither do these paints behave as ideal homogeneous phases. In this case we would expect to find the concentration of both sodium and chloride in the paint phase governed by mass action; i.e., the dimensionless solubilities of both sodium and chloride would be constant and equal. We therefore conclude that some strong specific interaction occurs in the paint phase. The specific interaction could be between any two of the four major components of the paint phase: sodium, chloride, water, or polymer. The electrostatic interaction between an ion exchange membrane and mobile ions is one type of specific interaction, but the data indicate that this phenomenon is not a primary consideration in these paints.

One possible type of specific interaction which has been considered in this study is ion association. This association results when the dielectric constant of the solvent (paint) becomes so low that the attraction between

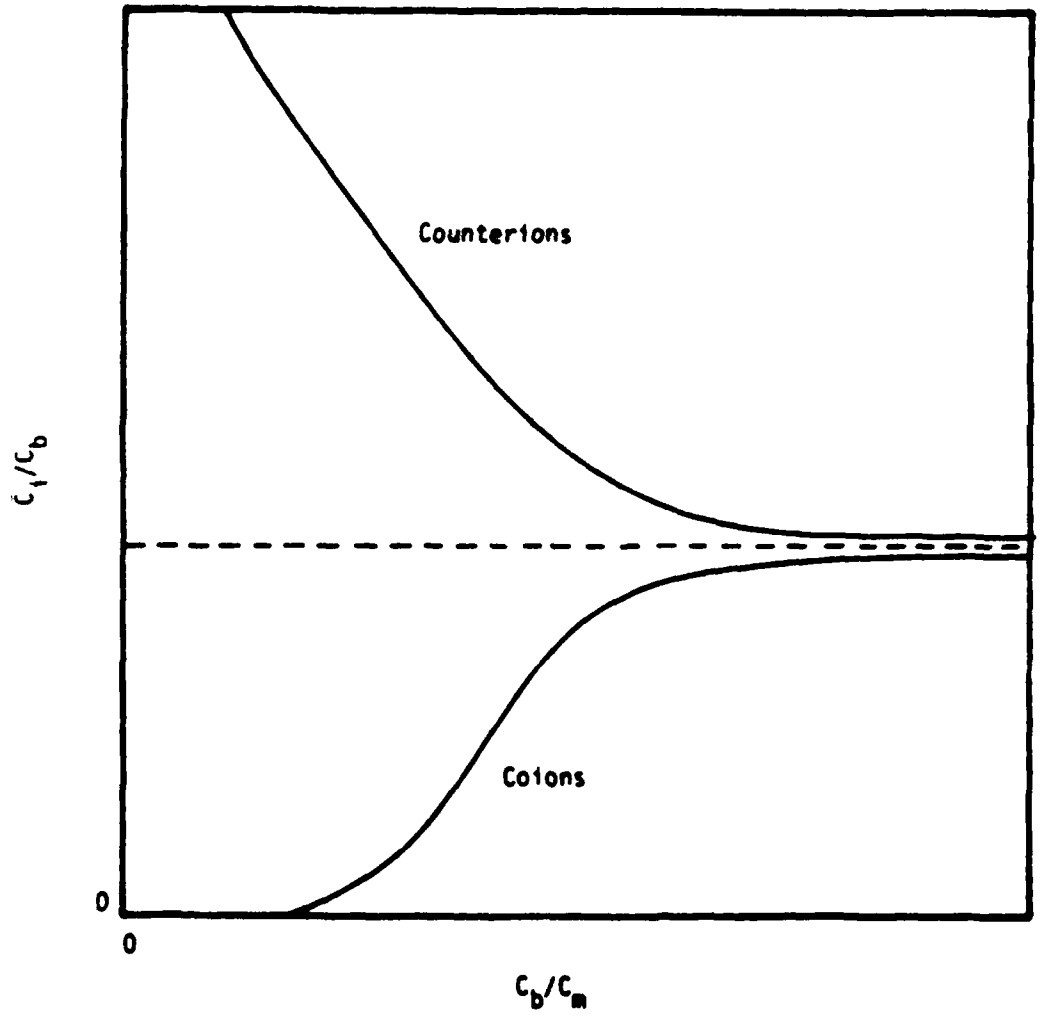

Fig. 8. Theoretical concentrations of coions and counterions in an ideal ion-exchange membrane.

ions can overcome the effects of entropy and solvation. The ion association theory of Fuoss (15) was tested to see if it could explain the experimental results. The theoretical results were in qualitative but not quantitative agreement with the experiments. The theory did suggest strongly that ion association occurs in paints. One limitation of the Fuoss theory is that it assumes the solvent (paint) is homogeneous, has uniform dielectric constant, and lacks any other specific interaction with all solute species. These assumptions are reasonable for many fluid solvents but are undoubtably invalid for some solids like polymers. It is therefore concluded that: ion association probably occurs in paints, and that there is some specific interaction between the polymer and the "ionic" solute species, but the exact nature of the specific interaction is not yet known.

Density of Paint Films

The densities of a number of paint films were determined by weighing specimens in air and under water. The results are listed in Table 9. It is clear that the pigments contribute a significant fraction of the weight to some of these films.

Average Water Permeability in Thick Paint Films

Experiments were continued to determine the average permeability of water in coatings. The diffusion-cup method (ASTM E-96 procedure BW) was used. The water flux through films of paint was determined by recording the rate of weight loss of the diffusion cups. The average permeability coefficient P was then determined from the equation

$$P = \frac{LJ}{C} \qquad (7)$$

where P = average permeability coefficient, cm^2/s

L = paint film thickness, cm

J = water flux, $mol/cm^2 \cdot s$

C = water concentration inside the cup, mol/cm^3

The permeability coefficient, P, depends on the diffusivity and the dimensionless solubility (16)

$$P = DS \qquad (8)$$

The solubility is defined

TABLE 9

Paint Densities

Paint	Density (g/cm^3)	Number of Specimens	Standard Deviation (%)
YP-Epoxy	1.808	4	0.78
GP-PUR	1.553	3	0.10
FP-PUR	1.538	4	0.27
ADPT	1.733	3	0.35
AD2	1.161	3	0.69
O PUR	1.137	3	0.9
O PUR	1.154	8	1.6
N PUR	1.156	4	2.9

$$S = \frac{C_m}{C} \tag{9}$$

where S = solubility

C_m = water concentration in the paint membrane, mol/cm^3

C = water concentration in the aqueous solution in the cup, mol/cm^3

The solubility is a thermodynamic parameter which can also be written as

$$S = \frac{\gamma}{\gamma_m} \tag{10}$$

where γ_m = the activity coefficient of water in the paint membrane

γ = the activity coefficient of water in the solution.

The permeability coefficients calculated according to Eq. 7 are shown in Table 10. The values of P shown in Table 10 compare reasonably well with those obtained with the crystal oscillator apparatus at 30°C (Table 6). Also shown in Table 10 are the activation energies, the corresponding linear correlation coefficients, and the number of experimental data points correlated. The permeability coefficients are functions of temperature, which affects both the diffusivity and solubility. The tabulated values of P have been extrapolated to 25°C according to the Arrhenius equation. Another permeability coefficient, P_c, is also shown in Table 10.

$$P_c = \frac{P}{\gamma} = \frac{D}{\gamma_m} \tag{11}$$

where the standard state for water has been taken as a pure liquid at 25°C. It was noted in these experiments that P_c is relatively independent of temperature.

The data illustrated in Table 10 provide order of magnitude estimates of the permeability coefficients. YP-Epoxy exhibits negative activation energies, possibly indicating that the solubility of water in the coatings decreases with temperature. A continuing polymerization reaction or some other chemical or physical change within the paint could also produce negative activation energies.

Adhesion Experiments

Experiments were conducted to determine the adhesion of three of the coatings to 7075-T6 aluminum which was either anodized or conversion coated.

Table 10

Permeability Coefficients and Activation Energies
for Permeation of Water Through Thick Paint Films

Paint	No. of Points	P at 25°C (cm^2/s)	E_a (kJ/mol)	Correlation Coefficient	P_c at 25°C (cm^2/s)	E_a (kJ/mol)	Correlation Coefficient
YP-Epoxy	5	4.04×10^{-10}	-27.0	0.701	7.42×10^{-10}	-70.3	0.932
YP-Epoxy	5	3.00×10^{-10}	-15.2	0.530	4.46×10^{-10}	-59.0	0.923
MDPT	4	5.18×10^{-10}	62.0	-0.995	4.43×10^{-10}	18.4	-0.950
MDPT	4	3.52×10^{-10}	55.4	-0.991	4.43×10^{-10}	13.4	-0.60
MDPT	3	6.67×10^{-10}	31.8	-0.852	2.81×10^{-10}	31.8	-0.85
FP-PUR	5	5.11×10^{-10}	111.	-0.940	3.9×10^{-10}	66.9	-0.857
FP-PUR	5	5.12×10^{-10}	65.8	-0.916	4.6×10^{-10}	22.2	-0.612
FP-PUR/ YP-Epoxy	5	2.50×10^{-10}	42.0	-0.889	2.3×10^{-10}	- 1.3	0.07
FP-PUR/ YP-Epoxy	4	3.02×10^{-10}	59.0	-0.973	9.8×10^{-10}	-34.3	0.423
FP-PUR YP-Epoxy	3	2.76×10^{-10}	58.7	-0.947	2.74×10^{-10}	15.3	-0.616

The tests were conducted at room temperature, 20°C, and utilized a cutting machine similar to the "Hesiometer" described by Asbeck (17-19). The results of the experiments have been analyzed according to Merchant's (20, 21) theories of cutting, and surface energies of adhesion have been obtained for two of the three coatings tested. The results were of questionable reliability because the data obtained in the experiments does not conform to the Merchant cutting theory. It was concluded that this method of determining the adhesion was unsatisfactory for paints on anodized or conversion-coated aluminum, and these studies were discontinued.

MATHEMATICAL MODELS

Introduction

Now that the transport properties of paints are known it is desired to reliably assess the relative importance of these properties in the corrosion process. As we have already pointed out the relative importance of the various parameters will change depending on such factors as age of the paint, temperature, geometry, oxygen availability, etc. Therefore, some model of the corrosion process is required to quantify how each parameter affects the corrosion rate. When this information is available, the relative importance of each parameter can be determined and each coating system can be rated on a relative scale for any prescribed set of physical conditions. The mathematical model described below is based on the results of experiments performed to date and forms the framework of this appraoch.

The average permeability coefficients of ionic species in GP-PUR, FP-PUR and YP-Epoxy are shown in Table 11. These data indicate that the dc conductivity of all three paints increases with the concentration of sodium chloride in the bathing electrolyte. These materials would therefore be classified as "direct" according to Mayne's criterion (10-14). Also according to Mayne the paint film resistance should be greater than $10^8\ \Omega cm^2$ for good corrosion protection. According to this theory the thickness of a coating must exceed a critical value to provide good protection of the metal. The critical thickness is also shown in Table 11. It is clear that it is impractical to use either FP-PUR or YP-Epoxy according to this criterion. Table 11 also shows that the primer coat, YP-Epoxy, is orders of magnitude

Table 11

Ionic Transport Parameters and
Critical Thickness of Paints at 25°C

Paint	NaCl Concentration (N)	Conductivity (S/cm)	Permeability Coefficient Cl^- (cm^2/s)	Permeability Coefficient Na^+ (cm^2/s)	Critical Thickness (cm)
GP-PUR	0.1	$6. \times 10^{-12}$	3×10^{-15}	1×10^{-14}	$6. \times 10^{-4}$
FP-PUR	0.1	1.9×10^{-9}	7×10^{-13}	2×10^{-12}	0.2
YP-Epoxy	0.1	2.8×10^{-7}	3×10^{-10}	1×10^{-10}	28.
GP-PUR	1.0	$9. \times 10^{-11}$			$9. \times 10^{-3}$
FP-PUR	1.0	1.2×10^{-8}	6×10^{-13}	8×10^{-13}	1.2
YP-Epoxy	1.0	2.1×10^{-6}	4×10^{-10}	6×10^{-11}	210.

more conductive than either of the topcoat paints. Thus the resistance of any practical two-layer system of primer and topcoat exhibits practically the same resistance as the topcoat would alone.

In YP-Epoxy the inhibitor is $SrCrO_4$ (1). It appears reasonable to assume that strontium and chromate ions have permeability coefficients in the topcoat paints no greater than sodium and chloride. In this case the inhibitor is essentially trapped in the primer layer between the metal and the topcoat.

It is instructive to determine the approximate time required for sodium chloride to penetrate from an external solution to the metal. Assume that all the resistance is in the topcoat which is approximately 51 μm thick. For GP-PUR the permeability coefficient is about 10^{-14} cm^2/s and the dimensionless solubility of NaCl is about 10^{-2}. The diffusivity is

$$D = \frac{P}{S} = 10^{-12} \text{ cm}^2/\text{s} \quad (12)$$

The time constant for sodium chloride diffusion is

$$t = \frac{L^2}{D} = 2.6 \times 10^7 \text{ s} \quad (13)$$

A similar calculation for YP-PUR yields

$$D = 10^{-11} \text{ cm}^2/\text{s} \quad (14)$$

$$t = 2.6 \times 10^6 \text{ s} \quad (15)$$

Thus sodium chloride will have completely penetrated the coating in a few weeks to months. In either case the time is short compared to the desired service life of the coating system. It is clear from these calculations that paints do not protect solely by preventing aggressive ions from reaching the metal.

Another calculation can be performed to determine if paints protect metals by limiting the rate of oxygen diffusion. Correlations were used to estimate the diffusivity and solubility of oxygen in polyurethane (22).

$$D(O_2) = 6 \times 10^{-8} \text{ cm}^2/\text{s} \quad (16)$$

$$C(O_2) = 3.2 \times 10^{-6} \text{ mol/cm}^3 \quad (17)$$

The limiting oxygen flux through a 51 μm thick film is then

$$J(O_2) = 3.8 \times 10^{-11} \text{ mol/(cm}^2 \cdot \text{s)} \quad (18)$$

The corrosion current for aluminum varies greatly and depends on many variables,

but it is usually in the range 10^{-9} A/cm^2 < i < 10^{-6} A/cm^2 (7-9). The maximum corrosion current of 10^{-6} A/cm^2 corresponds to an oxygen flux of

$$J'(O_2) = 5.2 \times 10^{-12} \text{ mol}/(\text{cm}^2 \cdot \text{s}) \quad (19)$$

Thus $$J'(O_2)/J(O_2) = 0.14 \quad (20)$$

This calculation demonstrates that paints do not retard the corrosion of aluminum primarily by limiting oxygen diffusion.

Similar calculations to determine if water could constitute a limiting reactant showed that the corrosion rate is not limited by the diffusion of water. Since, for uniform corrosion without physical separation of anodic and cathodic reaction sites, ion transport is not required, these calculations indicate that the transport properties of paints do not directly affect the uniform corrosion rate of aluminum. This result leads to the conclusion that corrosion kinetics, oxide breakdown, and passivation are the primary phenomena which control the corrosion of painted aluminum.

The preceding statements apply when no current is forced to flow through the coatings, i.e., when uniform corrosion occurs. Many, perhaps most, practical corrosion problems involve localized corrosion cells and involve physical separation of the anodic and cathodic reaction sites. Ionic current must flow between the anodic and cathodic sites. This raises the question of how these local corrosion cells are formed and maintained. Differential aeration is probably the best known mechanism of formation of local corrosion cells. Differential aeration can occur under paint coatings, but it is not a primary mechanism under uniform, intact coatings because oxygen is not excluded and is not a limiting reactant. Another mechanism appears responsible for the formation of local corrosion cells on painted aluminum. This mechanism is based on the fact that aluminum corrosion is auto catalytic (23). The coating reduces the flux of cations diffusing away from local anodic sites, and a buildup of cations results, increasing the anodic reaction rate. Thus the presence of the coating actually adds to the instability of the metal and enhances the possibility that a corrosion cell will develop. It is therefore reasonable to assume that separation of anodic and cathodic sites is the rule rather than the exception on painted aluminum.

Models

The models developed in this section are based on the principles discussed previously and the results of the experiments. The physical system which will be discussed is an 18 μm thick coat of YP-Epoxy covered by a 51 μm thick topcoat assumed to be GP-PUR. Some of the transport properties of these paints were listed in Table 11. Additional properties are presented in Table 12.

The Role of Inhibitors

Because the oxide film on aluminum controls the corrosion reaction rates we must be concerned with the phenomenon of passivation. Furthermore, the primer is filled with a chromate inhibitor which also has a direct affect on the passivity of aluminum. The subject of passivation is complex, and only certain essential characteristics of this phenomenon will be dealt with here.

It is known that the pitting of aluminum is a function of the concentration of both the aggressive and inhibitor anions. Bohni and Uhlig (24) have determined that, for a given concentration of inhibitor, a critical concentration of chloride ion can be specified. Pitting takes place when the chloride concentration exceeds the critical value, and log-log plots of critical chloride ion activity versus chromate ion activity are straight lines. These authors also showed that the pitting potential of aluminum varies inversely with the logarithm of the chloride ion activity. Later Kaesche (25) generalized these results and showed how the pitting potential depends on both chloride and chromate ion activities. These results have been used here to describe the role of paint inhibitors in reducing corrosion. It is assumed that the inhibitors act only through their effect on the pitting potential. Figure 9 shows approximately how the pitting potential of aluminum depends on both chloride and chromate ion activities.

Anodic Reaction

Aluminum is assumed to be passivated. A typical anodic polarization curve for aluminum in chloride solution is shown in Fig. 10 (26). The

Table 12

Physical Properties of Paints Used
To Form the Two-Layer Model System

Property	GP-PUR	FP-PUR	YP-Epoxy
Specific Gravity	1.553	1.538	1.808
Pigment			$SrCrO_4$
Wt % Pigment			52
Vol % Pigment			24
H_2O Permeability* (cm^2/s)(0.1 N NaCl)	5.4×10^{-10}	1.8×10^{-9}	2.5×10^{-10}
(1.0 N NaCl)	5.6×10^{-10}	1.4×10^{-9}	1.3×10^{-10}
H_2O Solubility** (g/g-paint)	0.025	0.025	0.012

* Determined by radiotracer method at 25°C.

** Determined with crystal oscillator at 30°C.

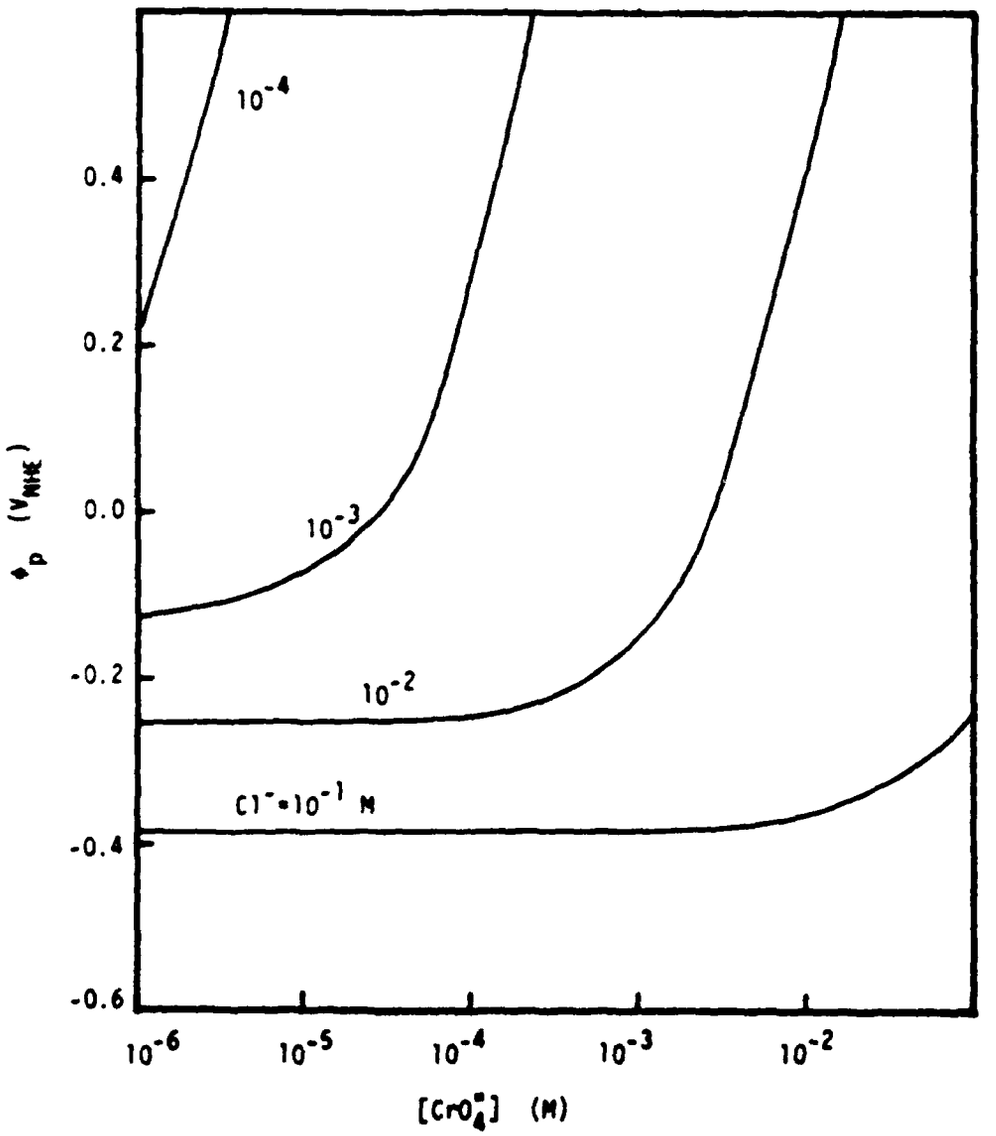

Fig. 9. Pitting potential of aluminum as a function of inhibiter ($CrO_4^=$) and chloride ion concentrations.

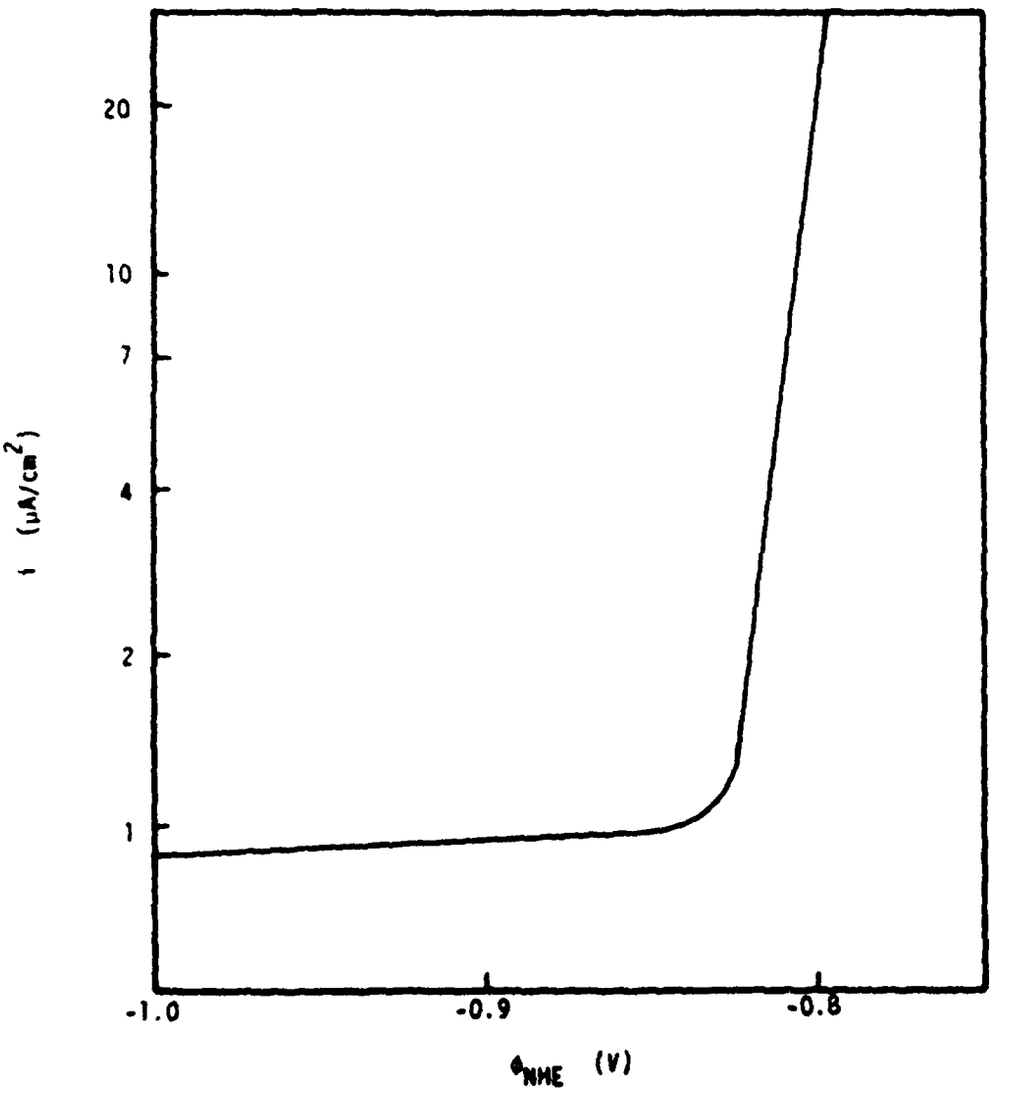

Fig. 10. Anodic polarization of 5083 aluminum in deaerated 3.5 wt % NaCl.

primary characteristics of this curve are the very low current density for potentials below the pitting potential and the steep rise in current density for potentials above the pitting potential.

A mathematical expression for this type of electrochemical reaction is

$$i_a = i_{oa}; \qquad \phi \leq \phi_p \tag{21}$$

$$= i_{oa} + A(\phi - \phi_p); \qquad \phi > \phi_p \tag{22}$$

This approximates the anodic reaction as function of potential only. In the region below the pitting potential (ϕ_p), i_a is a constant, and above ϕ_p it is linear in ϕ.

Cathodic Reaction

There are at least two possible cathodic reactions: the reduction of dissolved oxygen gas, and the reduction of hydrogen ions. It is generally accepted, however, that oxygen reduction is the faster reaction in areas where the electrolyte is saturated with oxygen. Since diffusion of oxygen through paint films is fast compared to general corrosion of aluminum, it is assumed that the reduction of oxygen is the primary cathodic reaction of interest. A typical cathodic polarization curve carried out in aerated electrolyte is shown in Fig. 11 (27).

The cathodic reaction is approximated by a Tafel type expression.

$$i_c = i_{oc} A_{O_2} \exp\left(-\frac{\alpha F}{RT}(\phi - \phi^o)\right) \tag{23}$$

where A_{O_2} = the activity of oxygen at the electrode surface, and the other terms have the usual significance.

If it is assumed that the coating does not interfere with the electrode kinetics then the constants in Eqs. 21 through 23 can be evaluated from experiments conducted in aqueous solution. In this way values of i_{oa}, A, ϕ_p, i_{oc}, α, and ϕ^o can be obtained. From the previous discussion it is expected that the pitting potential (ϕ_p) will be a function of the relative concentrations of chloride and chromate ions. This relationship may be in graphical form or expressed generally as

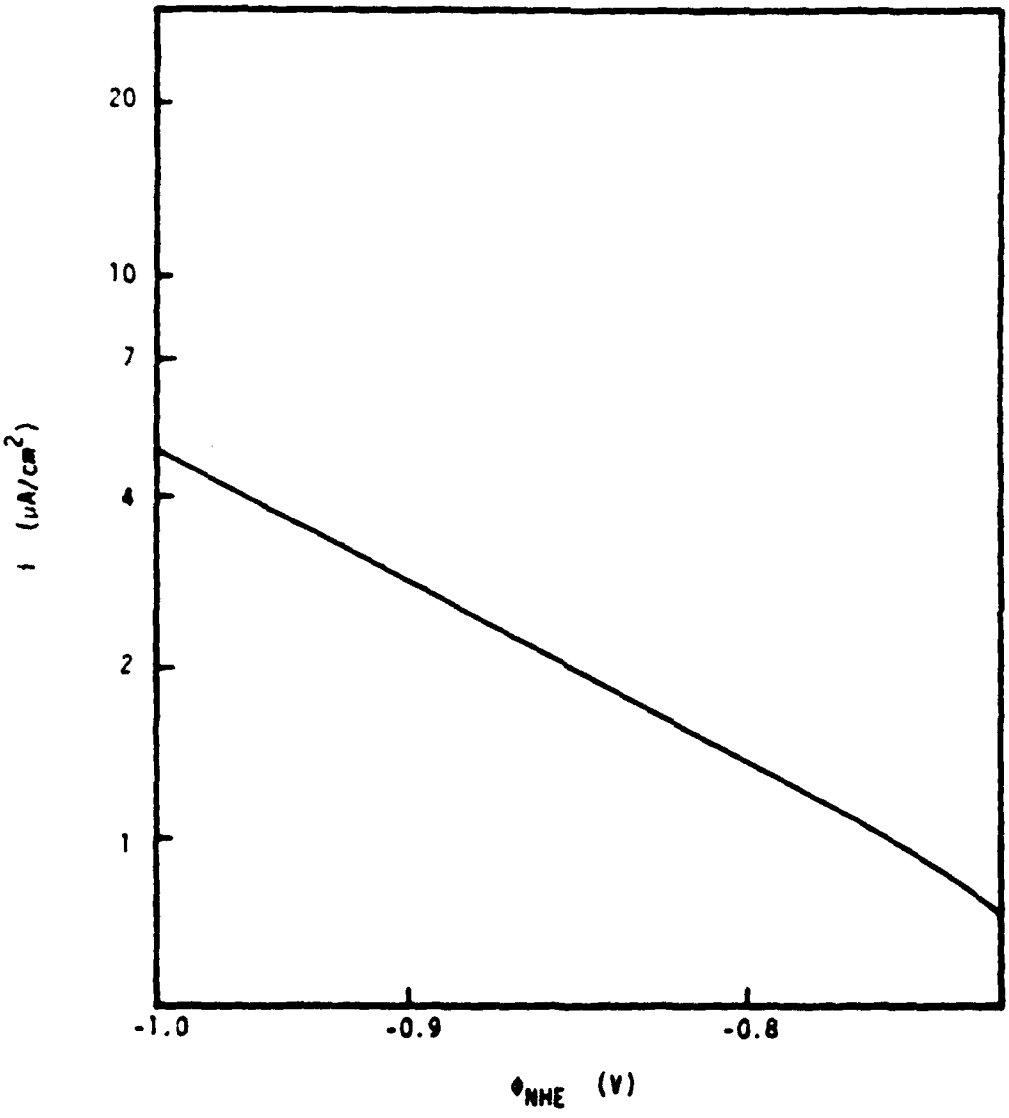

Fig. 11. Cathodic polarization of 5052 aluminum in air saturated sea water.

$$\phi_p = \phi_p\ (C_{Cl^-},\ C_i) \tag{24}$$

Some data are available on how the pitting potential varies with concentration of chromate and chloride ions.

Mass Transport

The general equation for mass transport of any mobile species, i, is

$$\frac{\partial C_i}{\partial t} = \vec{\nabla} \cdot \vec{j}_i + R_i \tag{25}$$

where C_i = concentration of species i
$\vec{\nabla}$ = del operator
$\vec{j}_i$ = flux of species i
R_i = rate of generation of species i

Experiments performed here and elsewhere (28) indicate that the dilute solution flux equation is adequate for paints.

$$J_i = - z_i D_i C_i \frac{F}{RT} \vec{\nabla}\phi - D_i \vec{\nabla} C_i \tag{26}$$

In general the diffusivity D_i is a function of both position, species concentration, and temperature

$$D_i = D_i\ (x,\ C_1,\ C_2 \ldots C_n,\ T) \tag{27}$$

Most mobile species of interest here are ions which have limited solubility in paints, and it is therefore often possible to neglect their effect on the diffusivity. Humidity-chamber results have shown that the diffusivity of water appears to be a strong function of coating thickness for coatings thinner than about 10 μm, but the diffusivity is relatively independent of coating thickness for thicker films. Most practical coatings are thicker than 10 μm, and, as a first approximation, we will neglect the effect of thickness on diffusivity. This evidence suggests, therefore, that the diffusivity is primarily a function of temperature and the water content of the paint

$$D_i = D_i\ (C_w,\ T) \tag{28}$$

It will also be assumed that the electroneutrality condition holds for paints

$$\sum_i C_i z_i = 0 \tag{29}$$

Equations 25, 26, and 29 are sufficient to solve for the concentrations (C_i) and potential (ϕ) as functions of time and position in isothermal systems. Isothermal systems will be assumed unless stated otherwise.

Boundary Conditions

Several types of boundary conditions may be used. One type of boundary condition specifies the equality of electrochemical potential between phases

$$\mu_i^{\alpha} = \mu_i^{\beta} \tag{30}$$

The generality of this equation is well accepted, but in practical application it is usually expressed as some type of distribution coefficient for the two phases (α and β)

$$\frac{C_i^{\alpha}}{C_i^{\beta}} = K_i \tag{31}$$

The potential is defined as that which would be measured with a reversible chloride ion electrode. This definition means that the potential is a function of the electrochemical potential of chloride ions. Therefore the potential is constant across phase boundaries in accordance with Eq. 30.

Initial conditions are often difficult to establish. However, usually we are primarily interested in what is taking place at relatively long times. Under these conditions the exact nature of the initial condition is often insignificant. In the paint systems studied here it is usually sufficient to specify uniform concentrations and potential at time zero. This type of initial condition usually leads to a step change in the concentration of a mobile species or potential at one of the boundaries at time zero. This procedure is a mathematical idealism, but it is sufficiently accurate for our purposes.

Stoichiometry also places mathematical restrictions on the corrosion model. In one dimension these restrictions take the form:

$$\sum_n \int_0^L i_a dx = \sum_n \int_0^L i_c dx \tag{32}$$

Equation 32 is simply the mathematical expression of the fact that the total anodic current must equal the total cathodic current.

In general there will be n mobile species. There will be n equations 25, n equations 26, and one equation 29 which must be solved for the n concentrations (C_i) and n fluxes (N_i) and one potential ϕ. The equations are subject to 2n boundary conditions similar to Eq. 30. There are n + 1 initial conditions. The two remaining boundary conditions involve potential and are usually an arbitrary definition of the zero of potential and Eq. 32.

Simplification

In general the procedure outlined above can be used to solve the required equations. The particular form of the solution depends on the values of the parameters involved (D_i, A, a, etc.) and on the geometry, but there are several approximations which will simplify the computations. We have assumed a two coat system of primer and topcoat. The experiments have shown the topcoats to be significantly less permeable to ions than the primer. As a first approximation it can be assumed that the topcoat is impermeable to ions. This assumption is certainly valid in the vicinity of a crack or other defect in the topcoat, and it will be assumed valid for all cases except the initial penetration of aggressive ions through an unblemished topcoat. A second simplification is that both topcoat and primer have uniform thickness and transport properties. This assumption is justified in most cases where the coating contacts liquid water and the temperature is constant. Salt spray tests conform to these requirements.

Corrosion Geometry Models

Flat Surface

The corrosion rate under an adherent two-layer coating on a flat plate is rarely high. In such a system the inhibitor is trapped beneath the topcoat and leaches out very slowly. The topcoat retards the penetration of aggressive ions (chloride), but if the external concentration is high, chloride will eventually penetrate to the metal surface thereby reducing the pitting potential. As the potential decreases the cathodic reduction of oxygen increases; however, the cathodic area is limited by the high resistivity of

the primer coating. The ionic current produced by both the anodic and cathodic reactions must flow through the primer which is attached to the surface of the metal (or metal oxide). The effective cathodic area is small because of the potential drop produced in the primer when ionic current flows.

Paint Edge

The paint edge is a geometry in which the two-coat paint ends, and bare metal is exposed to the bulk electrolyte. Under these conditions salt penetrates primarily through the primer layer and inhibitor diffuses out of the primer into the bulk electrolyte. Therefore, the ratio of the concentration of aggressive ion to the concentration of inhibitor varies with position relative to the edge of the paint. The anodic reaction rate is greatest where the inhibitor concentration is lowest, near the edge of the coating. Depending on how well the bulk electrolyte is stirred the inhibitor may provide some protection to the bare metal at a distance from the edge of the paint. At some point either on the bare metal or under the primer near the edge, the anodic reaction will occur. The cathodic reaction will occur primarily on the uncoated metal because the conductivity of the aqueous electrolyte is many orders of magnitude greater than the conductivity of the primer. According to this view we expect the corrosion rate and the position of the primary anodic site to change with time and to be controlled by the diffusion of salt and inhibitor in the primer.

Crack

Two adjacent edges form a crack. The general characteristics of a crack are the same as the edge except that the area of bare metal is much smaller. It is expected that the area at the base of the crack will become a local anode supported by a cathodic area under the coating adjacent to the crack.

Wedge

The wedge is a geometry in which the primer has become separated from the metal near an edge. The wedge has many of the properties of the typical

wedge-shaped corrosion cell except that oxygen and water can reach the metal by diffusion through the coating. In the vicinity of the edge the primary diffusion pathway is not through the coating, but farther away, toward the tip of the wedge, diffusion through the coating becomes most important. Ions are essentially excluded from diffusing in the coating. The position of the anodic reaction will be determined by two factors: the local ratio of inhibitor to chloride ions, and the reduced oxygen concentration resulting from the diffusion resistance of the coating. The primary cathodic area will be the bare metal beyond the edge of the coating.

Blister

A blister is assumed to be filled with an aqueous solution. The solution is trapped between the primer and the metal. The coating is assumed to be defect free and the coating is adherent to the metal everywhere except under the blister. There are many types of blisters in real paint systems. Some of these blisters are formed by entrapped solvent or lack of adhesion. We will consider only blisters which contain active corrosion cells. Apparently the corrosion blisters are not easily formed in dilute salt solutions because the inhibitor prevents local corrosion cells from forming. In concentrated salt solution the chloride ions swamp the inhibitor and blisters can form. The entire blister is a site for cathodic reaction. The area on the metal, near the center of the blister is farthest from a source of oxygen and this is the primary anodic site.

Examples

The purpose of the mathematical model is to provide a method of quantitatively evaluating paint performance. When the proper parameters are used in the model the anodic and cathodic reaction rates can be calculated as a function of position and time. The model is sufficiently general that the different geometries discussed above can be analyzed within the same framework.

Inhibitor Depletion Through the Topcoat

As an elementary example of how the experimental results can be used in a specific model, consider the time required for the inhibitor in a primer

to become depleted by diffusing through a 50 μm thick topcoat of GP-PUR. Assume the primer coat is 20 μm of YP-Epoxy containing 52 wt % $SrCrO_4$ as inhibitor. Assume the aqueous solution in the primer layer is saturated with $SrCrO_4$. Then the concentration in water is about 4×10^{-3} M. The total number of moles of $SrCrO_4$ available is 9.4×10^{-6} mol/cm^2 of painted area. It is assumed that the permeability coefficient of $SrCrO_4$ in the GP-PUR topcoat is $1. \times 10^{-14}$ cm^2/s, the same as that for NaCl. The flux of $SrCrO_4$ is then calculated to be

$$J_i = 7.7 \times 10^{-18} \text{ mol/cm}^2 \cdot \text{s} \tag{33}$$

The time to deplete the inhibitor is

$$t = \frac{9.4 \times 10^{-6}}{7.7 \times 10^{-18}} \text{ s} \tag{34}$$

$$= 4. \times 10^4 \text{ y} \tag{35}$$

This calculation shows that the corrosion inhibitor is held in the primer layer near the metal surface for a very long time when the topcoat is in good condition. Furthermore it is of little consequence which of the four topcoats is used. This result also indicates that practical paint systems prevent corrosion primarily through the use of inhibitors by changing the reaction kinetics of corrosion.

Permeation of NaCl to the Metal Surface

Now consider how long the example paint system provides protection against corrosion when immersed in a 0.1 N NaCl solution. Assume the permeability coefficient of GP-PUR is about 10^{-14} cm^2/s, and the salt concentration in the primer phase must remain less than about $4. \times 10^{-3}$ M. The volume fraction of inhibitor in YP-Epoxy is about 24%. Therefore, if all this volume is occupied by 4×10^{-3} M NaCl solution, there will be 1.9×10^{-10} moles of NaCl present in the primer phase. Thus

$$t = \frac{1.9 \times 10^{-10}}{N_{NaCl}} \text{ s} \tag{36}$$

$$J_{NaCl} = \frac{(10^{-14})(0.10)}{50 \times 10^{-4}} \frac{\text{mol}}{\text{cm}^2 \cdot \text{s}} \tag{37}$$

$$t = 950 \text{ s} \tag{38}$$

This calculation indicates first that even though the topcoat is effective in preventing the inhibitor from diffusing away from the metal it is not particularly good at preventing aggressive ions from reaching the metal. As a matter of fact the diffusional time-constant ℓ^2/s for the passage of ions through the 50 μm thick topcoat is only about 0.8 yrs. Thus it is clear that aggressive ions will be present on the metal after a relatively brief service life, and this is a factor which does depend on the transport properties and thickness of the topcoat.

Depletion of Inhibitor Near a Crack

Another example of this specific type of calculation is the diffusion and subsequent depletion of inhibiter through a crack in the coating. Consider the geometry illustrated in Fig. 12. The time required to reduce the inhibiter concentration at the bottom of the crack (point A) can be estimated as follows. The one dimensional rate of inhibiter transport out of the crack is

$$r_c = J_c W = \frac{D_w C W}{\ell_2} \tag{39}$$

The transport of inhibiter from inside the primer to point A is

$$r_p = J_p \ell_1 = \frac{P(C_{sat} - C)\ell_1}{x} \tag{40}$$

where x is the diffusion path length in the primer phase. The length x is related to the total quantity of inhibiter lost since formation of the crack, or in differential form

$$r_c = q \frac{dx}{dt} \tag{41}$$

where q = the available quantity of inhibiter in the primer (mol/cm^2). These three equations can be solved by equating r_c and r_p at all time, i.e., making the quasi-steady-state assumption. In dimensionless form the result is:

$$\frac{1}{2}\left(\frac{x}{\ell_1}\right)^2 + \frac{P}{D_w}\frac{\ell_2}{W}\left(\frac{x}{\ell_1}\right) = \frac{PC_{sat}}{\ell_1 q} t \tag{42}$$

where C_{sat} = the saturation concentration and the other variables have the usual meanings. In order to relate the time to the concentration at point A the following additional relation is required.

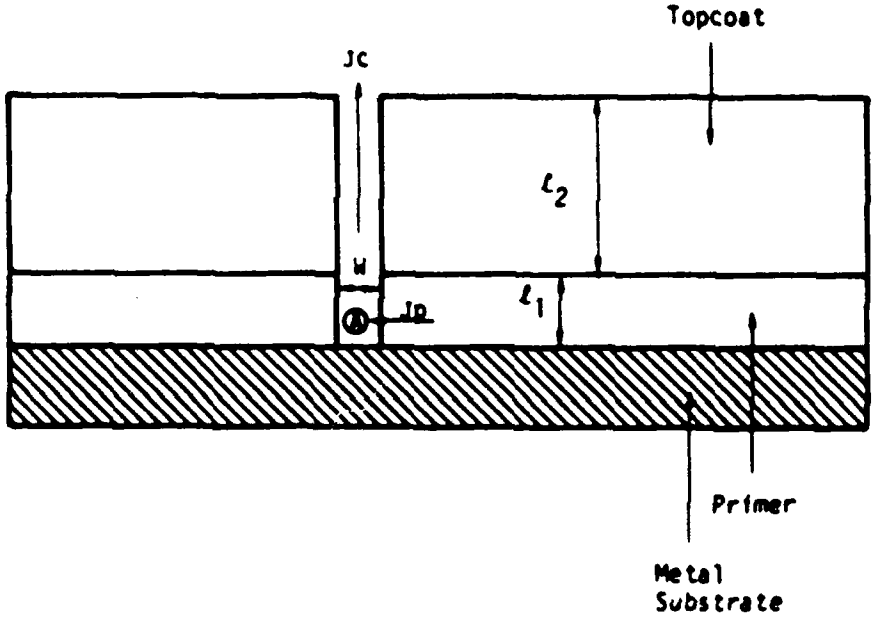

Fig. 12. Two-layer paint system with a one-dimentional crack defect.

$$\frac{x}{\ell_1} = \left(\frac{C_{sat}}{C} - 1\right) \frac{P}{D_w} \frac{\ell_2}{W} \tag{43}$$

The following values have been used to calculate results.

$\ell_1 = 20 \times 10^{-4}$ cm
$\ell_2 = 50 \times 10^{-4}$ cm
$P = 10^{-10}$ cm^2/s
$D = 10^{-5}$ cm^2/s
$C_{sat} = 4 \times 10^{-3}$ M
$q = 9.4 \times 10^{-6}$ mol/cm^2
$C_{sat}/C = 10$

First, assume $\ell_2/W = 100$. Then $x/\ell_1 = 9 \times 10^{-3}$ and t = 0.65 h. If $\ell_2/W = 5000$, $x/\ell_1 = 0.45$ and t = 1610 h or 67 d. These results demonstrate that the inhibiter is quickly depleted at the bottom of even a very thin crack. Also, the concentration of aggressive ion is expected to be high there.

Reduction of the Effective Cathodic Area by Paints

Another example illustrates one way that paints protect metals from corrosion. Consider the corrosion of a specimen of painted aluminum in which the primary anodic and cathodic sites have already become separated. Assume that the paint layers are intact and attached to the metal. As a simplification assume that the anode is unpolarizable and at the pitting potential. Consider also the limiting case where concentration gradients can be neglected and oxygen is not a limiting reactant. Equation 23 then has the form

$$i_c = Ae^{-B\phi} \tag{44}$$

where A and B are positive constants. The potential decreases as the distance from the anodic site increases. The relationship between the total current and potential is

$$i = \kappa \nabla \phi \tag{45}$$

The current varies with position according to the equation

$$t\frac{di}{dx} = -i_c \tag{46}$$

Combining Eqs. 43-46 yields

$$\nabla^2\phi = \frac{-A}{t\kappa} e^{-\beta\phi} \tag{47}$$

Equation 47 has no analytical solution, but a linearized approximation of the right hand side will be adequate for the present. For potentials near an arbitrary reference potential ϕ_r the linearized form of Eq. 47 is

$$\nabla^2\eta = \frac{-A}{t\kappa} (1 - \beta\eta) e^{-\beta\phi_r} \tag{48}$$

where $\phi = \phi_r + \eta$

The boundary conditions are most easily expressed as

$$\eta = \eta_o, \quad x = 0 \tag{49}$$

$$i \to 0, \quad x \to \infty \tag{50}$$

With these boundary conditions the solution is

$$\eta = [\sinh(cx) - \cosh(cx)] (1/\beta - \eta_o) + 1/\beta \tag{51}$$

where $c = \sqrt{\frac{A\beta e^{-\beta\phi_r}}{t\kappa}}$

Equation 51 shows that the potential is bounded. The other interesting point is that there is no contribution to the total cathodic current for $x > 1/c$. The maximum current occurs at $x = 0$. The current at $x = 0$ is

$$I_{total} \propto i \Big|_{x=0} = \sqrt{AB\kappa t e^{-\beta\phi_r}} (1/\beta - \eta_o) \tag{52}$$

Equation 52 shows that the total cathodic current is proportional to the square root of the thickness (t) and the conductivity (κ) of the primer coat. Other parameters occurring in Eq. 52 are generally not under experimental control. Equation 52 shows that the total corrosion current flowing to the anodic site can be minimized by reducing the thickness and conductivity of the primer. Ultimately the thickness could be reduced to zero, but not without affecting other properties, like adhesion and void volume, which have been assumed to remain constant in the derivation of Eq. 52. In the final analysis we will recognize that compromises must be made, but as a general rule it is expected that the corrosion can be reduced by reducing either t or κ.

Equation 52 provides one explanation of why blisters are a serious corrosion problem. When the primer ceases to adhere to the metal, the resulting void becomes filled with aqueous electrolyte. Usually the conductivity of the electrolyte is several orders of magnitude greater than that of the primer. It is therefore expected that a high corrosion current will flow between the local anodic and cathodic areas within the blister. Another way to look at this explanation is that the size of the cathodic area is proportional to $1/\epsilon$. Thus the cathodic area is proportional to $\sqrt{1/\epsilon}$, from the difinition of ϵ. If the conductivity of the aqeuous electrolyte inside a blister is 10^6 times the conductivity of the primer, the effective cathodic area in a blister is 1000 times greater than when the same primer adheres to the metal.

One aspect of the corrosion mechanism which is extremely difficult to quantify is adhesion. Equation 52 is based on the assumption that the primer and metal adhere to each other. When this assumption is not valid, a blister forms, and the local anodic rate increases dramatically. It would therefore be helpful if some criterion could be found for estimating the time required to break the adhesive bond. These criteria for disbonding may be unrelated to the adhesive energy itself. For example, a threshold charge density could be specified. Adhesion would be assumed normal for local charge densities below the threshold. Adhesion would be lost for charge densities above the threshold. Another criterion might be based on the local chemical composition. For example, either low or high values of pH might be expected to affect the oxide layer on aluminum and therefore the adhesive bond. In this case a time factor might also be important. Thus a local pH below one for more than 50 h might represent the desired criterion. Additional work needs to be performed in this area if quantitative estimates of the rate of coating disbonding are to be made.

Discussion

The examples illustrate that the mathematical model must in general be solved with a computer. Only relatively simple cases can be solved analytically. Nevertheless it is possible to use the model and the experimental results to ascertain certain qualitative features about the corrosion

of aluminum under paint. This qualitative analysis indicates that paints possess several good qualities which tend to reduce the corrosion rate and some bad qualities which tend to accelerate or localize corrosion. The primary advantage of the two-coat system appears to be that a relatively large quantity of inhibitor is trapped near the metal surface. The topcoat acts as a barrier to the diffusion of ions. This is an advantage when the painted specimen is initially exposed to electrolytes containing aggressing ions, but once the aggressive ions have reached the metal surface the topcoat tends to trap them there and its low ion permeability becomes a liability. This conclusion points up the importance of surface preparation and the need to paint on a surface free of ionic contaminants. The primer serves two important functions: it provides a vehicle for the inhibitor, and it improves adhesion. The inhibitor appears to function by raising the pitting potential, thereby decreasing the cathodic reaction rate and reducing corrosion currents. Adhesion is important because when the paints do not adhere to the metal surface (metal oxide) the corrosion current can flow through a relatively high-conductivity path, and the effective area of the cathode is greatly increased. The available data also indicate that neither oxygen nor water diffusion through the coating is the rate limiting step when the corrosion is uniform. In the limiting cases we have investigated the diffusion of ions through a resistive paint film adherent to the metal may be the rate limiting step. However, there are many instances, such as the initiation of a pit, when diffusion in the metal oxide or surface kinetics must represent the rate limiting step in the corrosion mechanism. The importance of the metal oxide as a barrier is further emphasized by the fact that aluminum is always in the passive or transpassive state under the conditions of interest. For this reason we can expect the bulk of observations of corrosion of painted aluminum to involve local corrosion cells.

Most of the undesirable effects of painting aluminum can be traced to the promotion of local corrosion cells. The mathematical model suggests that there are few problems associated with the corrosion of aluminum coated with an undamaged two-layer paint system even when exposed to dilute solutions containing chloride. Damaged coatings are another matter. When the topcoat becomes damaged the inhibitor diffuses out through the break. In a relatively

brief period the inhibitor becomes depleted in a region near the break. Further away from the break the inhibitor concentration is still high enough to prevent corrosion. This situation produces separate anodic and cathodic reaction areas and the formation of localized corrosion cells. These cells could take the form of pits, filiform corrosion, or a widening wedge of detached coating. The model also suggests that paints can promote corrosion by acting as barriers to the diffusion of ions. Pitting and localized corrosion of aluminum is known to be autocatalytic. The autocatalytic behavior is not yet well understood but appears to be related to a local buildup of some reaction product, possibly Al^{+3} or H^{+}. When these ions are produced beneath paint films they will tend to build up high concentrations because the coating acts as a diffusion barrier. Thus, not only does the coating reduce the separation of anodic and cathodic sites it increases the local concentration of reaction products. On some metals this retards the corrosion reaction, but when aluminum corrodes it apparently promotes the formation of local corrosion cells.

Conclusions

The following general conclusions are based on the experimental data and mathematical models studied here. They pertain to the mass transport properties of a limited number of paints and the corrosion of painted aluminum.

1. Some ion other than sodium or chloride carries a significant portion of current through many paints immersed in aqueous sodium chloride solution.

2. These paints do not provide a barrier to either oxygen or water sufficient to limit the uniform corrosion rate of aluminum.

3. Ionic inhibitors such as chromates are effectively retained near the metal by an undamaged topcoat.

4. Ionic inhibitors rapidly diffuse out of cracks and other defects in the topcoat leaving the metal unprotected from corrosion near the defect.

5. One general manner in which paints protect metals from corrosion is by forcing the current flowing to a local anode to pass through a highly

resistive medium, thereby reducing the effective cathodic area.

6. In general the mass transport properties of paints are quite complex, involving such phenomena as ion exchange, ion association, time varying properties, variations in physical and transport properties with position inside the paint film, and concentration dependent transport properties.

REFERENCES

1. Dave Pulley, private communication.

2. H. P. Gregor and H. H. Peterson, J. Phys. Chem., 68 (8), 2201-2205 (1964).

3. Electrochemical Technology Corp., Seventh Quarterly Report, January 1984, Contract No. N62269-82-C-0261, NADC.

4. Electrochemical Technology Corp., Final Report, October 1981, Contract No. N00014-79-C-0021, Naval Ocean Research and Development Activity, Bay St. Louis, MS.

5. W. Funke, J. Oil and Colour Chemists Assoc., 46, 975-979 (1963).

6. W. Funke, Corrosion Control by Coatings, H. Leidheiser, Ed., Science Press, Princeton, 1979, p 35.

7. H. P. Godard, The Corrosion of Light Metals, R. T. Foley, N. Hackerman, C. V. King, F. L. LaQue, and H. H. Uhlig, Eds., John Wiley & Sons, Inc., New York, 1967.

8. M. Pourbaix, Atlas of Electrochemical Equilibria in Aqueous Solution, NACE, Houston, 1974.

9. H. H. Uhlig, Corrosion and Corrosion Control, John Wiley & Sons, Inc., New York, 1963.

10. J. E. O. Mayne, J. Oil and Colour Chemists Assoc., 40, 183-199 (1957).

11. C. C. Maitland and J. E. O. Mayne, Official Digest, 34, 972-991 (Sept. 1962).

12. J. E. O. Mayne, Br. Corros. J., 5 (May), 106-111 (1970).

13. J. E. O. Mayne, Anti Corrosion, p 3, October 1973.

14. J. E. O. Mayne and D. J. Mills, J. Oil and Colour Chemists Assoc., 58, 155-159 (1975).

15. R. M. Fuoss and F. Accascina, Electrolytic Conductance, Interscience Publishers Inc., New York, 1959.

16. J. Crank and G. S. Park, Diffusion in Polymers, J. Crank and G. S. Park, Eds., Academic Press, New York, 1968.

17. W. K. Asbeck, "Adhesion and Cohesion," p 101, P. Weiss, Ed., Elsevier Publishing Co., New York, 1962.

18. W. K. Asbeck, IX FATIPEC Congr., p 78 (1968).

19. W. K. Asbeck, J. Paint Technol., 43, 84-91 (1971).

20. M. E. Merchant, J. Appl. Phys., 16, 267-75 (1945).

21. M. E. Merchant, J. Appl. Phys., 16, 318-24 (1945).

22. D. W. van Krevelen, Properties of Polymers, Their Estimation and Correlation with Chemical Structure, Elsevier Scientific Publishing Co., New York, 1976, ch. 18.

23. K. Sotoudeh, T. H. Nguyen, R. T. Foley, and B. F. Brown, Corrosion, 37 (6), 358-362 (1981).

24. H. Bohni and H. H. Uhlig, J. Electrochem. Soc., 116 (7), 906-910 (1969).

25. H. Kaesche, Localized Corrosion, NACE-3, Int. Corrosion Conf. Series, R. W. Staehle, B. F. Brown, J. Kruger, and A. Agerwal, Eds., 1974, p 516.

26. R. A. Patterson, Corrosion, 37 (8), 435-461 (1981).

27. H. T. Rowland and S. C. Dexter, Corrosion, 36 (9), 458-467 (1980).

28. A. Gemant, Ions in Hydrocarbons, Interscience Publishers, New York, 1962.

NOMENCLATURE

A	a constant
C	concentration, mole/cm^3
D	diffusivity, cm^2/s
F	Faraday constant
I	total current, A
i	current density, A/cm^2
J	flux, mole/($cm^2 \cdot s$)
K	distribution coefficient
L	membrane thickness, cm
l	paint thickness, cm
M	mass, g
P	permeability coefficient, cm^2/s
q	inhibitor content of the primer, mole/cm^2
R	gas constant
R	reaction rate, mole/($cm^3 \cdot s$)
r	transport rate, mole/(cm·s)
S	dimensionless solubility
T	temperature, °K
t	time, s
v	volume, cm^3
w	crack width, cm
x	position coeerdinate, cm
z	ionic charge including sign

Superscripts

*	radioactive species
o	reference value
α	alpha phase
β	beta phase

Greek

β	a constant, v^{-1}
γ	activity coefficient, cm^3/mole
∇	del operator
Δ	change, finite difference
η	electric potential, V
κ	electrical conductivity, S/cm
μ	Electrochemical potential, J/mole
φ	electric potential, V
ν	dimensionless electric potential, $z_i F\phi/RT$

Subscripts

a	anodic
ave	average value
b	bulk solution designator
c	corrected or normalized value
c	cathodic
e	experimental value
i	species designation
m	in the membrane or paint
n	normalized value
o	constant value, usually at time zero
p	in the paint phase
p	value at the pitting potential
r	reference value
sat	designates saturation
1	1st solution, species, or phase
2	2nd solution, species, or phase

APPENDIX A

HITTORF EXPERIMENTS

Apparatus

Both membrane-potential and Hittorf experiments were conducted in the same apparatus. Figure A1 illustrates the experimental cell which was made of Plexiglas. When assembled, each cell was composed of two cylindrical compartments separated by a paint membrane. The two compartments were aligned vertically. Both compartments were equiped with sampling ports and overflow tubes. The sampling ports were sealed with rubber septums, but the overflow tubes were open to the air. The overflow tubes were made of capillary tubing with one end drawn down to a small diameter. This construction reduced water evaporation to a negligible level. The overflow tubes from both the top and bottom compartments were bent above the cell so they were in the same horizontal plane. In this way the hydrostatic pressure difference across the membrane was minimized.

The cell was constructed in two halves. Internally, each cell was identical, but the external connections (sampling ports, overflow tubes, etc.) were in different positions in each of the half cells. The paint membrane was clamped between the two half-cells which were held together by four bolts. Viton O-ring gaskets were used to prevent the solutions from leaking between the paint and the Plexiglas.

Each compartment was equiped with a silver-silver chloride electrode. The electrodes were glued to the Plexiglas with epoxy. The electrode diameter was the same as the "active" diameter of the membrane, and both electrodes were parallel to, and equidistant from, the membrane.

Small Teflon-coated magnetic stir bars were used to stir the solutions in both compartments. The stir bar in the bottom compartment was held above the electrode surface by a circular disc of plastic window screen. Similar screens were clamped on each side of the paint membrane as

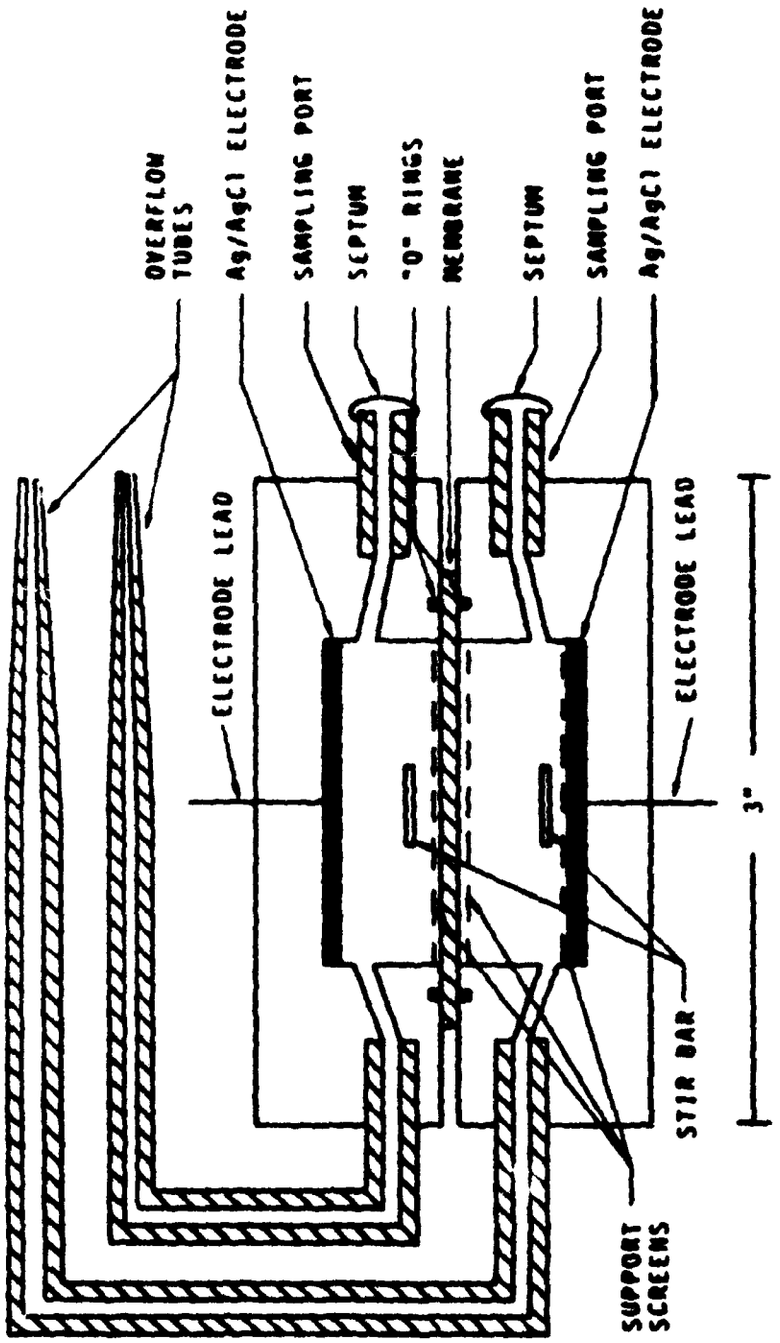

Fig. A1. Hitlorf Cell

physical supports. The stir bar in the top compartment rested directly on the upper support screen. Stirring speeds of approximately 100 rpm were achieved with a magnetic stir plate.

The assembled Hittorf cell was placed in a Faraday cage during experiments. A battery was used to control the cell potential between the two electrodes. The voltage difference and electrode current were measured with Keithley electrometers. Figure A2 is a schematic diagram of the electrical instrumentation. The electrometers contain retransmitting amplifiers with low output impedance. The output of these amplifiers was recorded on an Esterline Angus, model E1124E, strip chart recorder. The output of the electrometer recording the current was integrated with an Acromag, model 1752-K1-1, integrator. The total charge passed during the course of an experiment was obtained from the integrator. This instrumentation provided a permanent record of the voltage, current, and total charge for each experiment.

The experimental temperature was controlled with an air thermostat. A modified on-off household thermostat was used. Temperatures adjacent to the cell were measured with National Semiconductor, LX5600, temperature transducers. The transducers were purchased in TO-5 packages, and were equipped with radial-finned clip-on heat sinks. The cell temperatures were also recorded on the strip chart. A peak-to-peak temperature excursion of 1°C was observed with this apparatus.

All salts and solvents were ACS reagent grade, and the water was distilled. Radioactive hydrogen (^{3}H), sodium (^{22}Na), and chloride (^{36}Cl) were purchased in carrier-free form from commercial sources. Radiotracer standards, traceable to the National Bureau of Standards, were puschased and used to make reference solution. The radiotracer content of samples was measured with a Packard, model 2002, scintillation counter at the University of Washington.

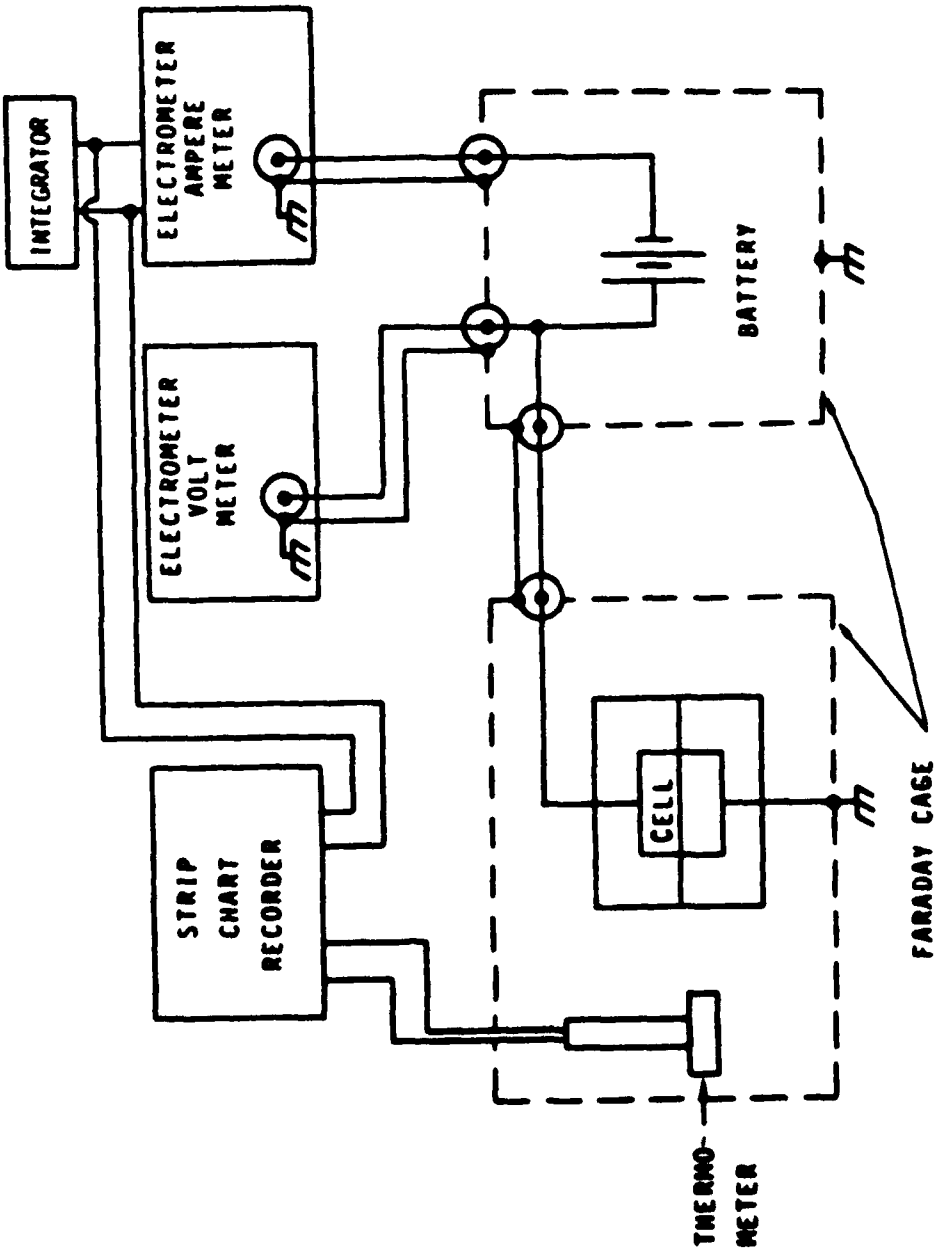

Fig. A2. Electrical schematic and instrumentation for a Hittorf experiment.

Procedure

In order to perform a Hittorf experiment, paint membranes unattached to any substrate were first prepared. Paints were first mixed according to the supplier's instructions. The paint was then spray applied to sheets of decal paper and allowed to dry. Drying took place in the ambient laboratory air at about 60% relative humidity and 23°C. The paint was protected from dust in a fume hood for about 24 hours. The coated pieces of decal paper were then placed in paper envelopes and stored in a wooden cabinet until needed. Storage times varied from two weeks to two years.

Immediately prior to use, specimens of paint were cut from the large sheets of coated decal paper. The decal paper was soaked in water for a few minutes until the paint could be easily removed. The free paint film was then washed in tap water till no mucilage could be detected by touch. Then the paint was rinsed in distilled water for a few seconds and dried with a paper towel. The dry paint film was allowed to stand in laboratory air for about 15 minutes before the thickness was measured with a micrometer. Twelve to 15 thickness measurements were made in the test area of the sample. The average coating thickness and standard deviations were then calculated. Free films with nonuniform thickness or high standard deviations were rejected. The membrane was next checked optically for defects: holes, dirt or dust particles, etc. Membranes which did not appear to be smooth and free of defects were rejected. The final pre-experiment check was a conductivity measurement. The membrane was mounted in a Hittorf cell and its dc conductivity was determined. If the conductivity differed more than a factor of about three from the average conductivity of similar membranes it was rejected. After a specimen passed all the pre-experiment tests it was ready for mounting in a Hittorf cell.

Prior to an experiment, the Hittorf-cell electrodes were checked. Solutions of differing salt concentration were placed in each half-cell, and the electrode potentials were measured relative to a standard reference electrode. If the "Nernst slope" for the Hittorf electrode exceeded 55 mV/decade, the electrode was considered acceptable. If the

electrode failed this test, the silver chloride layer was removed, and the silver was abraded, cleaned, and reanodized. Also, prior to the experiment the Plexiglas was inspected for scratches. If scratches were found, they were removed by polishing.

After the cell had been polished and the electrodes had passed inspection, both halves of the cell were rinsed in distilled water and then in methanol. The cell was then dried by blowing air through the injection ports and the overflow tubes. When the cell was completely dry, it was ready for assembly.

The cell was assembled in steps proceeding vertically from the bottom to the top. A screen was first placed in the bottom compartment over the silver-silver chloride electrode. A magnetic stir bar was then placed on the screen. Next, a second screen was placed over the mouth of the bottom compartment. The diameter of the second screen was greater than the compartment diameter. This screen supported the membrane. Next, the O-ring was coated with a thin layer of silicone stopcock grease and placed in its groove around the screen. Then the paint film was placed over the O-ring and the support screen. The paint film was always oriented in the Hittorf cell with the "air side" facing downward. The side of the free film which was exposed to air as the paint dried was termed the "air side." The opposite side, which was originally adjacent to the decal paper, was called the "paper side." When a voltage was applied, the polarity was such that the tracer ion was forced to migrate from the air side toward the paper side of the paint film. Next, a second support screen was placed on top of the paint, and another stir bar was placed on this second screen. Finally, the top half of the cell was placed on, and the entire assembly was bolted together. After the cell was assembled, a visual inspection was made. The inspection included checking the O-ring seals, the support screens, and the stir bars. If the inspection revealed no defects, the assembly was completed by placing rubber septums over the open ends of the injection ports.

Prior to filling the cell it was weighed. The assembled cell was then filled with electrolyte using a hypodermic syringe. The volume of electrolyte added to each compartment was measured with the syringe. The weight of the cell was also measured after each compartment was filled. This procedure provided two independent measures of the fluid volume in each compartment. The volume of fluid in the overflow tube was determined by the position of the liquid meniscus. Another visual inspection was performed after filling the cell. If bubbles with diameters greater than about 3mm (≈10% of the diameter of the compartments) were observed, the filling procedure was repeated. If the bubbles could not be removed, the compartments were emptied and the cell reassembled.

Electrolyte solutions were mixed just prior to assembling the cell. Various sodium chloride concentrations from 0.1 N to 1 N were employed. Radiotracers were added just prior to filling the cell. The solution containing the radiotracers was always placed in the bottom compartment. Solutions in both compartments contained the same concentration of salt, but no radiotracers were used in the top compartment. The bottom compartment always contained two radiotracers: tritium (^{3}H) and either sodium or chloride. In this way the water flux and one of the ion fluxes could be obtained.

After the cell had been filled, 10 μL samples were taken from each compartment. The cell was placed on a stir plate inside a thermostatically controlled glovebox. The mean temperature was maintained at 25°C ± 0.5°C. The cell was then connected to the battery and the electronic monitoring equipment. The cell was always connected to the battery with the polarity such that the salt radiotracer (^{22}Na or ^{36}Cl) was forced across the membrane. Experiments were conducted for various periods of time up to three months. The The cell voltage, current, and temperature were recorded. Radiotracer samples (10 μL) were periodically withdrawn with Hamilton micro-syringes through the rubber septums. The top compartment was sampled about every three days. The bottom compartment was sampled at two-week intervals. At the end of the experiment three samples were withdrawn from each compartment.

During the course of an experiment the positions of the menisci in the overflow tubes were periodically recorded. By comparing the relative positions of the two menisci, leaks could be detected. Experiments were terminated when leaks developed. At the conclusion of an experiment, the cell was dismantled and each half cell was leached for two weeks in separate distilled water baths.

The radiotracer samples were analyzed by liquid scintillation counting. The scintillation counter was capable of counting two radioisotopes simultaneously. The different isotopes were distinguished by the different energies of their β emissions. Chloride-36 could not be distinguished from sodium-22 because both radionulides have similar β-energy spectra. Therefore, tritium and either sodium or chloride were used in each experiment, and sodium and chloride fluxes were determined in separate experiments.

Approximately five standard samples were used to calibrate the scintillation counter during each counting session. The activities of the standards varied, covering a range approximately equal to that expected for the experimental samples. A least-squares matrix inversion method was used to determine counting efficiencies and cross-channel interference coefficients from the calibration data. The accuracy of each calibration matrix was also checked by counting mixtures of known composition. No quenching was observed with the small sample volumes (10 µl) used.

Transference numbers for sodium and chloride were calculated in the following way. First, the activity of the radiotracer (sodium or chloride) in the top compartment was obtained. These data were converted to equivalents of carrier (n_c) per ml by assuming a specific molar activity equal to that in the bottom cell. Then, the data were plotted as n_c versus charge passed. Different least-squares straight lines were then constructed through the data collected at each cell potential. Finally, the transference numbers were set equal to the slopes of the lines. This method was considered appropriate as long as two conditions were met. The radiotracer flux at zero applied voltage was negligible, and the fraction of radiotracer transported across the membrane was small. Both conditions were always satisfied in these experiments.

The diffusivity of water was calculated from measurements of the tritium concentration. It was assumed that tritium only passed through the membrane as water. This assumption cannot be easily verified. Other assumptions were the same as for sodium and chloride transport except that the fraction of tritium transported was usually large. In order to account for this fact, a differential mass balance was derived for the top compartment. The equation was solved to yield the tritium activity in the top compartment as a function of the water diffusivity and time. Experimental results were then inserted in the calculated solution, and a diffusivity was obtained for each of n experimental data points. The individual diffusivities were averaged to obtain the tabulated values.

TABLE A1

Experimental Results from Hittorf Experiments in

0.1 N NaCl solution at 25°C

Exp. No.	Paint Type	Specimen No.	Thickness (μm)	D. C. Conductivity ($\Omega^{-1}cm^{-1}$)	Applied Voltage (V)	Transference Numbers t_-	Transference Numbers t_+	Permeability Coefficients (cm^2/s) H_2O	Permeability Coefficients (cm^2/s) Cl^-	Permeability Coefficients (cm^2/s) Na^+
1A	PP-PUR	1	105	$1. \times 10^{-9}$	5.2	. 0.16		1.85×10^{-9}	1.62×10^{-12}	
					1.35	0.07			6.84×10^{-13}	
1B	PP-PUR	1	105	1.2×10^{-9}	0.95		0.48	1.84×10^{-9}		1.49×10^{-12}
2A	CP-PUR	2	83	6.0×10^{-13}	6.2		†	7.80×10^{-10}		†
					17.0		†			†
2B	CP-PUR	2	83	3.0×10^{-13}	23.0	†		5.95×10^{-10}	†	
3A	CP-PUR	3	80	5.5×10^{-12}	9.4		0.67	7.14×10^{-10}		1.07×10^{-14}
					22.0		0.62			9.43×10^{-15}
3B	CP-PUR	3	80	3.0×10^{-11}	15.3	0.16		1.83×10^{-10}	1.70×10^{-14}	

† A significant level of radioactivity could not be detected in the top compartment under these conditions.

TABLE A1 (Con't.)

Experimental Results from Hittorf Experiments in

0.1 N NaCl solution at 25°C

Exp. No.	Paint Type	Specimen No.	Thickness (μm)	D. C. Conductivity ($\Omega^{-1}cm^{-1}$)	Applied Voltage (V)	Transference Numbers t_-	Transference Numbers t_+	Permeability Coefficients (cm^2/s) H_2O	Permeability Coefficients (cm^2/s) Cl^-	Permeability Coefficients (cm^2/s) Na^+
4A	CP-PUR	4	78	2.0×10^{-12}	0.9	†		7.12×10^{-10}	†	
					22.3	~0.1			-8.5×10^{-16}	
4B	CP-PUR	4	78	1.0×10^{-10}	~12		0.32	5.74×10^{-10}		$\sim 1.7 \times 10^{-13}$
5A	YP-Epoxy	5	109	3.6×10^{-8}	2.6	0.27		7.8×10^{-10}	2.42×10^{-11}	
5F	YP-Epoxy	11	121	1.6×10^{-6}	1.2		0.08	2.9×10^{-11}		3.2×10^{-10}
6A	YP-Epoxy	6	104	2.0×10^{-7}	2.5		0.20	6.7×10^{-10}		3.61×10^{-11}
6F	YP-Epoxy	15	113	5.0×10^{-7}	1.4	0.52		†	7.6×10^{-10}	
7A	FP-PUR & YP-Epoxy	7	127	2.0×10^{-8}	1.74		0.421	1.77×10^{-9}		3.14×10^{-11}
7B	FP-FP-PUR/ YP-Epoxy	7	127	4.3×10^{-8}	1.14	0.026		4.07×10^{-9}	2.98×10^{-12}	
8A	FP-PUR & YP-Epoxy	8	148	2.0×10^{-8}	2.4	0.245		1.29×10^{-9}	3.8×10^{-12}	
8B	FP-FP-PUR/ YP-Epoxy	8	148	1.2×10^{-7}	2.3		0.54	1.38×10^{-9}		1.13×10^{-11}

† A significant level of radioactivity could not be detected in the top compartment under these conditions.

TABLE A1 (Con't.)

Experimental Results from Hittorf Experiments in

0.1 N NaCl solution at 25°C

Exp. No.	Paint Type	Specimen No.	Thickness (μm)	D. C. Conductivity ($\Omega^{-1}cm^{-1}$)	Applied Voltage (V)	Transference Numbers t_-	Transference Numbers t_+	Permeability Coefficients (cm^2/s) H_2O	Permeability Coefficients (cm^2/s) Cl^-	Permeability Coefficients (cm^2/s) Na^+
9B	MDPT	18	46	2.6×10^{-7}	1.35		0.56	11.0×10^{-9}		3.2×10^{-10}
10B	MDPT	20	51	5.0×10^{-8}	1.47	0.11		4.0×10^{-9}	6.1×10^{-12}	
11A	MD2	22	29	1.3×10^{-7}	1.33		0.33	3.1×10^{-9}		1.1×10^{-10}
12A	MD2	23	25	1.9×10^{-8}	1.46	0.63		1.4×10^{-9}	2.8×10^{-11}	

Table A2

Experimental Results from Hittorf Experiments in 1.0 N NaCl Solution at 25°C*

Exp. No.	Paint Type	Specimen No.	Thickness (μm)	D. C. Conductivity ($\Omega^{-1}cm^{-1}$)	Applied Voltage (V)	Transference Numbers t_-	Transference Numbers t_+	Permeability Coefficients (cm^2/s) H_2O	Permeability Coefficients (cm^2/s) Cl^-	Permeability Coefficients (cm^2/s) Na^+
1C	FP-PUR	1	105	3.4×10^{-8}	1.39	0.20		1.6×10^{-9}	1.7×10^{-12}	
1D	FP-PUR	21	116	4.1×10^{-9}	1.45		0.29	1.2×10^{-9}		2.9×10^{-13}
3C***	CP-PUR	3	79	4.2×10^{-11}	9.1		0.21	4.9×10^{-10}		1.4×10^{-14}
3D***	CP-PUR	3	79	1.9×10^{-10}	9.1	0.20		6.0×10^{-10}	8.0×10^{-14}	
6C***	CP-PUR	4	78	8.8×10^{-12}	8.8	0.11		5.5×10^{-10}	2.0×10^{-15}	
6D***	CP-PUR	4	78	1.1×10^{-9}	7.7		0.20	5.9×10^{-10}		7.7×10^{-13}
5D	YP-Epoxy	9	112	8.3×10^{-7}	1.3	0.58		2.1×10^{-11}	1.9×10^{-10}	
5E	YP-Epoxy	10	107	4.8×10^{-6}	1.0		0.12	5.2×10^{-11}		1.3×10^{-11}
6C	YP-Epoxy	12	111	1.2×10^{-6}	0.02		0.15	1.4×10^{-9}		7.2×10^{-11}
6D	YP-Epoxy	13	102	1.9×10^{-6}	1.37		0.58	2.7×10^{-10}		2.7×10^{-10}
6E	YP-Epoxy	14	114	4.2×10^{-6}	1.25	0.60		9.4×10^{-11}	6.1×10^{-10}	

Table A2 (Con't)

Experimental Results from Hittorf Experiments in 1.0 N NaCl Solution at 25°C*

Exp. No.	Paint Type	Specimen No.	Thickness (μm)	D. C. Conductivity ($\Omega^{-1}cm^{-1}$)	Applied Voltage (V)	Transference Numbers t_-	Transference Numbers t_+	Permeability Coefficients (cm^2/s) H_2O	Permeability Coefficients (cm^2/s) Cl^-	Permeability Coefficients (cm^2/s) Na^+
7C	FP-PUR & YP-Epoxy	15	137	9.7×10^{-10}	1.38		0.42	8.7×10^{-10}		2.7×10^{-12}
8C	FP-PUR & YP-Epoxy	16	152	1.4×10^{-9}	1.45	0.56		8.3×10^{-10}	2.9×10^{-12}	
9A	MBPT	17	45	2.6×10^{-8}	1.37		0.44	5.5×10^{-10}		3.4×10^{-12}
10A	MBPT	19	50	3.4×10^{-8}	1.42	0.38		6.1×10^{-10}	3.7×10^{-12}	

*The effect of this error is to reduce both the apparent sodium and chloride ion transference numbers. The conductivity and water permeability coefficient will also be affected, but the ion permeability coefficients will be approximately correct for a 0.1 N NaCl solution. The results from the experiments with GP-PUR separating solutions of unequal concentration have been included in the table for completeness, and to provide an order of magnitude estimate of the transport parameters of GP-PUR.

***Experiment conducted with 0.1 N NaCl in bottom compartment and 1.0 N NaCl in top.

APPENDIX B

Humidity Chamber Experiments

Crystal Oscillator Theory

Quartz crystals have been used to construct highly stable oscillators for many years. The crystal is a low-loss piezoelectric resonator which controls the oscillator's frequency. The fundamental frequency of a crystal is affected by temperature and several other environmental factors: however, the physical properties of the crystal have the greatest effect on the frequency.

The mass of the crystal is one property which has a great influence on frequency. This fact is the basis of several unusual uses of crystal oscillators, including sorption detectors (B1,B2). Highly sensitive sorption detectors have been constructed by coating a quartz crystal with a thin layer of absorbant (paint). The frequency of this "composite" crystal changes as its mass varies. By knowing the relationship between frequency change and mass change, microbalance weighing can be performed. Sensitivities on the order of 10^{-12} g have been estimated (B1).

The piezoelectric oscillation of a quartz crystal has been analyzed as an acoustic resonator (B3). In this one-dimensional theory, a wave disturbance is introduced at one surface of the crystal. The wave travels through the quartz with a constant velocity and attenuation until it reaches the opposite edge of the crystal. At the edge, the wave is completely reflected. This model is mathematically equivalent to an ideal transmission line with distributed loss, and a complete mathematical description is available.

When a quartz crystal is coated with another substance, a composite is formed. The acoustic resonator theory has been used to describe these composite resonators, but the analysis is more complicated than for the simple resonator. The complexity results from partial reflection of the traveling wave at the boundary between the quartz and the coating substance. Despite the complexity, Miller and Bolef (B3, B4) obtained an exact solution of the composite resonator. The theory showed that the only major effect of attaching the coating to the crystal was to shift the resonant frequency of the composite resonator (f) relative to the frequency of the simple quartz crystal (f_q).

Miller and Bolef's acoustic resonator theory is based on several approximations and assumptions. The assumptions appear to be appropriate, although they have apparently not been individually checked. However, the applicability of the entire theory to metal-coated crystals was proposed by Miller and Bolef (B4), and Lu and Lewis (B5) checked this application using three metals: copper, silver, and lead. The theory is in good agreement with experimental data for frequency shifts up to 15% of the "unloaded-crystal" frequency (f_q).

The acoustic resonance theory is based on the following assumptions (In the composite resonator the assumptions apply to the crystal and the coating separately.):

1. The system is one dimensional.
2. End faces are flat and parallel.
3. The wave travels with a constant velocity.
4. The attenuation per unit distance is constant.
5. The density of the medium is constant.
6. The crystal is oscillating at steady state (cw).
7. The coating is uniform over the entire "active" area.

   This theory does not treat the effects of crystal mounting or surface nonuniformities.

Lu and Lewis (B5) present three relations between the mass change of the composite crystal and the observed frequency shift. The most accurate equation, "exact solution," is based on Miller and Bolef's result (B3, Eq.9) with no losses in either the quartz or the coating. The exact equation is:

$$\tan\left[Z\pi\frac{f}{f_q}\frac{m_f}{m_q}\right] = Z \tan\left[\pi\frac{f_q - f}{f_q}\right] \qquad (B1)$$

where Z = the ratio of the shear-mode acoustic impedance of quartz to that of the coating

f = the frequency of the composite resonator

f_q = the frequency of the uncoated quartz crystal

m_f = the mass of the coating (film)

m_q = the mass of the uncoated quartz crystal

In this instance the composite-resonator frequency (f) depends on the acoustic impedance ratio (Z) as well as the mass of the applied coating (m_f).

The second equation presented by Lu and Lewis is the "period approximation." When Z = 1, or when $(m_f/m_q)<<1$, Eq. A1 simplifies to

$$\frac{m_f}{m_q} = \frac{f_q - f}{f} \qquad (B2)$$

The period approximation is adequate ($1<Z<2.29$) for frequency deviations less that about 5% (B5).

Also, when m_f/m_q is small, f has nearly the same value as f_q. Under these conditions Eq.A1 simplifies to the "frequency approximation,"

$$\frac{m_f}{m_q} = \frac{f_q - f}{f_q} \qquad (B3)$$

The frequency approximation is limited to a deviation of about 2% (B5)[1]. Once a particular quartz crystal has been selected, m_q and f_q are fixed. Then, f depends only on the mass of the applied coating. Eqs. B2 and B3 show this statement is true for both approximate models, but Eq. B2 is nonlinear.

[1] The total frequency change produced by the coating and absorption of water was less than 2% in all current experiments.

Diffusion Theory

The theory of sorption and desorption in thin sheets has been thoroughly discussed by Crank (B6). The basic equation describing the process is:

$$\frac{\partial c}{\partial t} = - \frac{\partial N}{\partial x} \tag{B4}$$

where c = the diffusant concentration (mol/m^3)

N = the diffusant flux ($mol/m^2 \cdot s$)

t = the time (s)

x = the linear dimension (m)

If the flux obeys Fick's first law,

$$N = - D \frac{\partial c}{\partial x} \tag{B5}$$

where D = the diffusivity (m^2/s)

Eq. B5 can be substituted into Eq. B4 to yield:

$$\frac{\partial c}{\partial t} = \frac{\partial}{\partial x} \left[D \frac{\partial c}{\partial x} \right] \tag{B6}$$

This is the basic equation of diffusion in a thin sheet and is equivalent to Fick's second law if the diffusivity is constant:

$$\frac{\partial c}{\partial t} = D \frac{\partial^2 c}{\partial x^2} \tag{B7}$$

In general the concentration depends on time, position, and the diffusivity, as well as the boundary conditions of a particular problem. Solutions of Eqs. B6 and B7 have been given for a variety of boundary conditions and diffusivities (B6, B7). Most of the published solutions require knowledge of the functional form of the diffusivity, but Crank and Park (B8) and Crank (B6) discuss practical ways of using the theory to evaluate the diffusivity from sorption and desorption isotherms.

One set of boundary conditions for which an analytical solution of Eq.B7 is available is:

$$\frac{\partial c}{\partial x} = 0 \quad @\ x = 0,\ t>0 \tag{B8}$$

$$c = 0 \quad @\ 0<x<\ell,\ t = 0$$

$$c = c_1 \quad @\ x = \ell,\ t>0$$

These boundary conditions represent a step change in surface concentration, at $x = \ell$, at time zero. For these conditions, the diffusivity is easily determined by plotting the dimensionless uptake of sorbate (R_u) versus the square root of time.

$$R_u = M_t/M_\infty \tag{B9}$$

where M_t = the total amount of sorbate present at time t

M_∞ = the total amount sorbed at long times (equilibrium).

$$M_t = \int_0^\ell c(x,t)dx \tag{B10}$$

This theory is equally applicable to desorption provided M_t and M_∞ represent quantities of diffusant lost.

At $t = 0$

$$\frac{dR_u}{d\sqrt{t}} = \frac{4}{\ell}\sqrt{\frac{D}{\pi}} \tag{B11}$$

The slope, $dR_u/d\sqrt{t}$, is nearly constant for $R_u<0.5$ (Rg. p16).

It is also easy to calculate the diffusivity at long time, provided an accurate value of M_∞ is known. At long times

$$\frac{d}{dt}\left[\ln\left(1-\frac{M_t}{M_\infty}\right)\right] = \frac{-D\pi^2}{\ell^2} \tag{B12}$$

If both Eqs.B11 and B12 are applied to a single sorpiton experiment, a single value of the diffusivity should be obtained. If this is not found, the diffusivity is not a constant.

Apparatus

The crystal oscillator apparatus was designed to subject the coated crystals to an isothermal, step-change in relative humidity. The crystal and the oscillator were suspended inside a metal chamber mounted inside a Plexiglas box. The crystal was first allowed to equilibriate with the atmosphere inside the inner (metal), chamber. Then, the inner chamber was opened and the crystal was exposed to the atmosphere in the Plexiglas box. A good step-change in relative humidity was reproducibly produced using this technique.

The "humidity chamber" apparatus is illustrated in Fig. B1. The outer chamber was constructed of 6.35 mm thick Plexiglas and was insulated with 3/4 in thick styrofoam. The volume of the outer chamber was 15 liters. The temperature in the box was controlled with a VWR #14370-030 proportional controller. The main constant-temperature bath was located outside the box and water was circulated from the bath through a finned-tube heat exchanger inside the box. The air inside the box was circulated with a fan. Three copper-constantan thermocouples were used to measure the temperature at different locations in the box. The maximum temperature difference between the different locations was 0.1°C, and a long-term temperature fluctuation of 0.5°C was observed.

The inner chamber was composed of two parts: a movable "cup," and a stationary "lid." The lid was attached to the Plexiglas box with a metal bracket. The cup could be raised and sealed against the lid to form the inner chamber, or lowered to open the chamber. The cup was aligned with the lid by a Plexiglas tube attached to the box. Both the alignment tube and the bracket supporting the lid were perforated with holes (≈10 mm diam.) to allow air to circulate completely around the inner chamber. In the raised position, the cup was supported by a Plexiglas column resting on a closed trapdoor. When the door was opened the entire cup-column assembly could be removed from the box. The cup and lid were both constructed of 1 mm thick sheet metal. The cup was 92 mm high and 55 mm in diameter, with a volume of 219 ml.

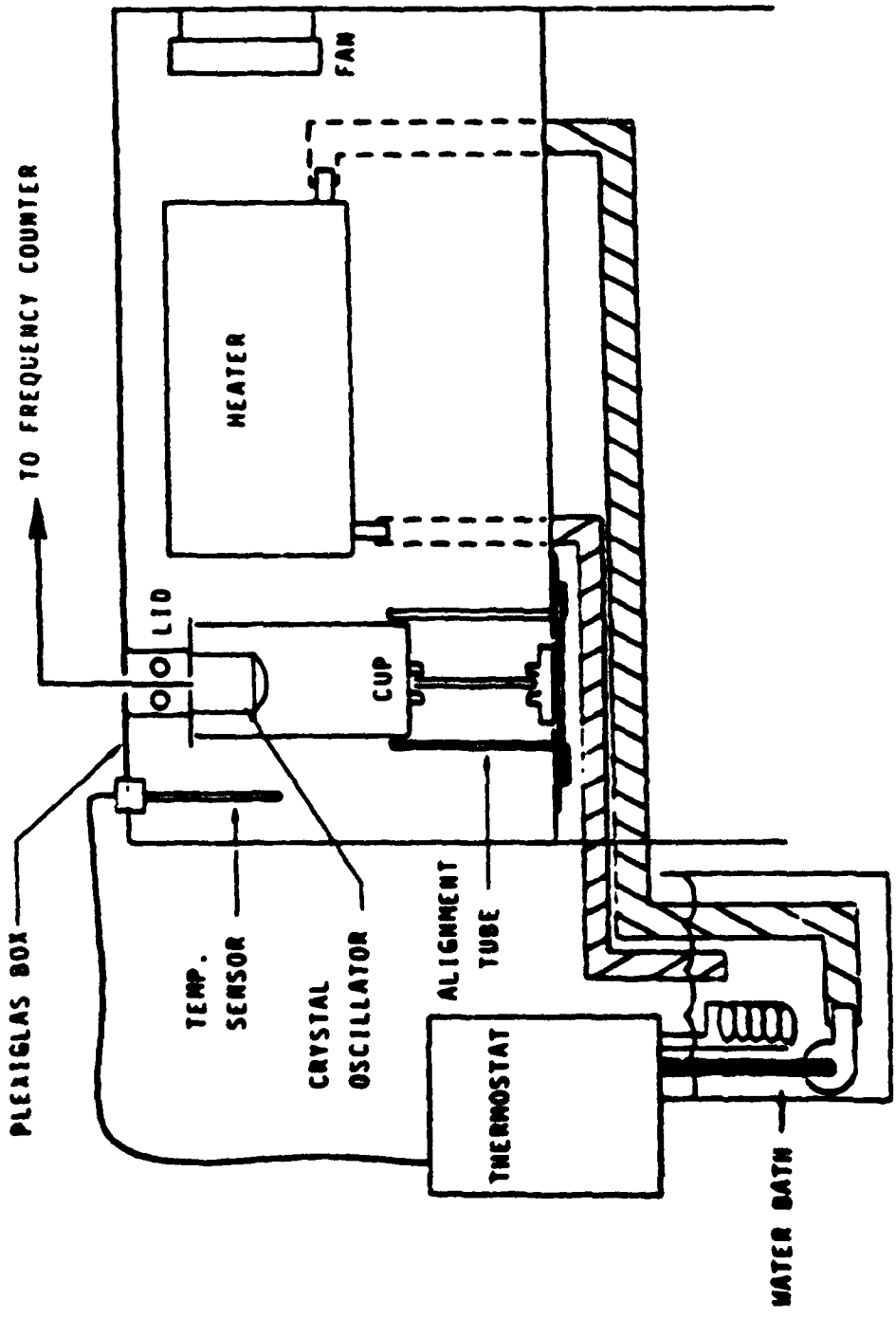

Fig. B1. Humidity chamber and crystal oscillator.

The oscillator and crystal holder comprised a single unit which was mounted on the inside surface of the lid. The oscillator was a "Digital Sensor Head," #900010, Sloan Technology Corp., Santa Barbara, Calif. The oscillator was powered by a 6 V regulated supply (Acopian, model 6E20D). The frequency was measured with a General Radio, model 1191 frequency counter and automatically recorded on paper tape with a Datil, model DPP-Q7 thermal printer. Only the "Digital Sensor Head" was inside the Plexiglas box. The circuit diagram of the electrical connections between the power supply, the oscillator, and the frequency counter is shown in Fig. B2. A low-pass filter (Fig. B2) was used between the oscillator and the frequency counter. The filter was not a necessary part of the circuit, but it reduced the effects of stray capacitance.

The crystals for the oscillator were purchased from Sloan Technology Corp. They were AT-cut quartz discs 12.5 mm in diameter and approximately 0.33 mm thick. The nominal frequency was 5.0 MHz. The as-received crystals had been coated on both sides with a thin layer of metal. The metal provided electrical contact with the crystal as it rested in the holder. Crystals with either gold or silver coatings were used. Only part of one surface of the crystal was exposed to air when it was in the holder. The exposed surface was visible through an 8.0 mm diameter hole in the crystal holder.

Procedure

The first step in the procedure was to record the base frequency (f_q) of the uncoated crystal in "dry" air at 31°C. Calcium sulfate (Drierite) desiccant was used to maintain dry conditions. Several of the crystals were also weighed on a Cahn, model gram-1501, electrobalance, with a reproducibility of ±10 µg. The base frequencies (f_q) and base weights (w_q) were measured at least three times for each crystal.

After the base data had been obtained, the crystals were prepared for painting. The crystals were flat only on one face. The other face was slightly convex. Lu and Lewis (B5) used similar crystals to confirm the acoustic resonator theory. Tests showed that the crystal could oscillate with the greatest mass attached to the flat side. Masks were used to produce uniform-diameter paint spots which were centered

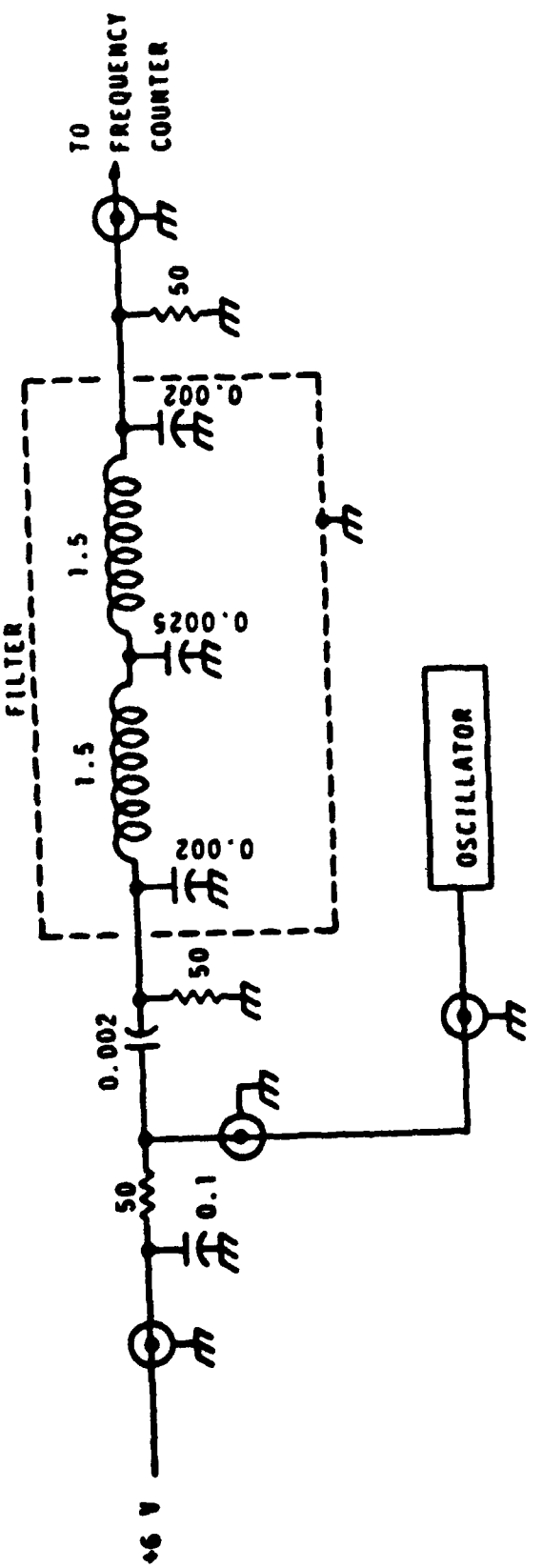

Fig.82. Crystal oscillator circuit diagram. Resistance values are ohms. Capacitance values are μF. Inductance values are μH.

on the flat side of the crystal. The masks were cut from plastic electricians tape with a cork bore. Various spot diameters were tested, but 5.8 mm was standard. The individual spot diameters were determined by averaging at least six measurements of the diameter (±0.3 mm) made with a metal rule. The paint was applied to the crystals with a 1 µl pipet. Different coating thicknesses were achieved by diluting the paints with the appropriate solvent prior to application. The coatings were allowed to dry for several days at ambient conditions. The average laboratory temperature was 23°C and the average relative humidity about 60%. After the coating had dried the mask was removed by soaking the crystal in an organic solvent. Several solvents have been used but hexane was one of the best. It dissolved the sticky side of the tape and had no apparent effect on the coatings. The crystals were soaked in hexane for ten to fifteen minutes; then the mask was lifted off with a pair of tweezers. The mask was inspected for visible traces of metal. If metal flecks were found the crystal was considered defective. Crystals were also classified as defective if any trace of the mask remained imbedded in the paint, or if any part of the paint became detached from the crystal.

After the masks had been removed, the crystals were rinsed with hexane and dried in laboratory air for at least several hours. The frequency (f_d) was then measured after equilibrating the crystals with a dry atmosphere. The crystals were also weighed (w_d) while being desiccated.

At this stage the painted c ,stals were ready for the diffusion experiments. The crystals were placed in the holder with the paint spot visible through the hole. The holder was then attached to the rest of the oscillator assembly, and oscillation was confirmed with the frequency counter or an oscilloscope. A saturated salt solution was placed inside the cup, and the cup was raised to seal the inner chamber. Desiccant, or a second salt solution, was placed in the outer chamber which was then sealed. Thermocouples were used to determine the temperatures in both the inner and outer chambers. When all thermocouples and the frequency had attained a steady state the printer was turned on, and the frequency counter was adjusted for a 1 s time period. A stopwatch

was started, and the cup was dropped at a well-specified time. The frequency (f) was automatically recorded every second for approximately 100 seconds. Then the time period was changed to ten seconds. Frequency measurements were continued in this manner until a total elapsed time of 300 seconds had passed. Most experiments had reached a "steady state" in 300 seconds, but some were extended up to 2 hrs. total time.

Each crystal was tested at least twice for each step change in relative humidity. The standard procedure was to allow the "closed-cup" system 16 hours to reach steady state. The first experiment was then conducted. When this experiment was complete (usually 5 to 20 min.) the cup was raised again and the system was allowed to stand for about 7 hours. A second experiment was then conducted as before. The frequencies obtained from the two experiments were compared at each time interval. If both experiments were in satisfactory agreement, the results of the first run were used to calculate the water diffusivity. If the experiments did not agree the sequence was repeated.

REFERENCES

B1. W. H. King, Research and Development, 28, April, 1969.

B2. W. H. King, Research and Development, 28, May, 1969.

B3. J. G. Miller and D. I. Bolef, J. Appl. Phys., 39, 4589 (1968).

B4. J. G. Miller and D. I. Bolef, J. Appl. Phys., 39, 5815 (1968).

B5. C. S. Lu and O. Lewis, J. Appl. Phys., 43, 4385 (1972).

B6. J. Crank, The Mathematics of Diffusion, 2nd ed., Clarendon Press, Oxford, 1975.

B7. H. S. Carslaw and J. C. Jaeger, Conduction of Heat in Solids, 2nd ed., Oxford University Press, London, 1959.

B8. J. Crank and G. S. Park, Eds., Diffusion in Polymers, Academic Press, New York, 1968.

APPENDIX B

Experimental Results
Water Solubility

Table B1

GP-PUR Paint Specimens Used
in the Crystal Oscillator Apparatus

Crystal Number	Paint Mass (mg)	Paint Thickness (μm)
59	0.263	6.3
60	0.304	7.3
72	0.293	7.0
73	0.581	13.9
74	0.276	6.6
75	0.176	4.2

Table B2

Solubility of Water in GP-PUR[a]

Paint Thickness (μm)	Temp. (°C)	Crystal	Solubility (g-H_2O/g-paint)
4.2	31.1	75	1.79 E-2
6.3	31.8	59	1.86 E-2
6.6	31.3	74	2.06 E-2
7.0	31.9	72	2.05 E-2
7.3	31.8	60	2.16 E-2
13.9	31.5	73	2.41 E-2
		Average	2.06 E-2
		σ	(±0.22 E-2)

[a]The equilibrium vapor pressure of water is 3.52 kPa.

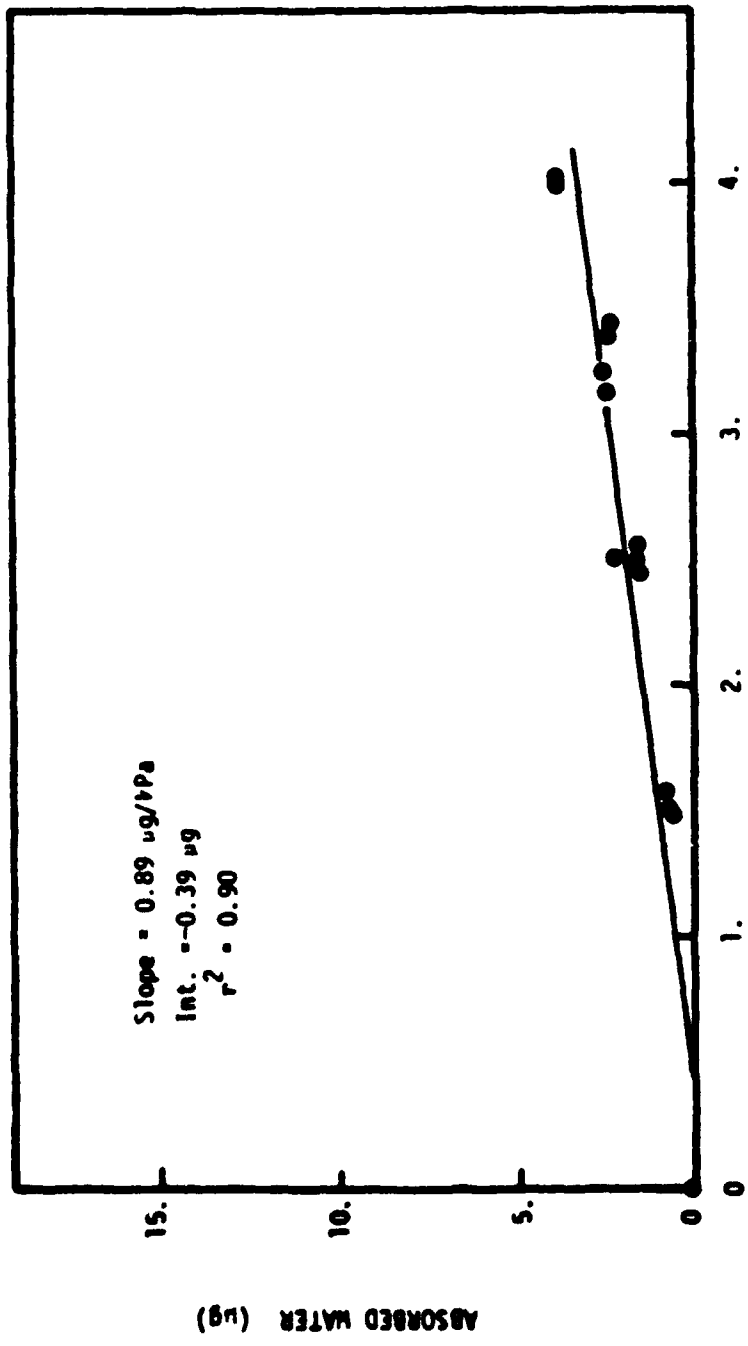

Fig. 83. Water absorption by GP-PUR at 31.1 ± 0.9°C. Crystal #75.

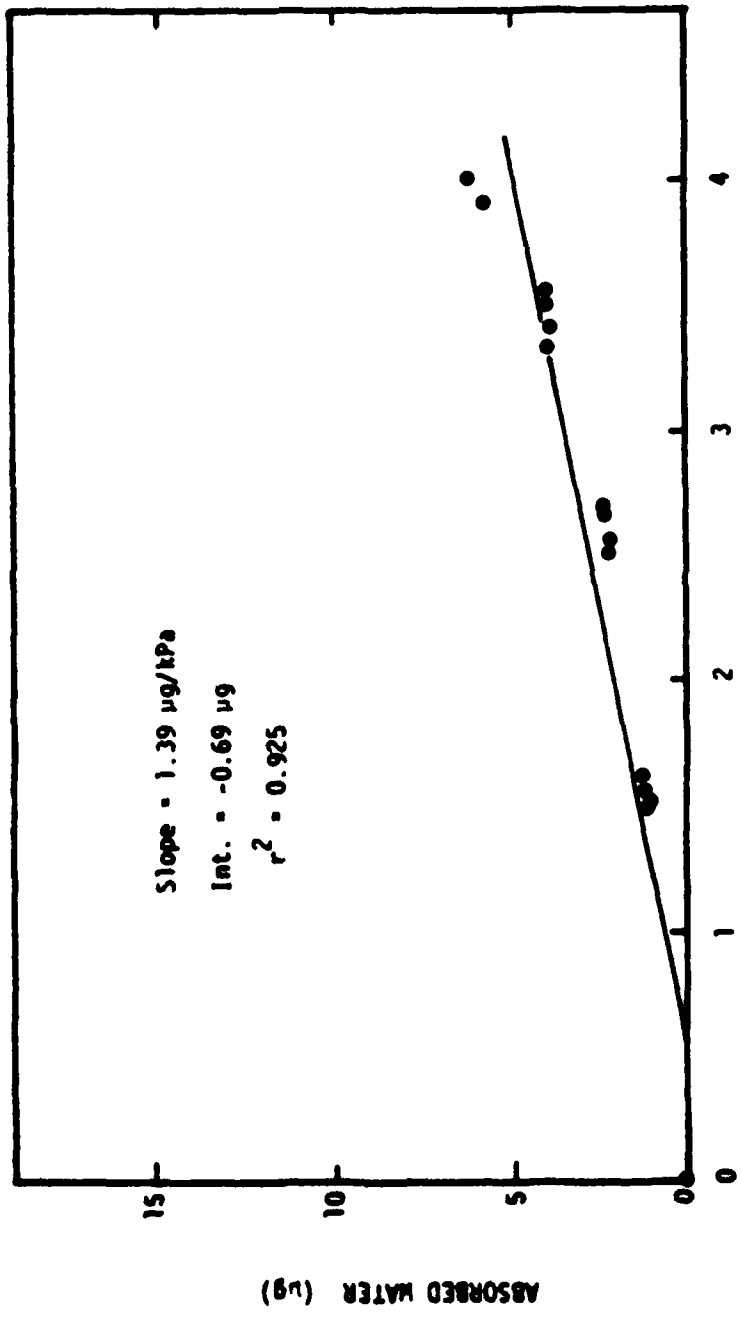

Fig. 84. Absorption isotherm for water in GP-PUR at 31.8°C. Crystal No. 59.

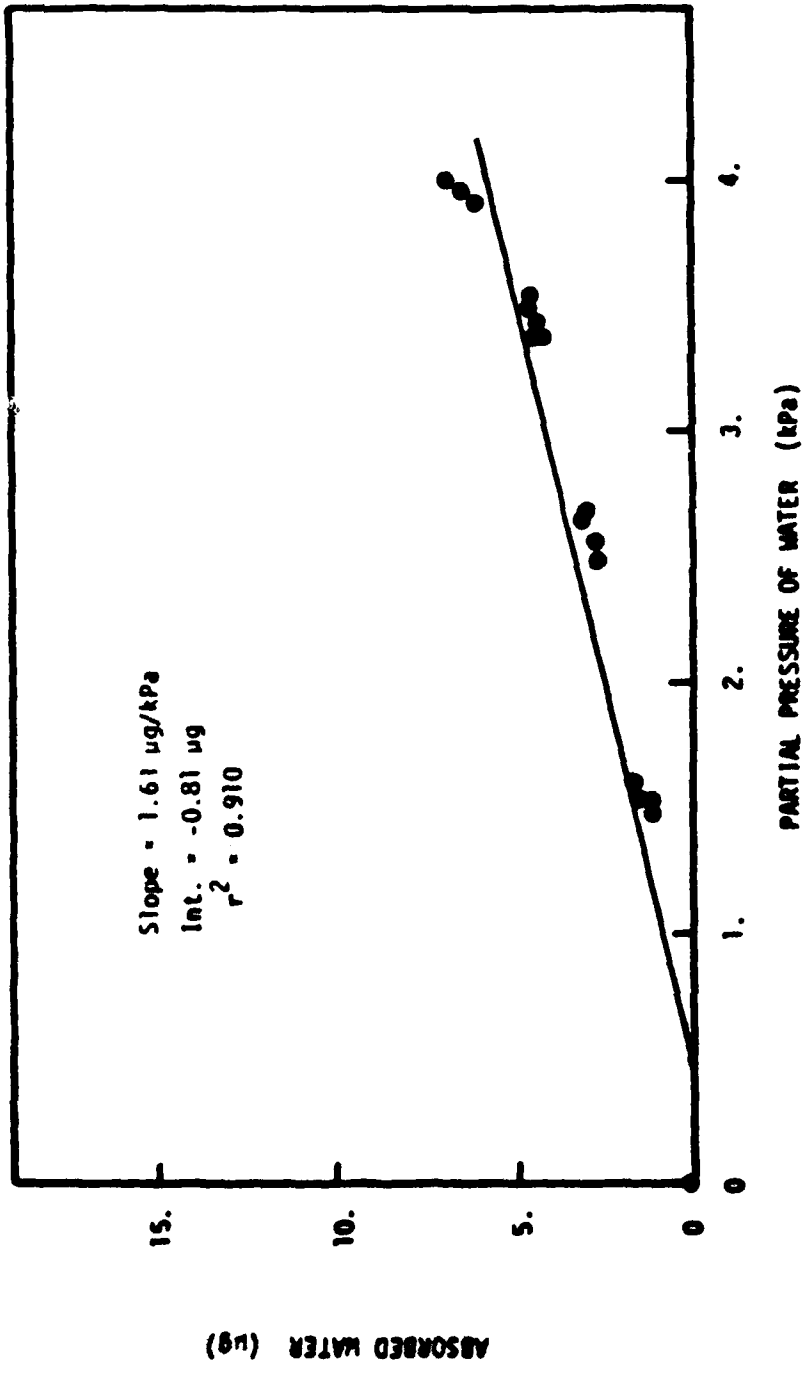

Fig. 85. Water absorption by GP-PUR at 31.3 ± 0.9°C. Crystal # 74.

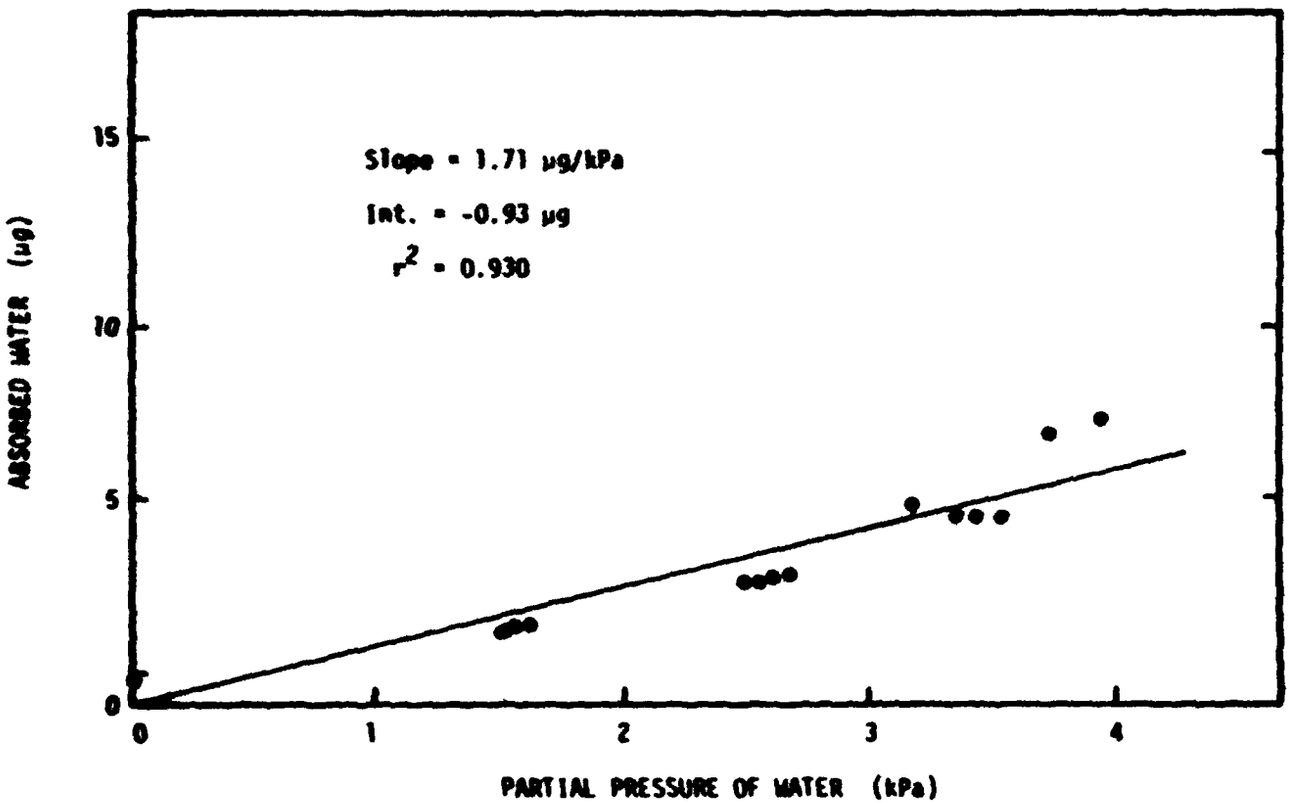

Fig. 26. Absorption isotherm for water in GP-PUR at 31.9°C. Crystal No. 72.

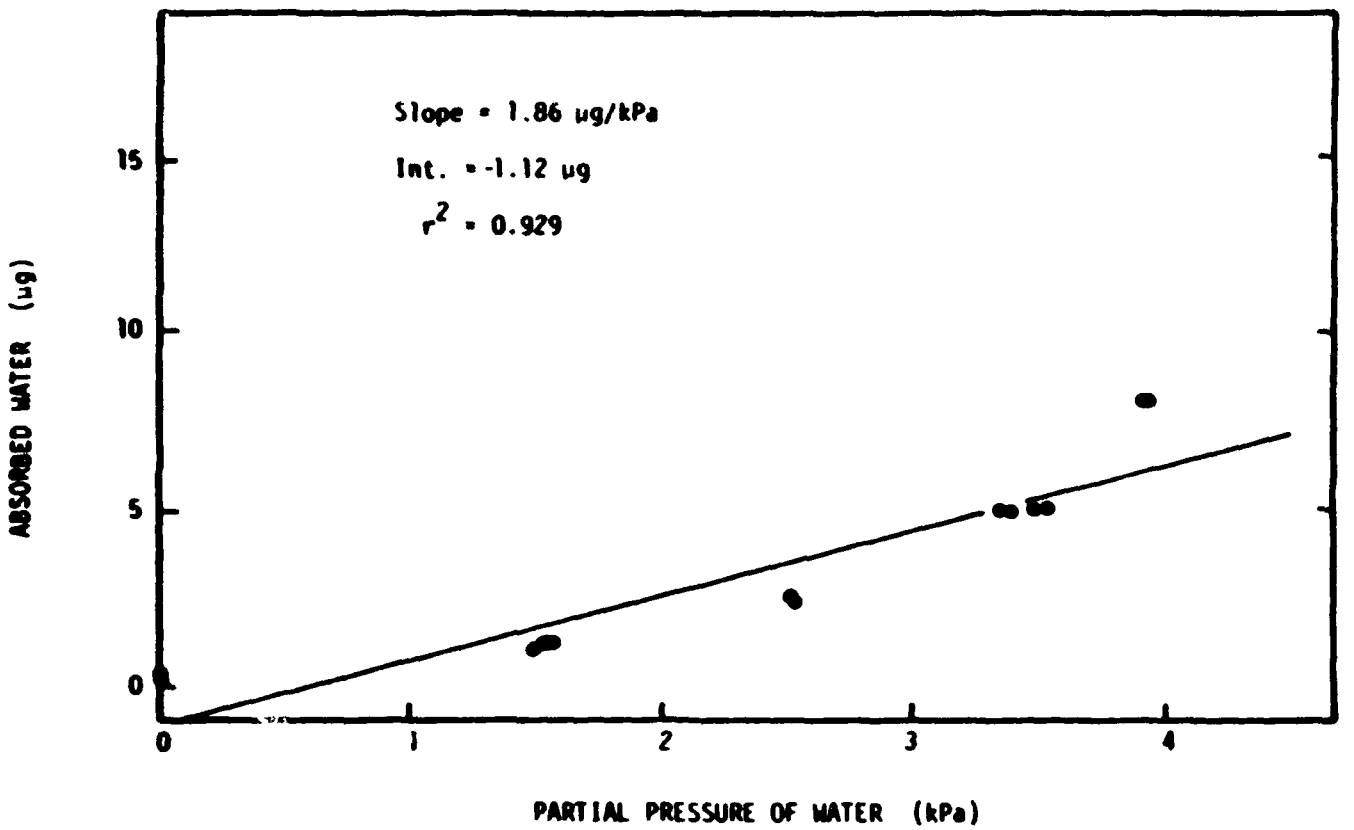

Fig. B7. Absorption isotherm for water in GP-PUR at 31.8°C. Crystal No. 60.

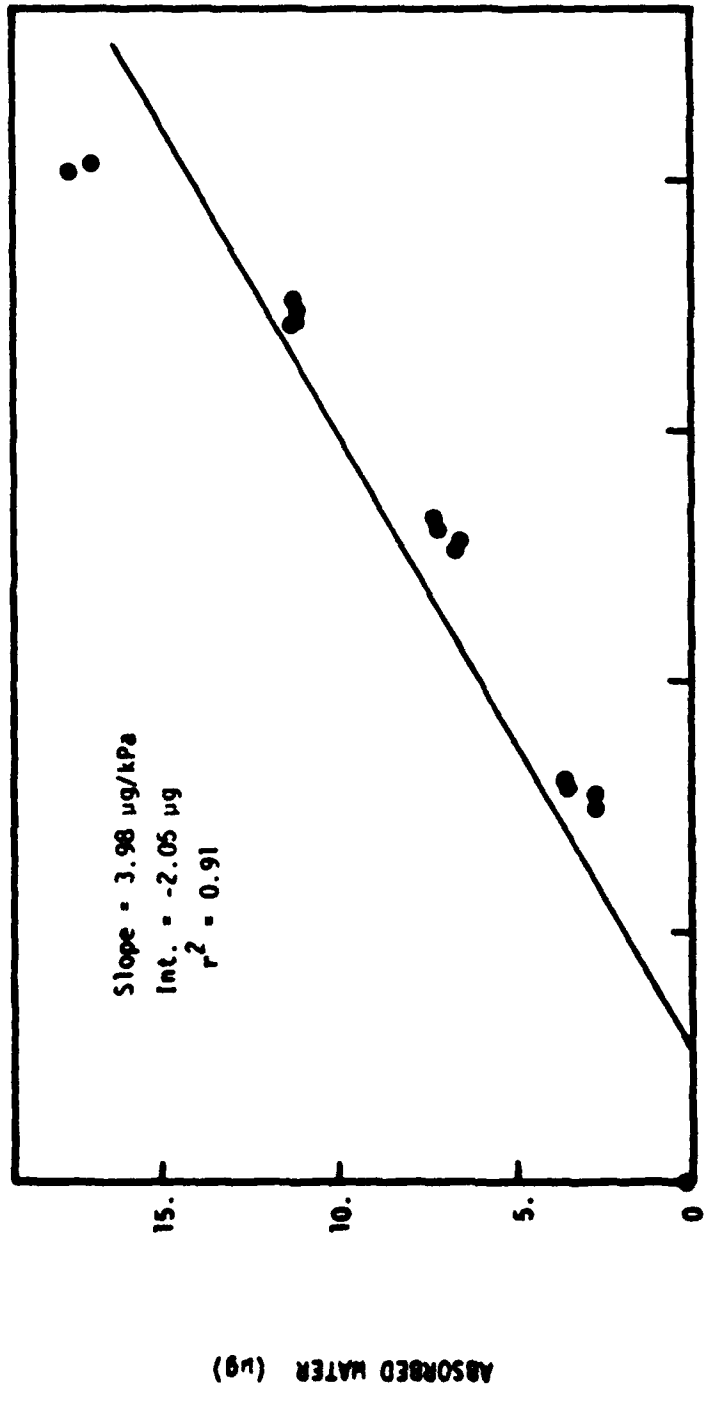

Fig. 88. Water absorption by GP-PUR at 31.5 ± 0.7°C. Crystal #73.

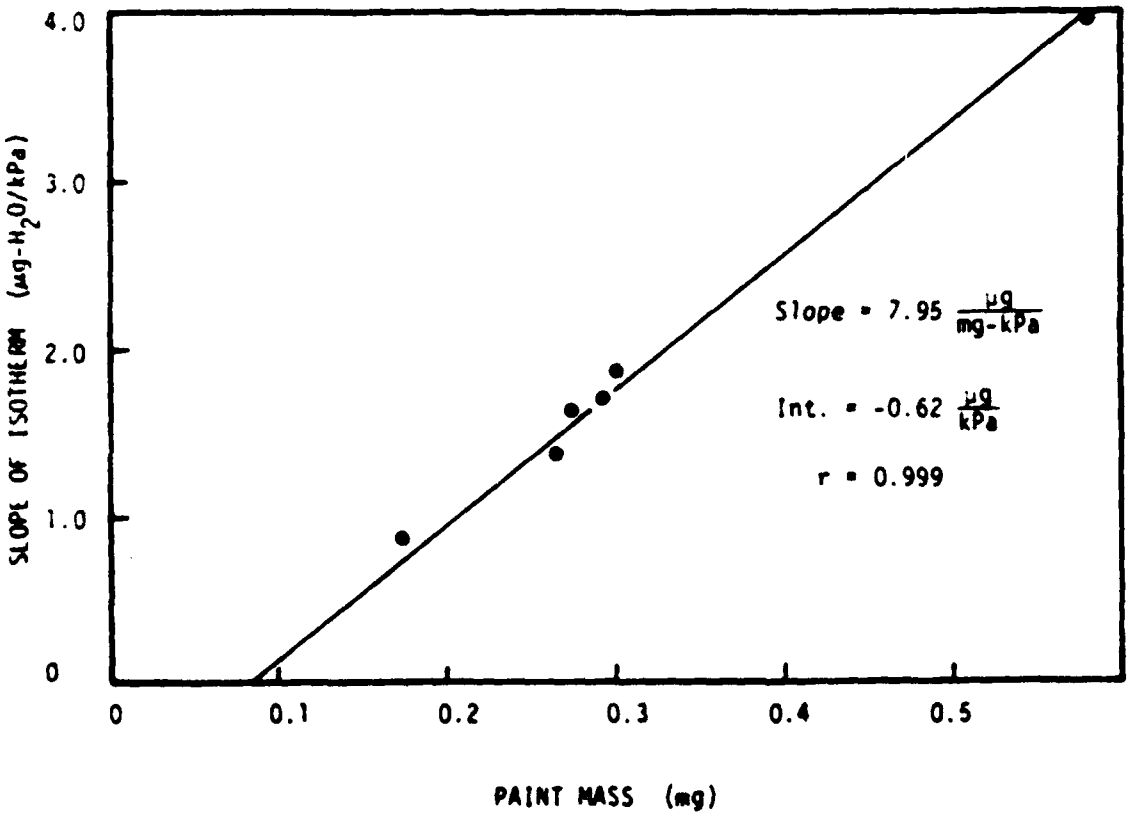

Fig. B9. Solubility of water in GP-PUR at 30.6°C.

Table B3

FP-PUR Paint Specimens Used
in the Crystal Oscillator Apparatus

Crystal Number	Paint Mass (mg)	Paint Thickness (μm)
77	.164	4.0
78	.218	5.3
62	.248	6.0
76	.258	6.3
61	.370	8.9

Table B4

Solubility of Water in FP-PUR*

Paint Thickness (μm)	Temp. (°C)	Crystal Number	Solubility ($g\text{-}H_2O/g\text{-paint}$)
4.0	32.0	77	2.55×10^{-3}
5.3	32.0	78	2.91×10^{-2}
6.0	31.9	62	2.63×10^{-2}
6.3	32.0	76	2.96×10^{-2}
8.9	31.9	61	2.87×10^{-2}
4.0	35.9	77	2.22×10^{-2}
5.3	35.9	78	3.17×10^{-2}
6.0	35.8	62	2.28×10^{-2}
8.9	35.7	61	2.88×10^{-2}
4.0	40.4	77	2.08×10^{-2}
5.3	40.2	78	2.56×10^{-2}
6.0	40.5	62	2.28×10^{-2}
8.9	40.3	61	2.33×10^{-2}

* Equilibrium vapor pressure of water is 3.52 kPa.

AD A147 799 APPLICATION OF ELECTROCHEMICAL ENGINEERING METHODS AND THEORY TO SOLVING..(U) ELECTROCHEMICAL TECHNOLOGY CORP SEATTLE WA R T RUGGERI ET AL. APR 84 NADC-84107-60

UNCLASSIFIED N62269-82-C-0261 F/G 11/6 NL

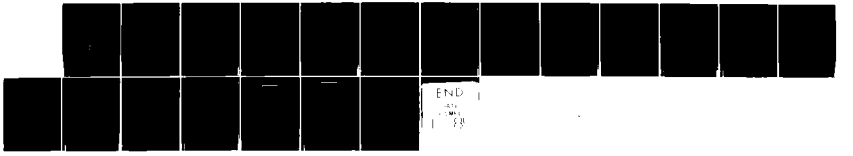

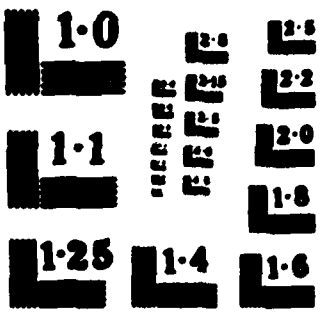
1·0
1·1
1·25
1·4
1·6
1·8
2·0
2·2
2·5

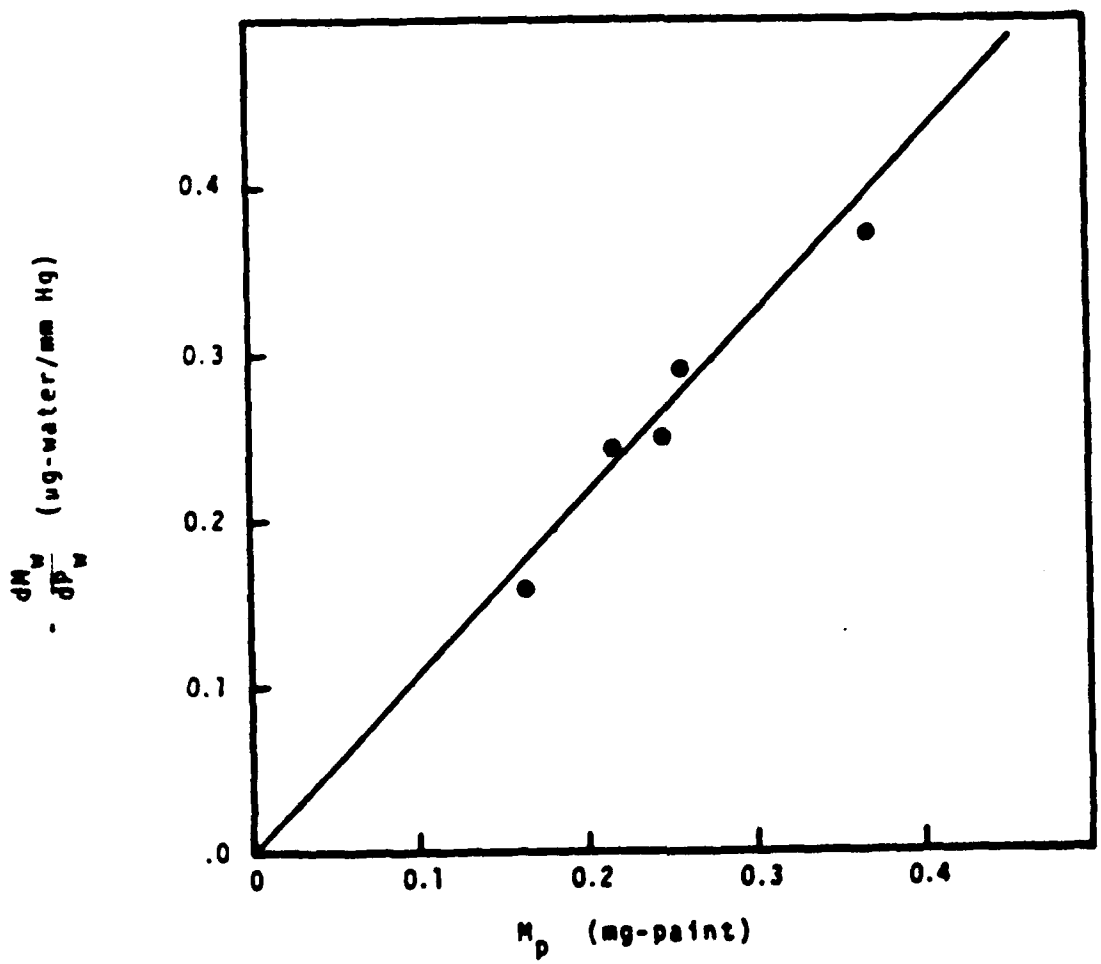

Fig. B10. Water sorption by FP-PUR at 32.0 ± 0.1°C. Linear regression forced through the origin: slope = 1.069 ug-water/(mg-paint · mm Hg), correlation coefficient = 0.999.

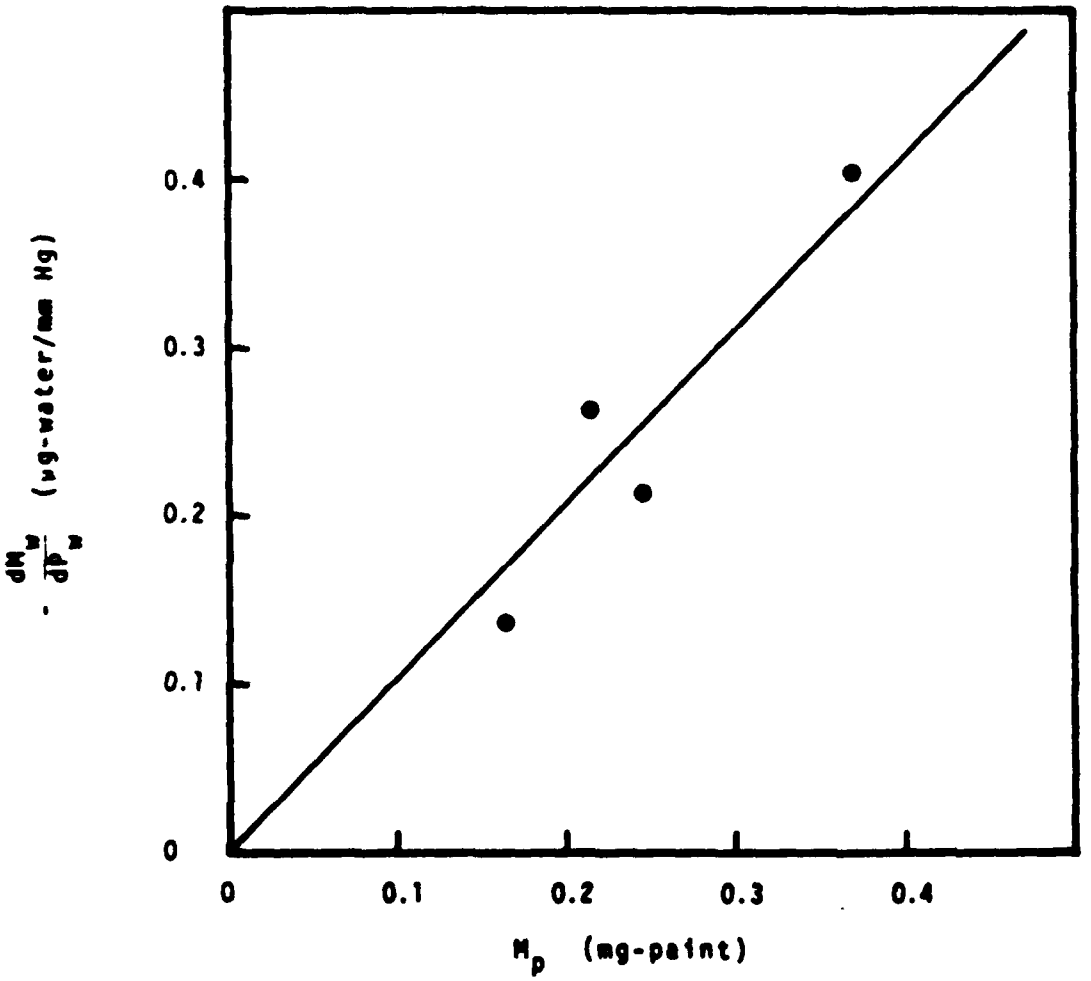

Fig. B11. Water sorption by FP-PUR at 35.8 ± 0.1°C. Linear regression forced through the origin: slope = 1.033 µg-water/(mg-paint · mm Hg), correlation coefficient = 0.992.

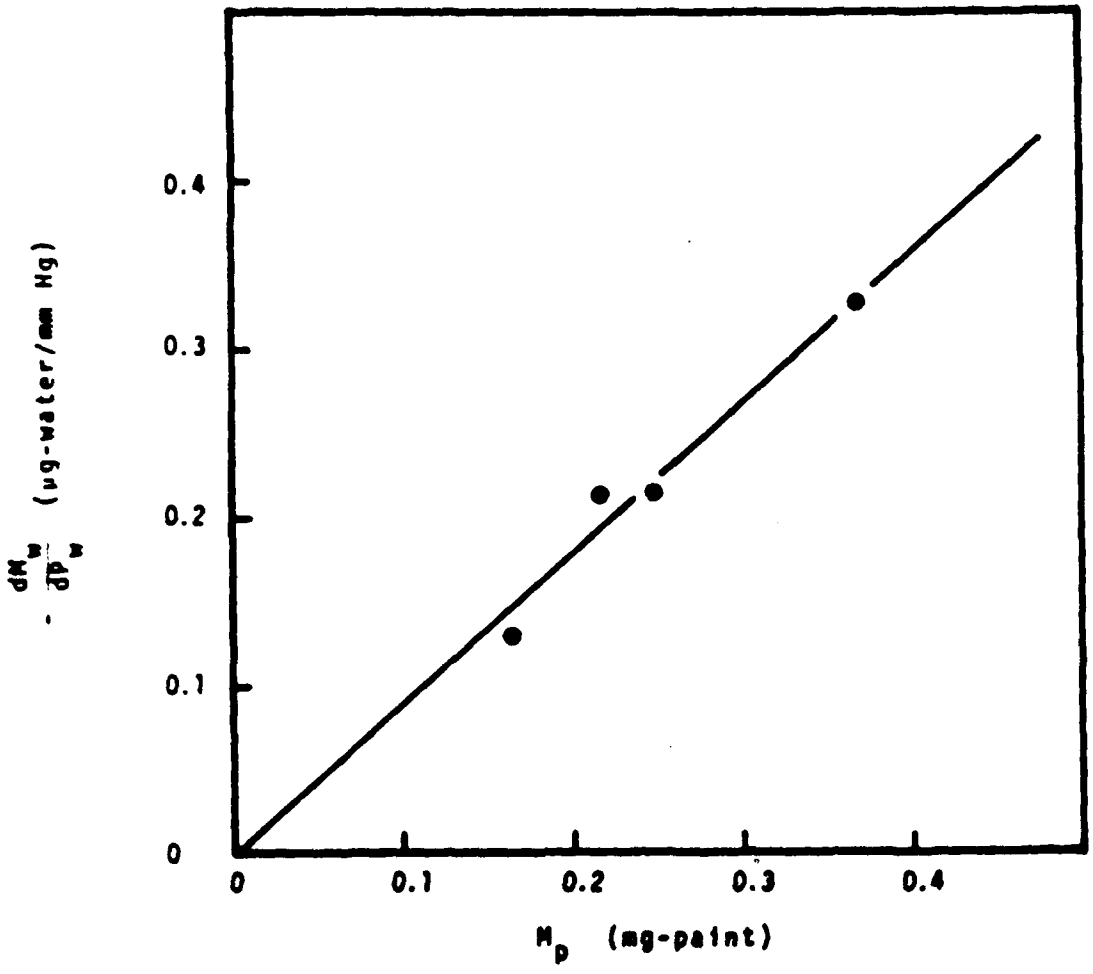

Fig. B12. Water sorption by FP-PUR at 40.4 ± 0.1°C. Linear regression forced through the origin: slope = 0.884 µg-water/(mg-paint · mm Hg), correlation coefficient = 0.999.

Table B5

YP-Epoxy Paint Specimens Used
in the Crystal Oscillator Apparatus

Crystal Number	Paint Mass (mg)	Paint Thickness (μm)
57	.276	5.6
58	.106	2.2
79	.204	4.1
81	.070	1.4

Table B6

Solubility of Water in YP-Epoxy*

Paint Thickness (μm)	Temp. (°C)	Crystal Number	Solubility (g-H_2O/g-paint)
1.4	30.5	81	1.98 E-2
2.2	30.7	58	8.90 E-3
4.1	30.1	79	1.43 E-2
5.6	30.7	57	1.25 E-2
		Average	1.39 E-2
		σ	($\pm$0.45 E-2)

* The equilibrium vapor pressure of water is 3.52 kPa.

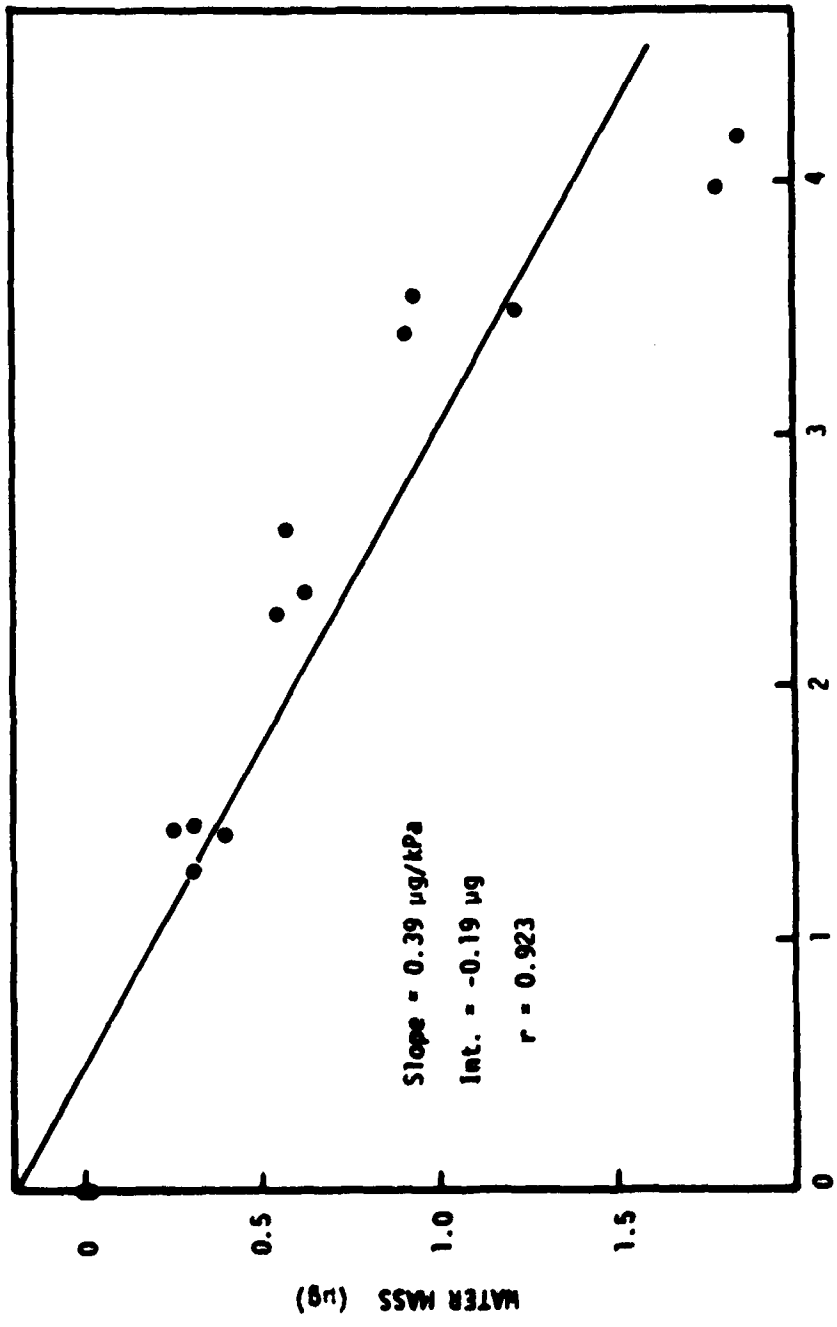

Fig. B13. Absorption isotherm for water in YP-Epoxy at 30.5°C. Crystal No. 81.

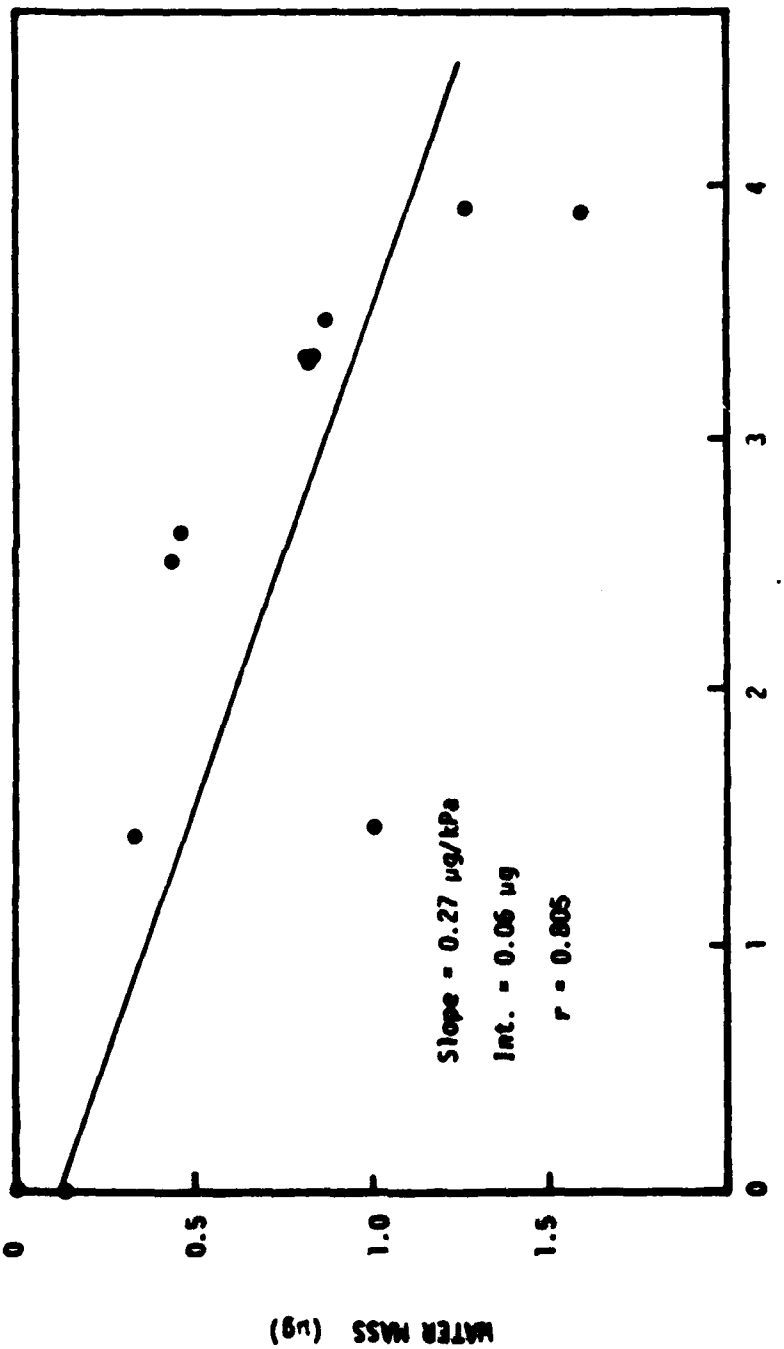

Fig. B14. Absorption isotherm for water in YP-Epoxy at 30.7°C. Crystal No. 58.

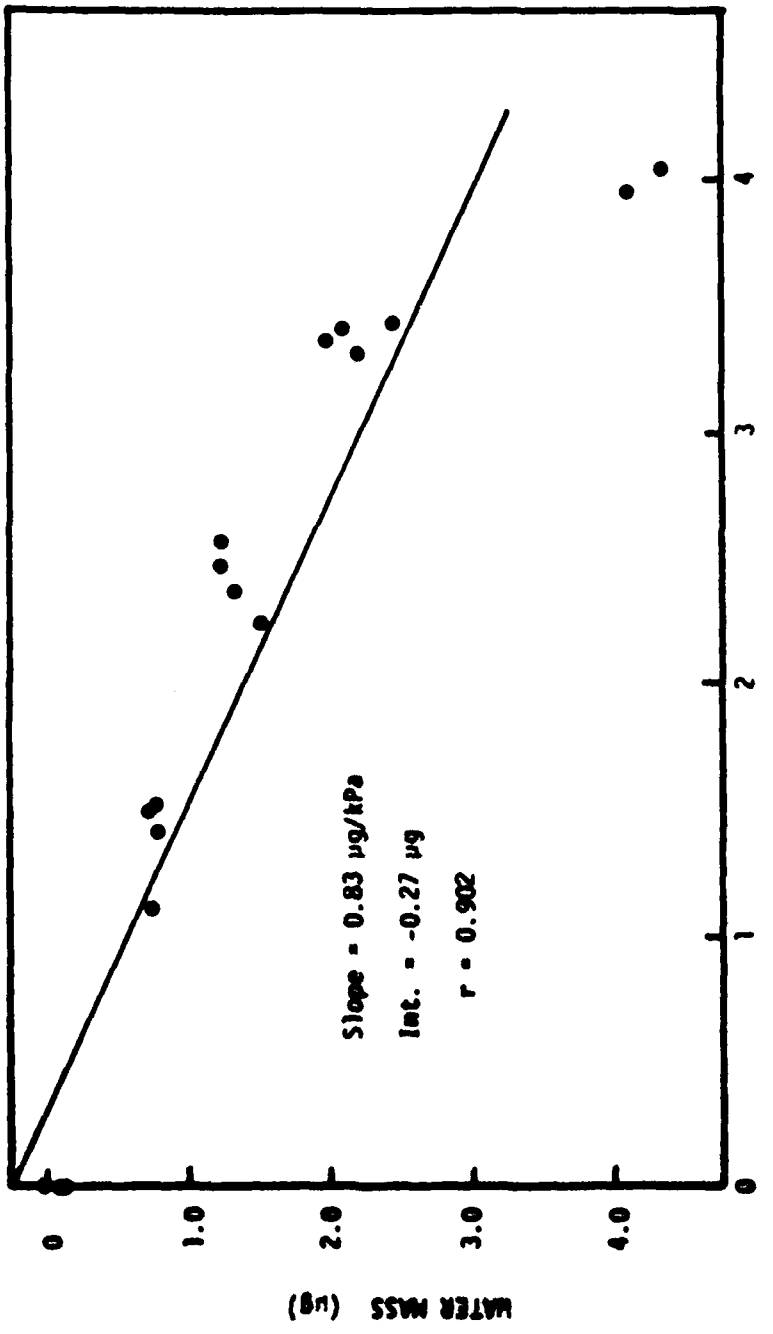

Fig. B15. Absorption isotherm for water in YP-Epoxy at 30.1°C. Crystal No. 79.

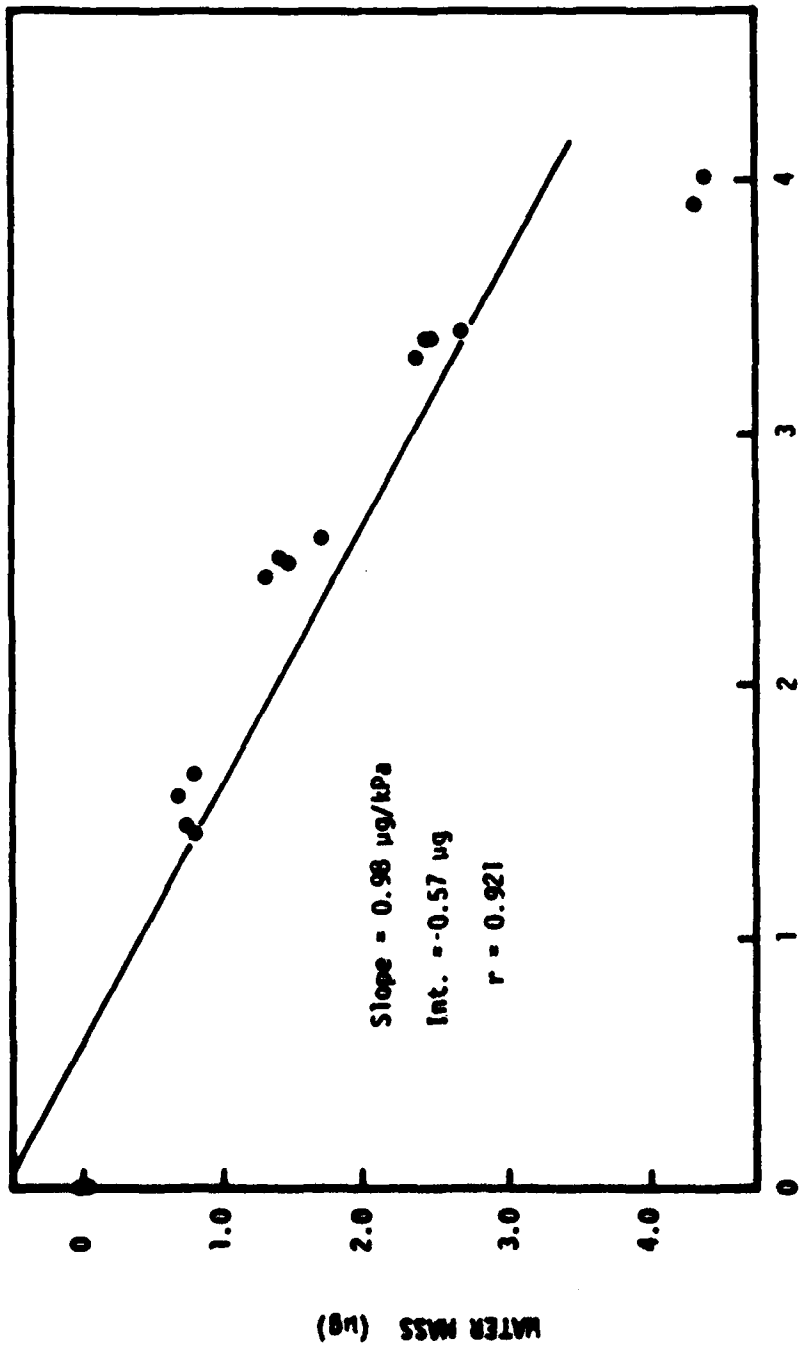

Fig. B16. Absorption isotherm for water in YP-Epoxy at 30.7°C. Crystal No. 57.

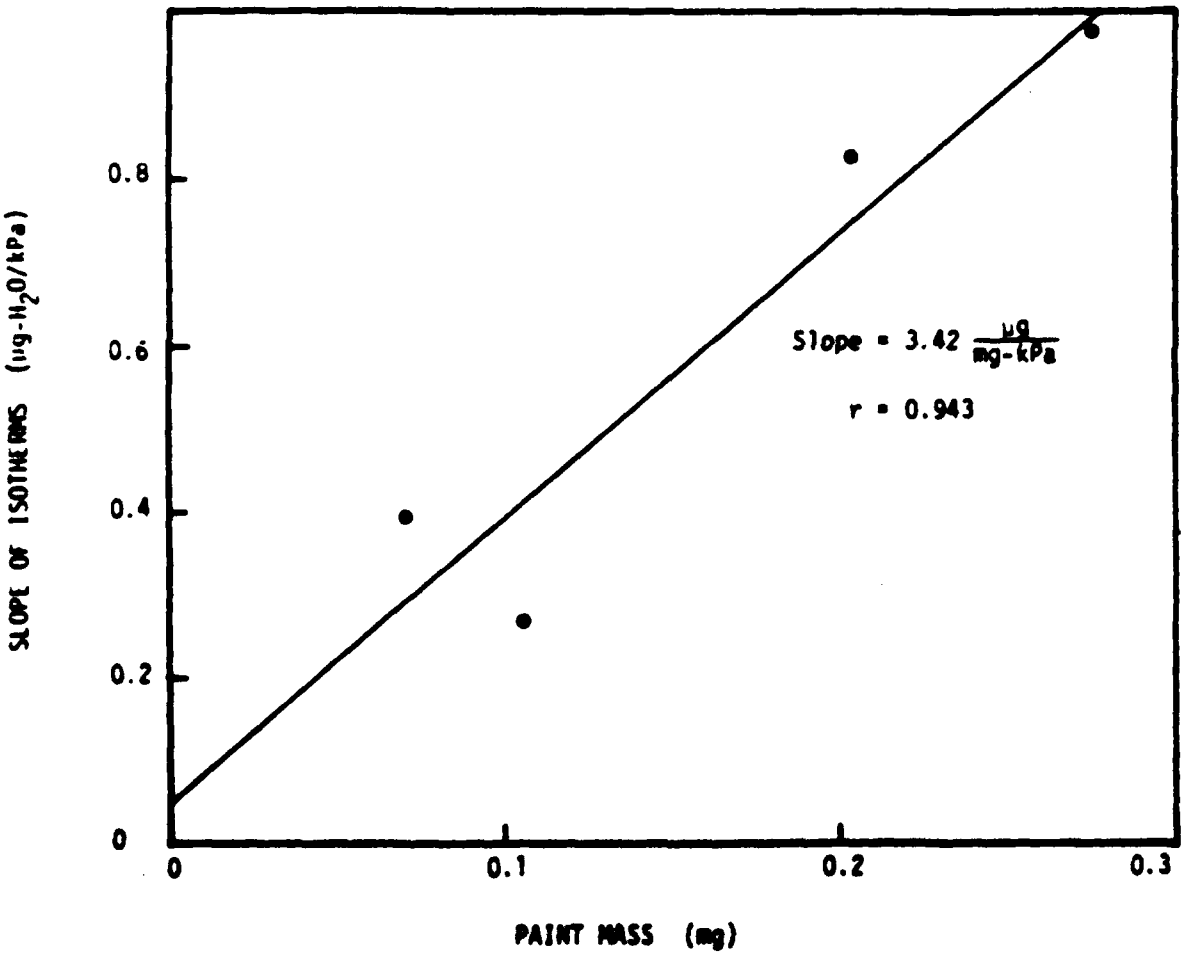

Fig. B17. Solubility of water in YP-Epoxy at 30.5°C.

APPENDIX B

Water Diffusivity

Table B7

Water Diffusivity in FP-PUR
Crystal #77, 0.164 mg of Paint
Thickness = 4.0 μm

10^{10} x Diffusivity (cm^2/s)	Relative Humidity Range (%)	Temperature (°C)	Date of Experiment
26.4	0 - 81.7	30.9	4/13/83
29.6	0 - 28.4	31.2	5/18/83
25.8	27.9 - 55.1	31.7	6/1/83
15.6	54.8 - 76.1	31.9	6/16/83
12.6	76.1 - 93.7	31.5	6/29/83
36.1	0 - 27.1	35.2	8/11/83
32.6	26.1 - 53.9	35.6	8/4/83
24.1	53.7 - 75.7	35.7	7/22/83
16.1	75.6 - 92.8	35.5	7/20/83
50.2	0 - 25.8	39.1	8/22/83
33.3	25.8 - 53.0	38.8	8/29/83

Table B8

Water Diffusivity in FP-PUR
Crystal # 78, 0.218 mg of Paint
Thickness = 5.3 μm

10^{10} x Diffusivity (cm^2/s)	Relative Humidity Range (%)	Temperature (°C)	Date of Experiment
75.5	0 - 81.7	30.7	4/18/83
75.5	0 - 28.3	31.4	5/18/83
75.5	27.9 - 55.1	31.7	5/20/83
53.9	54.9 - 76.2	31.3	6/24/83
42.7	76.1 - 93.7	31.5	6/27/83
75.5	0 - 26.9	35.6	8/10/83
75.5	26.7 - 53.9	35.6	8/8/83
80.0	53.8 - 75.6	35.6	7/22/83
60.5	75.6 - 92.7	35.8	7/21/83
75.5	0 - 25.9	38.9	8/24/83
75.5	25.8 - 53.0	38.8	8/25/83

Table B9

Water Diffusivity in FP-PUR
Crystal #62, 0.248 mg of Paint
Thickness = 6.0 μm

10^{10} x Diffusivity (cm^2/s)	Relative Humidity Range (%)	Temperature (°C)	Date of Experiment
43.1	0 - 81.9	29.5	9/13/83
38.9	0 - 28.4	31.2	5/16/83
45.5	27.8 - 55.1	31.9	6/7/83
28.8	54.8 - 76.1	31.8	6/13/83
27.7	76.1 - 93.7	31.2	7/5/83
60.5	0 - 27.0	35.5	8/12/83
68.0	26.7 - 53.9	35.5	8/3/83
44.2	53.7 - 75.6	35.7	7/25/83
36.2	75.6 - 95.8	35.3	7/15/83
75.5	0 - 25.8	39.1	8/17/83
75.5	25.8 - 53.0	38.8	8/31/83

Table B10

Water Diffusivity in FP-PUR
Crystal #76, 0.258 mg of Paint
Thickness = 6.3 μm

10^{10} x Diffusivity (cm^2/s)	Relative Humidity Range (%)	Temperature (°C)	Date of Experiment
36.3	0 - 81.7	30.7	4/14/83
35.8	0 - 28.4	31.5	5/17/83
36.4	27.9 - 55.0	31.9	6/6/83
22.3	54.8 - 76.1	31.9	6/15/83
20.9	81.5 - 93.7	31.4	6/30/83
29.8	75.6 - 92.8	35.5	7/18/83

Table B11

Water Diffusivity in FP-PUR
Crystal #61, 0.370 mg of Paint
Thickness = 8.9 μm

10^{10} x Diffusivity (cm^2/s)	Relative Humidity Range (%)	Temperature (°C)	Date of Experiment
39.4	0 - 81.5	29.3	9/10/82
34.4	0 - 28.3	31.4	5/9/83
40.3	27.9 - 55.1	31.8	6/9/83
34.7	54.8 - 76.0	31.8	6/10/83
32.4	76.1 - 93.6	31.5	7/6/83
54.9	0 - 26.9	35.8	8/15/83
64.4	26.9 - 54.0	35.3	8/1/83
54.0	53.9 - 75.7	35.2	7/29/83
43.6	75.6 - 92.8	35.2	7/14/83
75.5	0 - 25.9	39.1	8/16/83
75.5	25.6 - 52.8	39.8	9/2/83

Table B12

Water Diffusivity in GP-PUR

D x 10^{-10} (cm^2/s)	Relative Humidity Range (%)	Temp. (°C)	Date	Crystal
23.6	0 - 32.7	31.3	10/28/83	75
15.3	34.6 - 55.2	31.2	10/31/83	75
10.0	59.2 - 76.5	29.6	11/16/83	75
10.9	80.1 - 94.0	30.0	11/18/83	75
29.3	0 - 32.8	31.1	10/19/83	59
19.3	34.3 - 55.2	31.2	11/9/83	59
9.7	58.1 - 76.4	31.3	11/10/83	59
7.9	76.4 - 94.1	30.2	1/17/84	59
31.2	0 - 32.8	31.1	10/26/83	74
30.3	34.6 - 55.5	30.9	11/1/83	74
27.9	58.1 - 76.3	31.2	11/16/83	74
10.7	81.0 - 94.2	29.6	11/22/83	74
27.2	0 - 32.9	31.5	10/24/83	72
15.9	34.4 - 55.5	31.0	11/3/83	72
10.8	57.8 - 76.4	31.1	11/14/83	72
9.9	76.4 - 94.0	30.0	1/11/84	72
31.9	0 - 32.7	31.3	11/21/83	60
21.4	34.5 - 55.5	31.1	11/8/83	60
8.5	57.8 - 76.1	31.3	11/11/83	60
5.5	76.5 - 94.1	29.9	1/17/84	60
30.9	0 - 34.6	31.2	10/25/83	73
19.6	34.2 - 54.8	31.4	11/3/83	73
26.1	57.6 - 76.3	31.0	11/15/83	73
19.6	76.5 - 94.0	30.4	11/28/83	73

Table B13

Water Diffusivity in YP-Epoxy

10^{10} x Diffusivity (cm^2/s)	Relative Humidity Range (%)	Temp. (°C)	Date of Experiment	Crystal Number
78.44	0 - 36	29.7	2/17/84	57
50.84	34 - 56	30.5	2/7/84	57
31.33	55 - 76	30.9	2/3/84	57
17.44	76 - 94	29.8	1/19/84	57
70.22	0 - 34	30.3	2/16/84	58
10.47	34 - 55	30.8	2/8/84	58
6.74	56 - 76	30.6	2/3/84	58
2.87	76 - 94	29.7	1/23/84	58
64.68	0 - 32	26.7	2/21/84	79
23.41	33 - 56	29.1	2/10/84	79
7.09	55 - 76	31.2	2/1/84	79
4.42	76 - 92	30.0	1/24/84	79
4.75	0 - 33	28.3	2/13/84	81
2.76	34 - 56	29.3	2/13/84	81
1.25	56 - 76	30.6	2/2/84	81
0.92	76 - 99	30.1	1/26/84	81

[redacted]

DISTRIBUTION LIST
REPORT NO. NADC-84107-60

	No. of Copies
Army Aviation Research & Development Command (DRDAV-DS) 4300 Goodfellow Boulevard St. Louis, MO 63120	1
Army Materials & Mechanics Research Center (DRXMR-MM) Watertown, MA 02172	1
David Taylor Naval Ship Research & Development Center (2841) Annapolis, MD 21402	1
Defense Technical Information Center Cameron Station Alexandria, VA 22314	12
Lehigh University (H. Leidheiser) Bethlehem, PA 18015	1
Marine Corps Air Station (342) Cherry Point, NC 28533	1
Mobility Equipment Research & Development Command (DRDME-VO) Fort Belvoir, VA 22060	1
NASA-Ames Research Center (J. Parker) Moffett Field, CA 94035	1
National Bureau of Standards (M. McKnight) Washington, DC 20234	1
Naval Air Engineering Center (ESSD-9321) Lakehurst, NJ 08733	1
Naval Air Rework Facility (340) Naval Air Station Alameda, CA 94501	1
Naval Air Rework Facility Naval Air Station Jacksonville, FL 32212	1

DISTRIBUTION LIST (cont)

	No. of Copies
Naval Air Rework Facility Naval Air Station Norfolk, VA 23511	1
Naval Air Rework Facility Naval Air Station Pensacola, FL 32508	1
Naval Air Rework Facility Naval Air Station San Diego, CA 92135	1
Naval Air Station (AIRLANT-528A) Norfolk, VA 23511	1
Naval Air Station (AIRPAC-7412) North Island, San Diego, CA 92135	1
Naval Air Systems Command (AIR-310A, AIR-5304D) Washington, DC 20361	2
Naval Construction Battalion Center (L52) Port Hueneme, CA 93043	1
Naval Facilities Engineering Command (04B3) 200 Stovall Street Alexandria, VA 22332	1
Naval Research Laboratory (6120, 6123, 6124) 4555 Overlook Avenue Washington, DC 20375	3
Naval Sea Systems Command (05E1, 05M1) Washington, DC 20362	2
Office of Naval Research (471) 800 North Quincy Street Arlington, VA 22217	1
Warner-Robbins Air Logistics Command (MMTRC, MMEMC) Robbins AFB, GA 31098	2

DISTRIBUTION LIST (cont)

	No. of Copies
Wright Aeronautical Laboratories . . . . . (MLSA, MLBT) Wright-Patterson AFB, OH 45433	2
NAVAIRDEVCEN . . . . . (3 for 8131) (30 for 6062)	33